1-2023

Physiologically-Based Pharmacokinetic (PBPK) Modeling for the Preclinical Development of Spectinamide Antibiotics

Keyur R. Parmar

Physiologically-Based Pharmacokinetic (PBPK) Modeling for the Preclinical Development of Spectinamide Antibiotics

Abstract

Despite being an ancient disease caused by Mycobacterium tuberculosis (Mtb) and after decades of research, tuberculosis (TB) still affects millions of people every year worldwide. In 2018, the World Health Organization (WHO) reported that 10 million people developed tuberculosis and 1.5 million died of the disease. With the increase in the multidrug-resistant (MDR) and extensively drug-resistant (XDR) cases, the treatment for TB with the standard first and second-line therapy is becoming increasingly difficult. Therefore, there is an urgent need to find new anti-TB drugs as combination partners of existing and experimental classes of antimicrobial agents to shorten and simplify the treatment of MDR or XDR TB infection. Spectinamide 1599 and spectinamide 1810 are lead spectinamide compounds currently under preclinical development for the treatment of MDR and XDR tuberculosis. These compounds have previously been tested at various combinations of dose level, dosing frequency, and routes of administration in mouse models of Mtb infection and in healthy animals. Characterizing the disposition of a compound in the tissues of interest is important in understanding the pharmacology of novel antibiotic agents. TB is primarily a pulmonary disease, but extrapulmonary disease has been reported in 10-42% of patients. Thus, understanding the drug disposition and exposure in the tissues in which Mtb is residing is of utmost importance for any new antitubercular drug. Hence, we have used a physiologically-based pharmacokinetic (PBPK) approach for the prediction of drug pharmacokinetics in organs/tissues of interest and extrapolate their disposition across different species. In the current study, we built, qualified, and refined a minimalistic PBPK model that can describe and predict the pharmacokinetics of spectinamide antibiotics in various tissue, especially those relevant to Mtb infection. The model was expanded and qualified for multiple dose levels, dosing regimens, routes of administration, and various species. The model predictions in mice (healthy and infected) and rats were in reasonable agreement, and all predicted Area Under the Curve (AUCs) in plasma and tissues met the twofold acceptance criteria relative to observed data. To further explore tissue exposure in Mtb lesions, we also utilized the established Simcyp granuloma model to explore the distribution of spectinamide 1599 within granuloma substructures. Simulation results suggest substantial exposure in all lesion substructures, with particularly high exposure in the rim region and in macrophages of the lesion. The developed model may be leveraged as an effective tool in predicting the disposition of spectinamide antibiotics in further preclinical and clinical development to identify optimal dose levels and dosing regimens.

Document Type

Dissertation

Degree Name

Doctor of Philosophy (PhD)

Program

Pharmaceutical Sciences

Research Advisor

Bernd Meibohm, PhD

Keywords

granuloma model, interspecies extrapolation, intratracheal PBPK, mPBPK, spectinamides, subcutaneous PBPK

Subject Categories

Analytical, Diagnostic and Therapeutic Techniques and Equipment | Bacterial Infections and Mycoses | Diseases | Investigative Techniques | Medical Sciences | Medicine and Health Sciences | Other Pharmacy and Pharmaceutical Sciences | Pharmaceutics and Drug Design | Pharmacy and Pharmaceutical Sciences | Respiratory Tract Diseases | Therapeutics

UNIVERSITY OF TENNESSEE HEALTH SCIENCE CENTER

DOCTORAL DISSERTATION

Physiologically-Based Pharmacokinetic (PBPK) Modeling for the Preclinical Development of Spectinamide Antibiotics

---

Author:
Keyur Raman Parmar

Advisor:
Bernd Meibohm, PhD

A Dissertation Presented for The Graduate Studies Council of
The University of Tennessee Health Science Center
in Partial Fulfillment of the Requirements for the Doctor of Philosophy degree from
The University of Tennessee

in

Pharmaceutical Sciences: Pharmacometrics
College of Graduate Health Sciences

March 2023

DEDICATION

Dedicated to my beloved family and friends.

ACKNOWLEDGEMENTS

The journey for pursuing Doctor of Philosophy degree has been a life-changing experience for me, full of twists and turns, ups and downs, challenges, learning, and maturing. It would not have been possible without the endless support and encouragement of the following people. Here, I take this opportunity to extend my gratitude to all those who helped throughout this unforgettable journey at the University of Tennessee Health Science Center (UTHSC).

First and foremost, I would like to extend my sincere thanks to my mentor and advisor, Dr. Bernd Meibohm, for his inspiration, guidance, sheer optimism, and endless support throughout my Ph.D. journey. I could not have imagined having a better mentor for my Ph.D. program. I am immensely thankful to him for encouraging me to have a clear perspective of my research objectives, providing me with critical insights to solve difficult and complicated research problems. Moreover, I am grateful to him for helping me grow and mature not only as a scientist but also as a person. No words are sufficient to extend my gratitude to his efforts. I would also like to acknowledge my dissertation committee members: Dr. Andrea Edginton, Dr. Carl Panetta, Dr. Santosh Kumar, and Dr. Glen Palmer for their motivation, insightful comments, and continuous support. I would also like to extend my gratitude to our collaborators at St. Jude Children's Hospital: Dr. Richard Lee and his lab members for allowing me to work on the spectinamide project; and at Colorado State University, Dr. Anne Lenaerts and Dr. Mercedes Gonzalez-Juarrero for their research work on *Mtb*-infected animals and for providing pharmacokinetic data that was an integral part of my dissertation research. I am grateful to Dr. Aman Singh and Dr. Ganesh Mugundu for providing me internship opportunity that helped me in learning advanced modeling and simulation skills and contributed to my scientific and professional development.

I would like to extend my gratitude to our program director, Dr. Hassan Almoazen, for always being helpful and providing opportunities for professional development. I am sincerely grateful to all the faculty members and administrative staff at the UTHSC. I would like to thank our staff members, Ms. Kendra Golden, Ms. Shelley Cannioto, Ms. Patrice Shaw, and ex-staff Mary Newell for their administrative help. My heartfelt gratitude to the UTHSC, College of Pharmacy, and College of Graduate Health Sciences for providing all the necessary facilities, equipment, and financial support. I would also like to thank all the funding agencies: the National Institute of Allergy and Infectious Diseases and the Office of the Director of the National Institutes of Health (grants R01AI090810, R01AI120670, and S10OD016226), and ALSAC, St. Jude Children's Research Hospital. A special thanks to the ETD formatting and review manager, Ms. Shirley Hancock, for her constant effort and guidance in formatting and finalizing my dissertation.

I would like to thank my past and present lab members: Dr. Pradeep Lukka, Dr. Santosh Wagh, Dr. Ashit Trivedi, Dr. Ashish Srivastava, Zaid Temrikar, Paridhi Gupta, Hyunseo Park, Bhargavi Thalluri, and Christelle Mathieu for their wonderful company

and guidance. A special thanks from the bottom of my heart to Dr. Pradeep Lukka and Zaid Temrikar for their invaluable friendship and constant support throughout my graduate program.

I would like to extend my heartfelt gratitude to all my friends at UTHSC, Memphis for making my journey memorable. I greatly value their friendship and I deeply appreciate their belief in me. A special appreciation to Himani Darji, Maulik Shah, Manali Ghag, Reekin Dhaduk, and Utsav Patel for supporting me like a family, providing me strength to overcome challenges, and making my journey memorable.

Last but not the least, I would like to express my deepest gratitude towards my papa, Mr. Ramanbhai Bhulabhai Parmar, and my mummy Mrs. Bhartiben Ramanbhai Parmar for all their countless sacrifices, relentless efforts, and their belief in me to pursue my dream. I dedicate my work, achievements, and this dissertation to both. My sincere love and thanks to my sister, Mayuriben Rajesh Damania; brother-in-law, Rajesh Damania; brother, Vijay Ramanbhai Parmar; sister-in-law, Kinjal Parmar; and my lovely nephew; Heet Damania.

Finally, I owe my sincere gratitude to Almighty God for providing me wisdom, health, and strength.

PREFACE

Supplementary File

The Monolix model scripts used to run the intravenous, subcutaneous, and intrapulmonary model are presented in the **Model Script Supplemental Data** file mentioned in **Chapter 5**.

Note on PDF Navigation

Document navigation is greatly facilitated by using Adobe Acrobat's "Previous view" and "Next view" functions. For "Previous view," use quick keys Alt/Ctrl+Left Arrow on PC or Command+Left Arrow on Mac. For "Next view," use Alt/Ctrl+Right Arrow on PC or Command+Right Arrow on Mac. Using these quick keys in tandem allows the reader to toggle between document locations. Since every scroll represents a new view; depending on how much scrolling is done for a specific view destination, more than one press of the back or forward arrows may be needed. For additional navigational tips, click View at the top of the PDF, then Page Navigation. These Adobe Acrobat functions may not be functional for other PDF readers or for PDFs opened in web browsers.

ABSTRACT

Despite being an ancient disease caused by *Mycobacterium tuberculosis* (*Mtb*) and after decades of research, tuberculosis (TB) still affects millions of people every year worldwide. In 2018, the World Health Organization (WHO) reported that 10 million people developed tuberculosis and 1.5 million died of the disease. With the increase in the multidrug-resistant (MDR) and extensively drug-resistant (XDR) cases, the treatment for TB with the standard first and second-line therapy is becoming increasingly difficult. Therefore, there is an urgent need to find new anti-TB drugs as combination partners of existing and experimental classes of antimicrobial agents to shorten and simplify the treatment of MDR or XDR TB infection. Spectinamide 1599 and spectinamide 1810 are lead spectinamide compounds currently under preclinical development for the treatment of MDR and XDR tuberculosis. These compounds have previously been tested at various combinations of dose level, dosing frequency, and routes of administration in mouse models of *Mtb* infection and in healthy animals.

Characterizing the disposition of a compound in the tissues of interest is important in understanding the pharmacology of novel antibiotic agents. TB is primarily a pulmonary disease, but extrapulmonary disease has been reported in 10-42% of patients. Thus, understanding the drug disposition and exposure in the tissues in which *Mtb* is residing is of utmost importance for any new antitubercular drug. Hence, we have used a physiologically-based pharmacokinetic (PBPK) approach for the prediction of drug pharmacokinetics in organs/tissues of interest and extrapolate their disposition across different species. In the current study, we built, qualified, and refined a minimalistic PBPK model that can describe and predict the pharmacokinetics of spectinamide antibiotics in various tissue, especially those relevant to *Mtb* infection. The model was expanded and qualified for multiple dose levels, dosing regimens, routes of administration, and various species. The model predictions in mice (healthy and infected) and rats were in reasonable agreement, and all predicted Area Under the Curve (AUCs) in plasma and tissues met the twofold acceptance criteria relative to observed data. To further explore tissue exposure in *Mtb* lesions, we also utilized the established Simcyp granuloma model to explore the distribution of spectinamide 1599 within granuloma substructures. Simulation results suggest substantial exposure in all lesion substructures, with particularly high exposure in the rim region and in macrophages of the lesion. The developed model may be leveraged as an effective tool in predicting the disposition of spectinamide antibiotics in further preclinical and clinical development to identify optimal dose levels and dosing regimens.

TABLE OF CONTENTS

LIST OF TABLES

LIST OF FIGURES

LIST OF ABBREVIATIONS

API	Atmospheric Pressure Ionization
AUC	Area under the [plasma or tissue concentration] curve
AUClast	Area under the plasma or tissue concentration-time curve to the last measurable plasma concentration
BIW	Twice weekly dosing
BCS	Biosafety cabinet
BSL-3	Biosafety Level 3
CAD	Cationic amphiphilic drugs
cLogP	Calculated logarithm partition coefficient of a compound
C_{ss}	Steady state concentration
ELF	Epithelial lining fluid
F	Bioavailability
FDA	Food and Drug Administration
fe	Fraction of compound excreted unchanged in urine
FIH	First-in-human
fu	Fraction of compound unbound to plasma protein
IPA	Intrapulmonary aerosol
IS	Internal Standard
ISF	Interstitial fluid
IV	Intravenous
k(b/p)	Whole blood to plasma partition ratio of a compound
k(RBC/p)	Erythrocytes to plasma partition coefficient of a compound
Ka	First-order absorption rate constant
$K_{C\rightarrow I}^{Organ}$	First-order backflux rate constant from cellular to interstitial
$K_{I\rightarrow C}^{Organ}$	First-order influx rate constant from interstitial to cellular
LC-MS/MS	Liquid Chromatography with tandem mass spectrometry
MDR-TB	Multidrug-resistant tuberculosis
MIDD	Model Informed Drug Development
Mtb	*Mycobacterium tuberculosis*
OCT	Organic cation transporter
ODE	Ordinary differential equation
PAMPA	Parallel artificial membrane permeability assay
PBPK	Physiologically-Based Pharmacokinetic
PBR	Pulmonary blood reservoir
PBS	Phosphate-buffered saline
%CV	Percent coefficient of variation
pKa	Negative log of acid dissociation constant
QD5	Daily dosing for 5 consecutive days
Q_{Tissue}	Tissue-specific blood flow rate
RED	Rapid equilibrium dialysis
RSE	Relative standard error
RUV	Residual unexplained variability
SAEM	Stochastic Approximation Expectation Maximization

SC	Subcutaneous
TB	Tuberculosis
TIW	Thrice weekly dosing
V_{Tissue}	Volume of Tissue
WHO	World Health Organization
XDR-TB	Extensively Drug Resistant Tuberculosis

CHAPTER 1. INTRODUCTION

Physiologically-Based Pharmacokinetic (PBPK) Models

Pharmacokinetic models can be classified into empirical, semi-mechanistic, and compartmental models. These models are data driven and thus are useful for data interpolation and description. The modelling approach includes development, parameter estimation, and selection of the 'best fit' using statistical criteria [1]. However, the information content of these models does not extend beyond the available experimental data, and the models themselves do not represent the actual physiological spaces and thus are poor for extrapolation [2].

Physiologically-based pharmacokinetic (PBPK) models are mechanistic multicompartment models that incorporate the known anatomical and physiological knowledgebase for different species, as well as the physicochemical properties of the drug candidate to describe its pharmacokinetics in the organs and tissues of different mammalian species [3]. Each compartment in a whole-body PBPK model represents an organ or tissue with its known volume/weight and blood flow rate, which can provide a mechanistic understanding of drug disposition [4]. On the basis of this biological and mechanistic knowledge, the PBPK models allow the extrapolation of the pharmacokinetic behavior of drugs with respect to dose, route, and species [2].

Structural Framework of a PBPK Model

The basic framework of a whole body PBPK model includes building blocks such as body fluid/tissues/organs/systems connected *via* blood circulation (**Figure 1-1**). The PBPK model incorporates drug specific parameters such as binding to plasma proteins, *fu*; tissue-to-plasma distribution coefficient, Kp_T; tissue permeability-surface area product, PS_T; enzymatic activity, V_m/K_m [2]. The model is described mathematically by mass transfer differential equations (**Equation 1-1**):

$$\begin{aligned} Rate\ of\ change\ of\ X \\ = rate\ of\ gain\ of\ X - rate\ of\ loss\ of\ X \\ \pm\ rate\ of\ gain\ or\ loss\ of\ X\ by\ reaction \end{aligned} \qquad \textbf{Eq. 1-1}$$

The tissue compartment can be considered as perfusion-limited or permeability-rate-limited, depending on the underlying distribution mechanism of the compound in a tissue. The perfusion-rate-limited tissue models are the simplest, in which a tissue is represented as a single well-stirred compartment and the distribution of a compound in the whole volume of tissue is instantaneous with the incoming blood flow (**Figure 1-2A**). On the other hand, when the membrane permeability is assumed to be the rate-limiting factor.

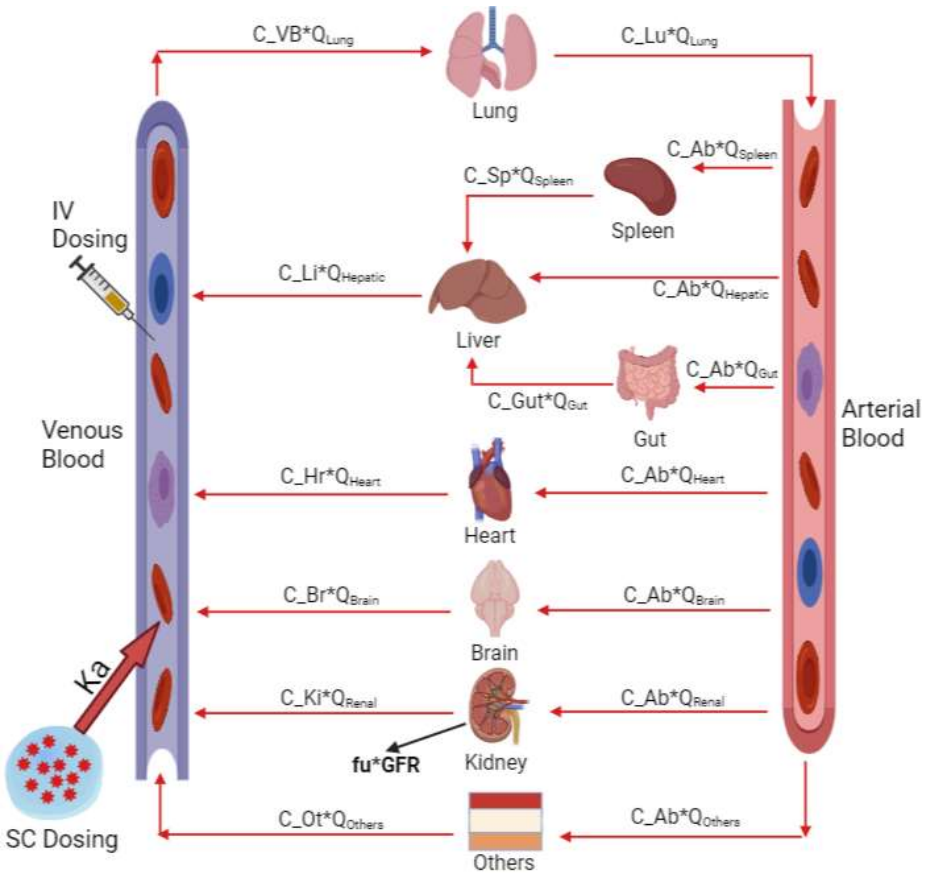

Figure 1-1. Schematic diagram of a whole body PBPK model consisting of blood compartments (venous and arterial) and organs (lung, liver, spleen, gut, heart, brain, kidney), and all the remaining organs lumped together as "others," connected by blood circulation.

C = concentration; Q = blood flow rate; IV = intravenous route of administration; SC = subcutaneous route of administration; and Ka = first order absorption rate constant.

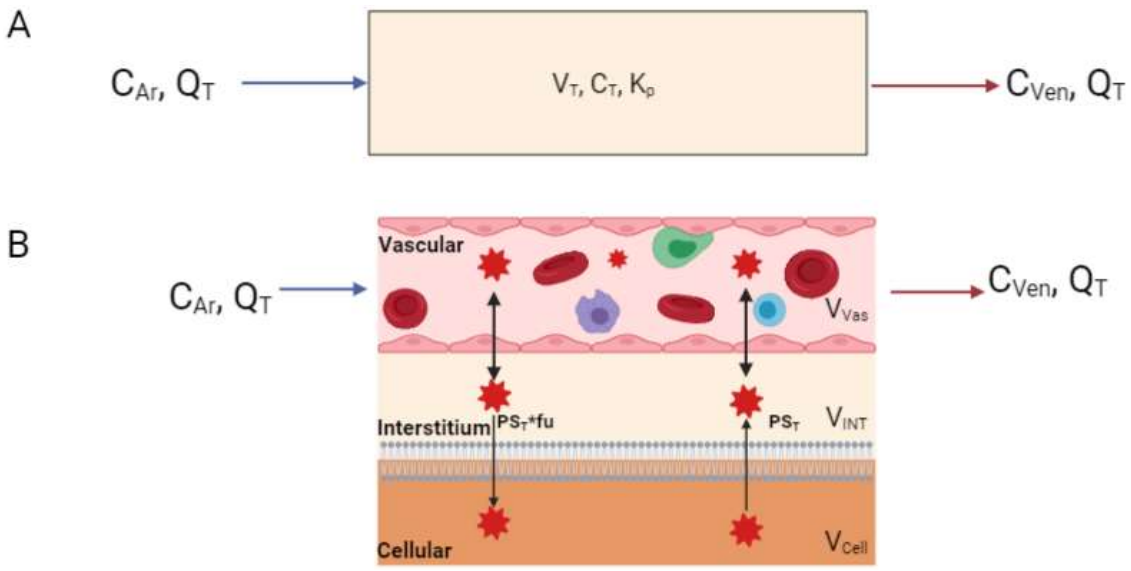

Figure 1-2. Diagram for a perfusion limited tissue (A) and a permeability rate-limited tissue (B).

C = concentration; Kp = tissue:plasma distribution coefficient; PS_T = permeability surface area coefficient; *fu* = fraction of compound unbound to plasma protein, Q = blood flow; V = volume; subscripts Ar, Cell, INT, T, Vas, and Ven = arterial, tissue cellular compartment, tissue interstitial compartment, tissue compartment, tissue vascular compartment and venous, respectively.

for the distribution of a compound in a tissue, the tissues could be divided into 2 or 3 well-stirred sub compartments and the distribution of a compound could be addressed by tissue-specific permeability surface area product (PS_T) **Figure 1-2B**).

The perfusion limited tissue structure can be described mathematically by the differential equation mentioned below in **Equation 1-2**. The commonly used two-compartment permeability-limited tissue structure can be mathematically described by the differential equations presented in **Equations 1-3** and **1-4**. In the two-compartment tissue structure, the whole tissue is divided into two sub compartments, one is well stirred or in rapid equilibrium with the blood flow and the other one is a delayed equilibrium compartment, limited by the permeability surface area product of the tissue. Also, the common assumption is that only the unbound fraction of the drug in plasma is distributed in the delayed equilibrium compartment:

$$\frac{dC_T}{dt} = \frac{\left(Q_T \cdot C_{Ar} - Q_T \cdot \frac{C_T}{Kp}\right)}{V_T} \qquad \textbf{Eq. 1-2}$$

$$\frac{dC_V}{dt} = \frac{Q_T \cdot C_{Ar}}{V_V} - \frac{Q_T \cdot C_V}{V_V} - \frac{PS_T \cdot fu \cdot C_V}{V_V} + \frac{PS_T \cdot C_{EV}}{V_{EV}} \qquad \textbf{Eq. 1-3}$$

$$\frac{dC_{EV}}{dt} = \frac{PS_T \cdot fu \cdot C_V}{V_V} - \frac{PS_T \cdot C_{EV}}{V_{EV}} \qquad \textbf{Eq. 1-4}$$

Building a whole body PBPK model requires various physicochemical parameters and concentration-time profiles in numerous tissues. A model could be reduced to a less complex structure requiring some empirical adjustment in order to increase transparency and enhance the ease of application, while retaining the key mechanistic features [5]. Such models are called minimal PBPK (mPBPK) models which allow one to focus on specific tissues of interest for which the data are available while lumping the other tissues into a single compartment [4].

A PBPK model development could be initiated based on either of these three approaches: 1) bottom-up, 2) top-down, and 3) middle-out approach. The “bottom-up” approach is based on the *in vitro* understanding of the compound-specific ADME mechanisms. The model is integrated with all the known physicochemical properties of the compound, along with the system-specific parameters, and used to predict the concentration-time profiles. An alternative to “bottom-up” approach is developing a PBPK model based on the observed data, known as “top-down” approach. The base model is fitted to a set of observed concentration-time profiles by estimating relevant parameters. The last approach, a hybrid of both “bottom-up” and “top-down” approaches, is called “middle-out” approach. In this approach, the base model relies on the physicochemical, *in vitro*, preclinical, and mass-balance data. This approach provides enhanced flexibility by applying the “predict, learn, confirm, apply paradigm” and allows *a priori* decision-making [3].

Qualification, Verification, and Refinement of PBPK Model

Apart from model development, it is crucial for a PBPK model to be qualified, verified, and refined to gain confidence in the model's predictive performance—i.e., that the model is performing as intended

Model Qualification. Qualification of a model refers to a set of prerequisites that ensure "permission" to handle the intended use [3]. It requires documentation covering three components of a PBPK platform: the software/computational framework, system-dependent/physiological framework, and the drug properties. The computational framework consists of model code, model structure, mathematical equations, and runtime engine. The physiological framework includes the population-specific physiology of humans or preclinical species, which serves as a database to create virtual populations. The drug component consists of drug-dependent parameters that are necessary to define the ADME properties of the drug.

Model Verification. Verification refers to the predictive performance of the model, i.e., how well the model fits or describes the observed data. The predictive performance of a model mainly depends on the underlying mechanisms and assumptions within the related physiological system. The valid general model assumptions and the incorporation of correct drug and system parameters allow the model to simulate any drug regardless of the mechanism of elimination or enzymes involved. A compound model for a particular use or application is considered to be verified if the predictive performance for that particular use is satisfactory, based on the commonly accepted criteria [3], for example:

- Visual inspection of overlays of predicted and observed concentration-time profile indicates good agreement.
- The observed data are within the 95% prediction interval.
- Comparison of predicted and observed key pharmacokinetic parameters such as area under the curve (AUC), maximum concentration (C_{max}), clearance (CL), volume of distribution (Vd), time to peak concentration (T_{max}) indicates that the predicted values are within twofold of the observed values.

Model Refinement. PBPK model development is an iterative process involving multiple cycles of "predict, learn, and confirm" [3]. The improvement in the model predictive performance is done by adjusting individual model parameters, which are selected based on physiological understanding and scientific evidence. After the prediction from the refined model is checked against available PK data and commonly accepted criteria, the model is considered verified. Sensitivity analysis and uncertainty analysis play an important role in model refinement.

Sensitivity Analysis. Sensitivity analysis is used to identify the parameters that have the greatest influence on the prediction of concentration-time profiles. The selection of the parameters and their range is based on the known mechanistic basis and scientific

rationale. Identifying the parameters having a significant impact on the simulation outcome is very important, as it helps in deciding which experiment to perform at what stage of drug development to precisely determine these parameters and the resources to be invested in obtaining a particular parameter [6, 7]. Thus, it is recommended that sensitivity analysis be used throughout the model development process.

Uncertainty Analysis. Uncertainty analysis is used to account for the variability and uncertainty in the PBPK model parameters. The predictions are a result of a stochastic process instead of a single deterministic concentration-time curve, which is used to calculate 95% prediction intervals. This helps to obtain central tendencies and characterization of variability and uncertainty in the concentration-time profiles of various tissues [1]. One commonly used method is the Monte Carlo simulation procedure in which the statistical distribution of the input parameters is specified and defined quantitatively based on the observation or various assumptions (e.g., log-normality distribution assumption of clearance). Multiple sampling and computation of the model outputs from these distributions are used for calculation of 95% confidence intervals of pharmacokinetic parameters and hypothesis testing [3].

Application of PBPK Modeling

In the last decade, physiologically-based pharmacokinetic (PBPK) modeling and simulation has earned its rank in the model-informed drug development paradigm affecting various stages of drug development, from early compound selection to first in human (FIH) dose selection to dosing recommendations in product labeling [8]. The results from PBPK analyses have been routinely found in the clinical pharmacology section of investigational new drug (IND) and new drug application (NDA) submissions to the Food and Drug Administration (FDA) [9].

The PBPK modelling approach has three major advantages over empirical approaches: 1) richer information content (system- and drug-specific information), 2) modular structure (anatomical and physiological), and 3) universality (structure common across all mammalian species) [1]. This allows the extension of a PBPK model in performing inter-route, inter-species, and inter-drug extrapolation, rendering it most appropriate in understanding the disposition of a compound in plasma and tissues across various dosing levels, regimens, routes of administration, species, and structurally similar compounds. Here, we aim to utilize this extensive application of a PBPK model for the preclinical development of two leading spectinamide compounds and to leverage it in predicting the disposition in human tissues.

Spectinamide 1599 and 1810: Lead Compounds in the Treatment of Drug-Resistant Tuberculosis

Spectinamides are a novel class of semisynthetic analogs of the naturally occurring antibiotic spectinomycin. This modification of a natural product provides

advantages over spectinomycin in terms of increase in the potency, narrowing the antimicrobial spectrum, and, most importantly, evading the efflux from *Mycobacterium tuberculosis* (*Mtb*) [10]. The mechanism of action of spectinamides is similar to that of spectinomycin, exhibiting the anti-bacterial activity by binding to the bacterial 30S ribosomal subunit, resulting in the inhibition of the translocation and subsequently inhibiting protein synthesis [11]. These compounds are effective against both the susceptible as well as the resistant (MDR and XDR) strains of tuberculosis. Spectinamides are reported to reduce the *Mtb* burden in mice lungs both in acute as well as chronic models [12, 13].

In terms of physicochemical properties and pharmacokinetic behaviors, spectinamides are highly hydrophilic compounds with a cLogP of -2.5 and an acid dissociation constant (pKa) of 8.69, suggesting that the compounds are largely in ionized form at the physiological pH of 7.4. This is the likely reason for their poor membrane permeability and negligible oral bioavailability. Also, spectinamides have low plasma protein binding, excellent stability when incubated in liver microsomes, and are predominantly eliminated unchanged in urine. Thus, spectinamides are classified in the BDDCS class 3, compounds with high aqueous solubility, low permeability (BCS), and low metabolism [12].

The *in vivo* efficacy of the spectinamide compounds has been determined in tuberculosis-infected mouse models. The preliminary evaluation in the acute *Mtb* infection model showed a significant reduction in the lung bacterial burden compared to saline control and comparable to streptomycin. Also, in the chronic infection model the compounds showed significant reduction in the lung bacterial burden compared to a saline control group and similar to streptomycin and isoniazid [10]. Later, spectinamide 1599 and 1810 were tested alone and in combination with the existing frontline and new anti-TB agents in acute and chronic infection mouse models. Both compounds showed a significant reduction in the bacterial burden in the mouse lung. Moreover, spectinamide 1599 demonstrated appreciable synergy in anti-bacterial activity when combined with rifampin (RIF) [13]. These studies were performed by administrating the compounds *via* subcutaneous route and the maximum effective dose of spectinamide 1599 was 200 mg/kg given every day for 5 days (QD5) for 4 weeks [14]. The limitations of this approach are that the effective dose of 200 mg/kg is very high, and the subcutaneous route of administration does not directly target the lungs.

To overcome these limitations, spectinamide 1599 was tested at various dose levels and frequencies *via* the intrapulmonary route of administration (IPA) to healthy and infected (acute and chronic) mouse models. Conducted at the same dose level as given *via* the subcutaneous route, the intrapulmonary aerosol administration of spectinamide 1599 showed ~50-fold higher lung exposure and ~85-fold higher maximum concentrations with a relative bioavailability of 101%. The IPA administration demonstrated higher systemic deposition in lung, decent plasma exposure, negligible pulmonary metabolism, and rapid absorption into the alveolar space and peripheral region of lungs compared to SC administration [14]. Moreover, the IPA administration of spectinamide 1599 at a 200 mg/kg dose given 3 days a week for 4 weeks resulted in a

significant reduction in the lung bacterial burden, equivalent to that of RIF. With this route of administration, higher macrophage uptake of spectinamide 1599 was observed compared to spectinomycin, and a substantial fraction of dose was retained in the lung for a prolonged time despite rapid absorption. These experiments demonstrated that IPA administration could provide better efficacy through targeting the lungs directly, at a lower dose compared to the subcutaneous administration.

CHAPTER 2. HYPOTHESIS, OBJECTIVE, SPECIFIC AIMS[1]

Hypothesis

In 2018, the World Health Organization (WHO) reported that 10 million people developed tuberculosis, of which 1.5 million died. In the same year, WHO reported 484,000 new cases of multidrug-resistant (MDR) tuberculosis worldwide, of which 6.2% were estimated to have extensively drug-resistant (XDR) tuberculosis [15]. The treatment of tuberculosis is becoming extremely difficult due to increasing instances of resistance to the standard first-line as well as second-line therapy. Also, it has been reported that the *Mtb* can reside within lung macrophages and dendritic cells, and these intracellular bacilli are difficult to treat with the current drug regimens [16]. Therefore, there is an urgent need to find new anti-TB drugs as combination partners of existing and experimental classes of antimicrobial agents to shorten and simplify the treatment of MDR or XDR TB infection [13]. As of 2023, there are six new anti TB drug candidates in the pre-clinical development phase, including spectinamide 1810, six in Phase I, ten in Phase II, and three in Phase III clinical trials [17].

Spectinamides are a novel class of anti TB agents that is currently under preclinical development. The lead compounds, 1599 and 1810, are potential drug candidates, reported to have promising results in terms of efficacy against *Mycobacterium tuberculosis* (*Mtb*) when tested in mouse models of TB infection *via* various dosage levels, dosage regimens, and routes of administration, including subcutaneous injection and intratracheal aerosol delivery [13, 14, 18]. TB is primarily a pulmonary disease, but extrapulmonary manifestation has been reported in 10-42% of patients [19]. Therefore, it is imperative to understand the tissue distribution of novel anti TB drug candidates, particularly in the sub-compartments of pulmonary tissues such as epithelial lining fluid, alveolar macrophages, and TB lesions.

In the last decade, physiologically-based pharmacokinetic (PBPK) modeling and simulation has earned its rank in the model-informed drug development paradigm affecting various stages of drug development, from early compound selection to dose selection for first-in-human (FIH) trials to dosing recommendations in product labeling [8]. PBPK models are mechanistic, compartmental models that utilize the known anatomical and physiological knowledge base for humans and various preclinical species, in conjunction with the known physicochemical properties of a drug candidate to describe its *in vivo* pharmacokinetics in plasma and tissues [3]. Each compartment in a whole-body PBPK model represents an organ/tissue of known volume/weight and blood flow rate to provide a mechanistic understanding of drug disposition [4]. Thus, the PBPK approach can be used to predict the pharmacokinetics of drug candidates in organs/tissues

[1] Modified from to-be-submitted article with permission. Keyur Parmar, Pradeep B. Lukka, Santosh Wagh, Zaid Temrikar, Richard E. Lee, Miriam Braunstein, Anthony J. Hickey, Gregory T. Robertson, Mercedes Gonzalez-Juarrero, Andrea Edginton and Bernd Meibohm. Development of a Minimalistic Physiologically-Based Pharmacokinetic (mPBPK) Model for the Preclinical Development of Spectinamide Antibiotics.

of interest and to extrapolate their disposition behavior between different preclinical species and humans in support of drug development activities.

Objective

The objective of this study was to build, qualify, and refine a PBPK model with the help of drug-specific parameters, and observed plasma and tissue data in rodents (mouse and rat) after different routes of administration, including intravenous, subcutaneous, and intratracheal administration. This model is intended to describe and predict the pharmacokinetics of spectinamide compounds in various tissues, especially those relevant to *Mtb* infection and across various species, thereby supporting further drug development steps. We hypothesize that a common PBPK model can be developed for spectinamide 1599 and 1810 which can reliably and accurately predict the concentration-time profiles in tissues relevant for *Mtb* infection across various dose-levels. dosing frequencies, routes of administration, health conditions (infected and healthy), and different species.

Specific Aims

Specific Aim 1

To measure, collect, and integrate the drug-specific physicochemical, *in vitro* ADME, and *in vivo* pharmacokinetic parameters of spectinamide 1599 and 1810.

The drug specific parameters, such as molecular weight, lipophilicity, dissociation constants, fraction unbound to blood cells and plasma proteins, tissue to plasma partition coefficients, tissue permeability, metabolic stability, and blood to plasma ratio are crucial in defining the pharmacokinetic properties of a particular molecule [1]. The following drug specific and system specific parameters are used as building blocks in defining the PK properties of a test compound and are derived from *in vitro* and *in vivo* experiments or predicted from *in silico* tools [1].

- Tissue volumes
- Blood flow rates
- Molecular weight
- Lipophilicity (cLogP or $LogD_{octanol:water}$)
- Dissociation constant (pKa)
- Fraction unbound in plasma protein (*fu*)
- Tissue to plasma partition coefficient ($Kp_{T:pl}$)
- Tissue permeability (*Pe*)
- Blood to plasma partition ratio (k(b/p))
- Stability toward drug metabolizing enzymes (CL_{int}, V_{max}, K_m)
- In vivo PK parameters (V_{ss}, CL, $t_{1/2}$, etc.)

- Fraction of compound excreted unchanged in urine (*fe*)

Specific Aim 2

To build, qualify, verify, and refine a murine PBPK model for spectinamide 1599 and 1810 based on the parameters established in Aim 1 and observed tissue and plasma data.

The model structure will include the core tissues for which the experimental data are available, such as blood, lung. liver, spleen, and kidney, while all the remaining organs will be lumped together for the mass balance of the compound. The model will be built by integrating the known physiological and physicochemical parameters of the compounds, and the dynamic pharmacokinetic processes will be described in terms of linear ordinary differential equations. The predictions from the base model will be compared with the observed PK data (intravenous single dose or intravenous single ascending dose studies), and model parameters will be selected and adjusted based on sound physiological and scientific evidence to improve the predictive performance of the model. The predictive performance of the refined model will be confirmed by comparing the prediction with the additional plasma and tissue (lung, ELF, granulomas, liver, and spleen) PK data obtained from single ascending dose (SAD) and multiple ascending dose (MAD) studies at the dosage levels of 10-200 mg/kg *via* intravenous, subcutaneous, and intrapulmonary aerosol routes of administration. The model will be expanded to predict the pharmacokinetic profiles in infected animals to test the hypothesis that there are no significant differences in the PK profiles between healthy and infected animals.

Specific Aim 3

To perform the inter-species extrapolation of the model to predict the plasma and tissue concentration profiles in healthy rats.

The established murine PBPK model will be scaled to describe the tissue distribution of spectinamides in another species (rat) [20-23]. The scaling will be done using the physiological parameters of the scaled species, such as tissue flows and weights, and some drug-specific information, such as *in vitro*-derived metabolism, absorption, and protein binding. Specifically, the P BPK model will be scaled to rats by updating the model with the system- and drug-specific parameters pertaining to a healthy rat. The model predictions will be verified against the observations *via* visual inspection and twofold acceptance criteria of PK parameters.

Specific Aim 4

To perform the exploratory simulations to understand the relative distribution of spectinamide 1599 in granulomatous lesion substructures.

One of the recurrent questions and challenges in anti-TB drug development is to assess the exposure of new drug candidates not only in the interstitial sub-compartment of the lungs but also in the substructures of granulomatous lesions [24]. To predict the relative exposure of spectinamide compounds in different substructures of a granulomatous lesion, we will utilize the established multicompartmental human PBPK model of the lung and granuloma within the Simcyp simulator V21 R1 (Certara, Sheffield, UK). The known physicochemical parameters, as listed in Specific Aim 1**,** will be used to define Spectinamide 1599 within the Simcyp simulator. Simulations will be performed to translate our experimentally observed drug exposures in the lung interstitial sub-compartment into relative drug exposure in the rim-blood capillary, rim-interstitial fluid, macrophages, and necrotic caseum substructures.

CHAPTER 3. MODEL BUILDING BLOCKS: SYSTEM SPECIFIC AND DRUG SPECIFIC PARAMETERS[2]

Physicochemical Parameters of Spectinamide 1599 and 1810

The drug specific parameters such as lipophilicity, ionization constant, the extent of plasma protein binding, metabolic stability, and permeability are important in defining the PK properties of a compound. These parameters are either calculated from *in silico* tools or determined from *in vitro* experiments. These parameters can be used to mechanistically understand the absorption, distribution, metabolism, and elimination (ADME) of a compound. The mechanistic understanding of ADME ultimately assists in selecting an appropriate model structure. Here, we have obtained various drug- specific parameters which were used as building blocks for the PBPK model development.

Lipophilicity

The lipophilicity of a compound is its affinity towards the lipids present in the organ tissue, most commonly as phospholipid membranes. As a descriptor of lipophilicity, LogP or cLogP, LogMA (membrane affinity at physiological pH), and $LogD_{o:w}$ (partition coefficient of both ionized and unionized species in saturated *n*-octanol and phosphate buffer saine (PBS) at pH 7.4) could be used. In PBPK modeling, tissue to plasma partition coefficient ($Kp_{T:pl}$) can be predicted using the mechanistic tissue-composition-based equation (**Equation 3-1**) developed by Poulin and coworkers [25, 26]:

$$Kp_{T:pl} = \frac{\left[\left(f_{NL,T} + 0.3 \cdot f_{PL,T}\right) \cdot P + \left(f_{water,T} + 0.7 \cdot f_{PL,T}\right)\right] \cdot f_{u,pl}}{\left[\left(f_{NL,pl} + 0.3 \cdot f_{PL,pl}\right) \cdot P + \left(f_{water,pl} + 0.7 \cdot f_{PL,pl}\right)\right] \cdot f_{u,T}} \qquad \textbf{Eq. 3-1}$$

Where P is the antilog value of $LogP_{octanol:water}$ for non-adipose tissues, f is the fractional tissue volume content of neutral lipid (NL), phospholipid (PL), or water in tissue (T), plasma (pl), $f_{u,pl}$ is the fraction of compound unbound in plasma, and $f_{u,T}$ is the fraction of compound unbound in tissue.

cLogP. The calculated LogP values for spectinamide 1599 and 1810 obtained from the ChemDraw (PerkinElmer, Waltham, MA) software package are -2.52 and -3.03, respectively.

$LogD_{octanol:water}$. We performed a miniaturized shake-flask assay to determine the LogD values of spectinamide 1599 and 1810. The methodology we used to

[2] Modified from to-be-submitted article with permission. Keyur Parmar, Pradeep B. Lukka, Santosh Wagh, Zaid Temrikar, Richard E. Lee, Miriam Braunstein, Anthony J. Hickey, Gregory T. Robertson, Mercedes Gonzalez-Juarrero, Andrea Edginton and Bernd Meibohm. Development of a Minimalistic Physiologically-Based Pharmacokinetic (mPBPK) Model for the Preclinical Development of Spectinamide Antibiotics.

experimentally measure the LogD values, such as the procedure obtained from the literature [28] and the required chemicals and reagents are listed below:

Chemical and Reagents. Spectinamide 1810 (2-(5-hydroxypyridin-2-yl)-N-((2R,4R,4aS,5aR,6S,7S,8R,9S,9aR,10aS) -4a,7,9-trihydroxy-2-methyl-6,8-bis(methylamino)decahydro-2H-benzo[b]pyrano[2,3-e][1,4]dioxin-4-yl)acetamide), Spectinamide 1599 (2-(5-chloroypyridin-2-yl)-N-((2R,4R,4aS,5aR,6S,7S,8R,9S,9aR,10aS) -4a,7,9-trihydroxy-2-methyl-6,8-bis(methylamino)decahydro-2H-benzo[b]pyrano[2,3-e][1,4]dioxin-4-yl)acetamide) were synthesized in Dr. Richard E. Lee's laboratory at St. Jude Children's Research Hospital, Memphis, TN, as previously described [11]. Methanol and *n*-octanol were purchased from Fisher Scientific (Pittsburg, PA). Phosphate buffer saline (1x PBS) was purchased from Thermo Fisher Scientific (Waltham, MA).

Procedure. Log D values of spectinamide compounds were estimated using a miniaturized shake-flask method using saturated *n*-octanol and phosphate buffer saline (PBS) at pH 7.4, as described in literature [27]. Equal proportions of *n*-octanol and PBS were mixed in a 50 mL conical tube and kept for saturation on a shaker mixer for overnight; both the phases were then separated and used for the assay. The 10 mg/mL stock solution of spectinamide 1599 and 1810 was prepared in MilliQ water. The 10 mg/mL stock solution of caffeine, which was used as a positive control, was prepared in DMSO. In a 2 mL Eppendorf tube, 500 µL of saturated *n*-octanol and 500µL of PBS was pipetted; 5µL of the stock solution was spiked, and the tubes were capped and sealed with parafilm tape. The tubes were then vortexed at 1,300 RPM at 37 °C for 3 hr. After 3 hr of shaking, the tubes were kept undisturbed for the separation phase. The octanol fraction and PBS fraction were collected in 1.5 mL HPLC tubes and were subjected to HPLC-PDA analysis. **Equation 3-2** was used to calculate the LogD values for spectinamide 1599 and 1810:

$$LogD = Log\ \frac{[Peak\ area]_{octanol}}{[Peak\ area]_{PBS}} \qquad \textbf{Eq. 3-2}$$

Results. We were unable to experimentally determine the LogD values of spectinamide 1599 and 1810 due to their high hydrophilicity and concentrations in the octanol fraction being below the limit of detection.

Acid Dissociation Constant (pKa)

Acid dissociation constants, or pKa, refer to the acidic form of a compound; a lower pKa value indicates a stronger acid. In PBPK modeling, pKa can be used to calculate $LogD_{vo:w}$ (partition coefficient of both ionized and unionized species at pH 7.4), as shown in **Equation 3-3** (for monoprotic bases). Also, pKa can be used to calculate unbound tissue to plasma partition coefficient ($Kp_{T:pl,u}$) based on the electrostatic interaction of ionized species with acidic membrane phospholipids [28], as shown in **Equation 3-4** (for strong bases having pKa > 7.0):

$$Log\ D_{vo:w} = Log\ P_{vo:w} - Log(1 + 10^{pKa-pH}) \quad \textbf{Eq. 3-3}$$

$$Kp_{T:pl,u} = f_{EW} + \left(\frac{1 + 10^{pKa-pH_{IW}}}{1 + 10^{pKa-pH_{pl}}} \cdot f_{IW}\right) + \left(\frac{K_{a,AP^-} \cdot [AP^-]_T \cdot 10^{pKa-pH_{IW}}}{1 + 10^{pKa-pH_{pl}}}\right) + \left(\frac{P \cdot f_{NL} + (0.3 \cdot P + 0.7) \cdot f_{NP}}{1 + 10^{pKa-pH_{pl}}}\right) \quad \textbf{Eq. 3-4}$$

Where f is the fractional tissue volume of neutral lipids (NL), neutral phospholipids (NP), extracellular water (EW), and intracellular water (IW); $[AP^-]_T$ is the concentration of acidic phospholipids in tissue; and $K_{a,AP-}$ is the association constant of the compound with the acidic phospholipids. These physiological values have been described in the literature [25, 26, 28]. pKa is the dissociation constant of the protonated base; P is the antilog value of $LogP_{vo:w}$ calculated from $P_{oc:w}$ using **Equation 3-5**:

$$Log\ P_{vo:w} = 1.115 \times Log\ P_{oc:w} - 1.35 \quad \textbf{Eq. 3-5}$$

The pKa values for spectinamide 1599 and 1810 were obtained from the Schrödinger Maestro software (Schrödinger, Inc., New York, NY) and are shown in **Figure 3-1**. The pKa values of the secondary amines for both compounds are the same, 8.69 and 6.95, respectively. However, the pKa values of the pyridine nitrogen are different: 3.42 for spectinamide 1599 and 4.92 for spectinamide 1810 due to different functional groups on the pyridine ring. At pH 8.69, both the compounds, which are weak bases, will have 50% of the fraction ionized and 50% of the fraction unionized. Thus, these compounds are expected to be largely in ionized form at the physiological pH of 7.4.

Permeability

Permeability can be determined using *in vitro* assays, such as Parallel Artificial Membrane Permeability Assay (PAMPA), Caco-2-cell permeability assay, or MDCK-cell permeability assay. For compounds with low permeability values, the assessment by experimentation is likely challenging and the associated uncertainty is high. In such case, the predicted or calculated permeability values could be used instead of experimentally determined values. The cellular permeability can be calculated from the physicochemical properties of a compound using the PK-Sim standard, which is one of the methods within the PK-Sim® software platform (Bayer Technology Services GmbH, Leverkusen,

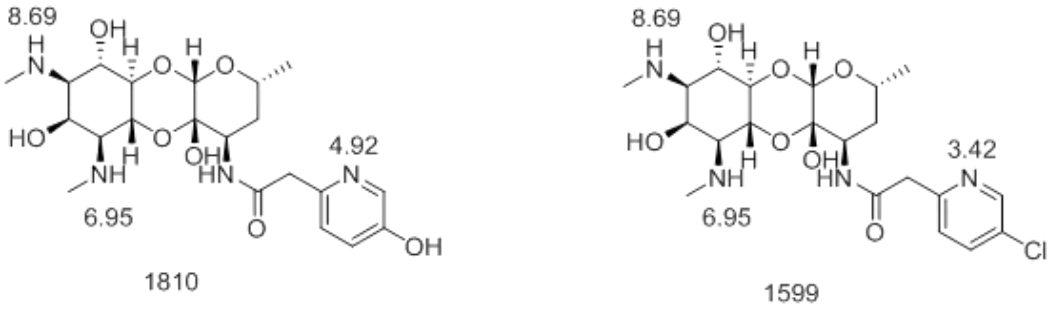

Figure 3-1. Chemical structure and pKa values of spectinamide 1599 and 1810.

Germany), as shown in **Equation 3-6**:

$$Cellular\ permeability = \left(\frac{MW_{eff} \times 10^8}{336}\right)^{-6} \times \frac{10^{LogMA}}{5} \times 10^{-5} \times 10^{-2} \quad \textbf{Eq. 3-6}$$

Where MW_{eff} is the effective molecular weight and LogMA is the membrane affinity at the physiological pH.

We performed the Parallel Artificial Membrane Permeability Assay (PAMPA) to determine the *in vitro* passive permeability of spectinamide 1599 and 1810 according to the protocol published in the literature [29, 30]:

Chemical and Reagents. Dodecane, methanol, and acetonitrile were purchased from Fisher Scientific (Pittsburg, PA). Caffeine and L-phosphatidylcholine were purchased from Sigma-Aldrich (St. Louis, MO). The 0.4 µm PCTE membrane MultiScreen filter plate was purchased from Millipore Corporation (Billerica, MA). Phosphate buffer saline (1x PBS) was purchased from Thermo Fisher Scientific (Waltham, MA).

Procedure. In this assay, membrane was treated with 2% solution of phosphatidylcholine in dodecane and dried at room temperature for 10 min. The 10 mg/mL stock solution of spectinamide compounds was prepared in MilliQ water, and reference standards were prepared in DMSO, which were then further diluted to 100 and 50 µg/mL as working solutions. The dosing solutions were prepared by spiking the working solutions in the mixture of DMSO and PBS (5% DMSO), pH 7.4, to yield the final assay concentrations of 1 and 0.5 µg/mL. An aliquot of 150 µL of the dosing solutions was added to the coated donor plate in triplicate. The 300 µL of blank PBS containing 5% DMSO was added to each well of the acceptor plate. The donor plate was then placed on the acceptor plate cautiously to avoid any damage to the membrane while making sure the underside of the membrane was in contact with the buffer in the acceptor wells. The plate assembly was then kept undisturbed at 37 °C for 5 hr. Meanwhile, the equilibrium mixture was prepared by mixing 150 µL of the dosing solution and 300 µL of the blank PBS containing 5% DMSO to obtain a theoretical equilibrium mixture. After the incubation, 50 µL from the acceptor region was added to a deep-well plate and mixed with 150 µL of methanol containing 10 ng/mL internal standard (spectinamide 1369). Similarly, 50 µL of the equilibrium mixture was mixed with 150 µL of methanol containing 10 ng/mL internal standard, followed by brief mixing and centrifugation. The samples were then subjected to LC-MS/MS analysis. The Faller equation (**Equation 3-7)** was used to determine permeability rates (Pe):

$$Log\ Pe = \log\left\{C \cdot -ln\left(1 - \frac{[drug]_{Acceptor}}{[drug]_{Equilibrium}}\right)\right\}, \quad \textbf{Eq. 3-7}$$

$$Where\ C = \frac{V_D \cdot V_E}{(V_D + V_E) \cdot Area \cdot Time}$$

Where V_D is Volume of donor compartment expressed in cm^3, 150 µL is 0.15 cm^3; V_A is Volume of acceptor compartment expressed in cm^3, 300 µL = 0.3 cm^3; and Area is Active surface area of membrane defined as membrane area x porosity. For the membrane in MultiScreen Permeability Filter Plate, area is 0.24 cm^2 x 100% or 0.24 cm^2; Time is Incubation time for the assay expressed in seconds; 1 hr = 3600 sec; $[drug]_{Acceptor}$ is Concentration/area ratio of compound in the acceptor compartment; and $[drug]_{equilibrium}$ is Concentration/area ratio of compound at theoretical equilibrium.

Results. We were unable to experimentally determine the effective passive permeability or Log Pe values of spectinamide 1599 and 1810 due to their high hydrophilicity and concentrations in the acceptor compartment being below the limit of detection. Both spectinamides 1599 and 1810 have very low passive permeability and cannot be integrated in the PBPK model. As an alternative, we have estimated the tissue-specific influx and backflux rate constants by fitting the model to the observed plasma and tissue concentration-time profiles to address the permeability-limited distribution of the compounds across the subcompartments of a tissue.

Blood to Plasma Partition Coefficient

Blood to plasma ratio is the distribution of a compound between red blood cells and plasma, which was estimated experimentally for spectinamide 1599 and 1810. In PBPK modeling, blood-to-plasma ratio is used to convert plasma concentration to arterial blood concentration or *vice versa*, as shown in **Equation 3-8** [31]:

$$C_a = R_B \cdot C_p \qquad \textbf{Eq. 3-8}$$

Where R_B is the blood-to-plasma ratio, C_a is the arterial blood concentration, and C_p is the plasma concentration.

We performed an assay to measure the blood-to-plasma ratio of spectinamide 1599 and 1810 in mouse, rat, and human blood by following the protocol published in the literature [32, 33]:

Chemical and Reagents. Lithium heparin tubes were purchased from BD Vacutainer™ (Franklin Lakes, NJ). Spectinomycin was purchased from Fisher Scientific (Pittsburg, PA). Heparinized human blood was purchased from Tennessee blood bank (Memphis, TN). Methanol and acetonitrile were purchased from Fisher Scientific (Pittsburg, PA).

Procedure. Fresh blood was collected from BALB/c mice and Sprague-Dawley rats via cardiac puncture in tubes with lithium heparin as anticoagulant. Hematocrit was measured using a VetScan HM5 hematology analyzer (Abaxis, Union City, CA). Heparinized human blood was purchased from the Tennessee Blood Bank (Memphis, TN). For each species, control plasma was obtained from aliquots of the available blood

by centrifugation at ~3,750 ×g for 10 min at 4 °C. Aliquots of pre-warmed whole blood and plasma were spiked with the test compounds and incubated at 37°C. After 1 hour of incubation, the incubated whole blood was removed, and the plasma was separated by centrifugation. Aliquots of the incubated control plasma were also removed after 1 hour of incubation. Plasma samples were treated with 8 volumes of ice-cold methanol containing internal standard (100 ng/mL spectinomycin) and analyzed for drug concentrations by LC-MS/MS [32].

The whole blood-to-plasma ratio k(b/p) was calculated by taking the ratio of the concentrations measured in the control plasma over the concentrations measured in the plasma centrifuged from the incubated whole blood, as shown in **Equation 3-9**. The erythrocyte to plasma partitioning coefficient k(RBC/p) was calculated from the whole blood to plasma ratio by accounting for the measured hematocrit, as shown in **Equation 3-10:**

$$k(b/p) = \frac{C_{CP}}{C_P} \qquad \textbf{Eq. 3-9}$$

$$k(RBC/p) = 1 + \left(\frac{1}{H}\right)\left[\left(\frac{C_{CP}}{C_P}\right) - 1\right] \qquad \textbf{Eq. 3-10}$$

Where C_{CP} is the concentration of the test compound in the control plasma, C_P is the concentration of the test compound in the plasma centrifuged from the incubated whole blood, and H is the measured hematocrit value.

Results. The blood-to-plasma partition ratio for both compounds was measured in mouse, rat, and human blood:

- 1599 partition ratio: 0.552 in mouse, 0.812 in rat, and 0.693 in human
- 1810 partition ratio: 0.604 in mouse, 0.785 in rat, and 0.680 in human

The partition ratio ranges from 0.552 to 0.812 (< 1) suggest that the distribution of spectinamide compounds is higher in plasma compared to blood cells.

Fraction Unbound to Plasma Protein (*fu*)

The extent of binding of the compounds to the plasma proteins determines the distribution in tissue. The fraction unbound of spectinamide 1599 and 1810 unbound in human, rat, and mouse plasma was measured using equilibrium dialysis following a previously described assay protocol [34]. In PBPK modeling, the fraction unbound in tissue (fu_T) can be calculated from fu_{pl} using the albumin concentration ratio between the plasma and tissue [26], as shown in **Equation 3-11**, assuming that albumin is the major binding protein:

$$fu_T = \frac{1}{1 + \left[\frac{(1 - fu_{pl})}{fu_{pl}} RA\right]}$$ **Eq. 3-11**

We performed the plasma protein binding assay of spectinamide 1599 and 1810 using the rapid equilibrium dialysis method.

Chemical and Reagents. Rapid Equilibrium Device (RED) was purchased from Thermo Scientific (Rockford, IL). Methanol and acetonitrile were purchased from Fisher Scientific (Pittsburg, PA). Ranitidine and warfarin were purchased from Sigma-Aldrich (St. Louis, MO). Phosphate buffer saline (1x PBS) was purchased from Thermo Fisher Scientific (Waltham, MA).

Procedure. Plasma protein binding was determined by equilibrium dialysis using a RED device (8 kDa molecular cutoff) containing plasma and buffer chambers for dialysis and a base plate. Two concentrations (0.5 and 5 mg/L) of 1599 and 1810 were prepared in mouse plasma from BALB/c mice and rat plasma from Sprague-Dawley rats, and an aliquot of 300 µL was added in the plasma chamber in duplicate. A 500 µL aliquot of PBS was added in the buffer chamber for dialysis. Then the base plate was covered with sealing tape and incubated at 37°C at approximately 100 RPM on an orbital shaker for 4 hr to achieve equilibrium. After incubation, 50 µL of each sample was pipetted from the plasma and buffer chambers into separate micro-centrifuge tubes. 50 µL of plasma were added to the buffer samples and an equal volume of PBS to the collected plasma samples and vortexed. Samples were processed by protein precipitation and analyzed for bound and unbound drug concentrations by LC-MS/MS. Ranitidine (0.5 and 5 mg/L) was included as a positive control. The fraction of compound unbound to plasma proteins (*fu*) was calculated from the measured concentrations in the plasma and buffer chambers using **Equation 3-12**:

$$fu = 1 - \left(\frac{C(Plasma\ Chamber) - C(Buffer\ Chamber)}{C(Plasma\ Chamber)}\right)$$ **Eq. 3-12**

Results. The unbound fraction of spectinamide 1599 and 1810 ranges from 0.436 to 0.693 between all three species, suggesting that these compounds have low plasma protein binding:

- 1599 unbound fraction: 0.602 in mouse, 0.563 in rat, and 0.436 in human
- 1810 unbound fraction: 0.693 in mouse, 0.607 in rat, and 0.649 in human

Microsomal Stability

The microsomal stability assay is performed as a primary screening assay to investigate the *in vitro* metabolism (usually Phase I) of compounds by liver enzymes in the presence of co-factor NADPH. The microsomal stability can be used to predict the *in vivo* metabolic stability using *in vitro-in vivo* extrapolation (IVIVE) [35]. We have

performed an *in vitro* assay to determine the stability of spectinamide 1599 and 1810 in rat and human liver microsomes by following the protocol from literature [36].

Chemical and Reagents. Pooled human liver and Sprague-Dawley rat liver microsomes were purchased from Corning Life Sciences (Oneonta, NY, USA). Dibasic and monobasic potassium phosphate, methanol, and acetonitrile were purchased from Fisher Scientific (Pittsburg, PA). PlasmaLyte A was purchased from Baxter international (Deerfield, IL).

Procedure. Microsomes (20 mg/mL) were thawed on ice and diluted using phosphate buffer (100 mM, pH: 7.4), resulting in protein concentration of 1 mg/mL. Stock solutions (10 mg/L) of spectinamide 1599 and 1810 were prepared in water (50%) and PlasmaLyte A (50%). A final concentration of 0.5 mg/L was incubated with the liver microsomes. NADPH (final concentration: 1 mM) was used as a co-factor. All the above solutions except NADPH were added to individual wells (12-well) in triplicate and were allowed to equilibrate for 5 min at 37 °C. A 50 µL aliquot of NAPDH was added.to initiate the reaction. The samples from the incubation mixture were withdrawn at predefined time points (0, 5, 10, 20, 30, 45, 60 and 90 min). The reaction was quenched by adding ice-cold methanol (4 volumes) to the sample aliquots. The samples were then briefly mixed and centrifuged at 4000 RPM. The supernatants were collected and were subject to LC-MS/MS analysis. Verapamil was used as a positive control. The *in vitro* half-life ($t_{1/2}$) and intrinsic clearance (CL_{int}) were calculated using **Equations 3-13** through **3-16**:

$$ELimination\ rate\ constant\ (k) = Absolute\ value\ of\ the\ slope\ (min^{-1}) \quad \textbf{Eq. 3-13}$$

$$Half\ life\ (t_{1/2})(min) = \frac{0.693}{k} \quad \textbf{Eq. 3-14}$$

$$V\ (\mu L/mg) = \frac{Volume\ of\ incubation\ (\mu L)}{Protein\ in\ the\ incubation\ (mg)} = \frac{400\ \mu L}{0.4\ mg} = 1000 \quad \textbf{Eq. 3-15}$$

$$Intrinsic\ Clearance\ (CL_{int})(\mu L/min/mg\ protein) = \frac{V \times 0.693}{t_{1/2}} \quad \textbf{Eq. 3-16}$$

Results. Both spectinamide compounds demonstrated an excellent microsomal stability in rat and human liver microsomes, with half-lives exceeding 300 min.

Lysosomal Trapping

Lysosomes are membrane-bound acidic organelles with the luminal pH ranging from 4.5 to 5 that play a key role in the breakdown of biomolecules, cell signaling, energy metabolism, waste disposal, autophagy, and apoptosis. One of the key roles is to regulate the turnover of phospholipids; impairment can lead to phospholipidosis, which is a lysosomal storage disorder characterized by the excess accumulation of phospholipids in tissues. Phospholipidosis can be induced by trapping or sequestration of drugs in the lysosome, which is governed by the physicochemical properties of drugs. The objective of this study was to investigate if the spectinamide compounds are accumulated in the lysosomes, which might be the reason for the observed slow redistribution phase in the pharmacokinetic profiles of spectinamides.

Lipophilic and amphiphilic drugs—also known as cationic amphiphilic drugs (CAD)—are common targets of lysosomal sequestration. Many lipophilic amines (LogP > 1) with ionizable amine group (pKa > 6) have an appreciable unionized fraction at physiological pH (7.2-7.4), which can diffuse across the cell membranes by passive diffusion [37]. These drugs become protonated when diffused into lysosomes because of the acidic environment, and the protonated species have a restricted diffusion back into the cytosolic space. This pH partitioning of the drugs into acidic environments is the main mechanism of lysosomotropism. Cellular uptake by active transporters such as organic cation transporters (OCTs) may also play a role for certain lipophilic amines at plasma concentration at or below K_m value [38]; for higher concentrations, passive diffusion is predominant. For acidic drugs, hepatic OATP1B1/1B3 or renal OATP1/3 may be involved in active uptake [39]. The pH partitioning mechanism is shown in **Figure 3-2**.

Competition for lysosomal trapping has been the subject of some speculation as a potential mechanism of drug-drug interactions (DDIs) [38, 40-43]. There is a possibility that concomitant administration of lysosomotropics could lead to elevated drug exposure levels as competition for lysosomal sequestration increases or lysosomal pH is elevated by amine accumulation [43, 44]. These drugs can inhibit the accumulation of the marker compound LysoTracker Red by the following mechanisms:

1. Competition with LysoTracker Red for lysosomal accumulation
2. Elevation of lysosomal pH by drugs via permeabilizing the lysosomal membrane to protons
3. Inhibition of lysosomal V-ATPase (maintains the acidic environment in the lysosome) by drugs
4. Drug-induced cellular toxicity

The Fa2N-4 cells are SV40 virus large T antigen-transformed human hepatocytes that do not express the constitutive androstane receptor and do not retain significant transporter activity [45]. Liver is a lysosome-rich organ and thus hepatocytes serve as a suitable system to evaluate the potential for lysosome-based accumulation and drug-drug

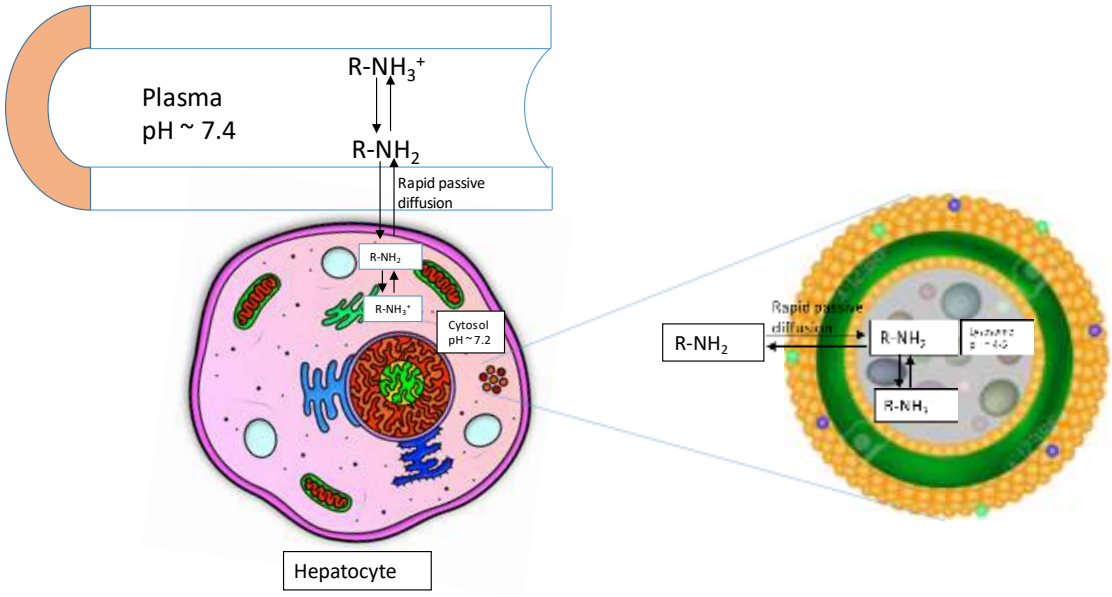

Figure 3-2. Schematic diagram of pH partitioning of a lipophilic amine in the lysosomes.

interaction. Red DND-99, or LysoTracker Red, is a lysosome-specific fluorescent lipophilic amine probe with LogP of 2.10 and pKa of 7.5 [46] used for *in vitro* evaluation of lysosomotropism of compounds of interest. We measured the concentration-dependent inhibition of LysoTracker Red fluorescence in Fa2N-4 cells by the test compounds.

Chemical and Reagents. Propranolol and ibuprofen were purchased from Sigma-Aldrich (St. Louis, MO); LysoTracker Red was purchased from Invitrogen (Eugene, OR); Fa2N-4 Line - 96 well - Collagen Coated Plate, multifunction enhancing (MFE) plating media (components A and B) from MFE support media. Modified Chee's medium was purchased from Sekisui XenoTech, LLC (Kansas City, KS); 1 × phosphate buffer saline (PBS) was purchased from Thermo Fisher Scientific (Waltham, MA).

Procedure. Fa2N-4 cells (50,000 cells/well) plated in a collagen-coated 96-well microtiter plate were purchased from Sekisui XenoTech. The plate was received, and the media was aspirated immediately under a class II biosafety cabinet (BSC) and replaced with 75 µL of pre-warmed (37 °C) MFE support media. The plate was acclimatized by incubating in a cell incubator at 37 °C with 95% humidity and 5% CO_2 for 3 days. Before performing the assay, the MFE support media was removed, and the wells were rinsed with 100 µL of pre-warmed (37 °C) 1× PBS. 100 mM stock solution of propranolol and ibuprofen was prepared in methanol, spectinamide 1599 and 1810 was prepared in sterile water for injection and diluted with modified Chee's medium such that the final incubation concentrations of each compound were 5, 10, 50, 100, 500, and 1000 µM. LysoTracker Red was added to each test drug solution to give a final incubation concentration of 50 nM. Incubation with the cells was performed at a final volume of 100 µL in triplicate for 30 min at 37 °C with 95% humidity and 5% CO_2. After the incubation, the matrix was aspirated, and the wells were rinsed twice with 200 µL of 1× PBS (at room temperature). After the rinsing step, the cells were solubilized by adding 100 µL of acetonitrile, followed by shaking at 900 RPM. Samples were then analyzed for LysoTracker Red fluorescence (λex 530 nm, λem 590 nm) with a BioTek Cytation™ 5 plate reader (BioTek, Winooski, VT).

Results. The spectinamide compounds 1599 and 1810, along with a positive (propranolol) and negative (ibuprofen) control, were tested for their ability to inhibit LysoTracker Red fluorescence in a concentration-dependent manner. The positive control propranolol, which is a known lysosomotropic, blocked LysoTracker Red partitioning and the IC_{50} value obtained was 113.2 µM (literature value: 92 µM), whereas, the negative control ibuprofen did not give a measurable LysoTracker Red IC50 value within the concentration range tested. The results suggest that the spectinamide compounds do not accumulate in the lysosomes, as shown in **Table 3-1** and **Figure 3-3**. However, the Fa2N-4 cell line is devoid of any transporter, and the passive diffusion is the key mechanism for the diffusion of a compound, which could be the reason for the lack of accumulation of spectinamide compounds in the lysosomes.

Table 3-1. Predicted/computed physicochemical properties and experimentally determined LysoTracker Red IC_{50} values.

Molecular Species	Drug	Drug Class	LogP	Acidic or Anionic pKa	Basic or Cationic pKa	LysoTracker Red IC_{50} µM	Literature Value [37]
Base	Propranolol	Beta blocker	2.58	-	9.67	113.2	92
Acid	Ibuprofen	NSAID	3.84	4.85	-	>1000	>500
Base	1599	Antituberculosis	-2.52	-	8.69	>1000	-
Base	1810	Antituberculosis	-2.50	-	8.69	>1000	-

*LogP = the octanol-water partition coefficient, pKa = the acid dissociation constant, and IC_{50} = the half-maximal inhibitory concentration.

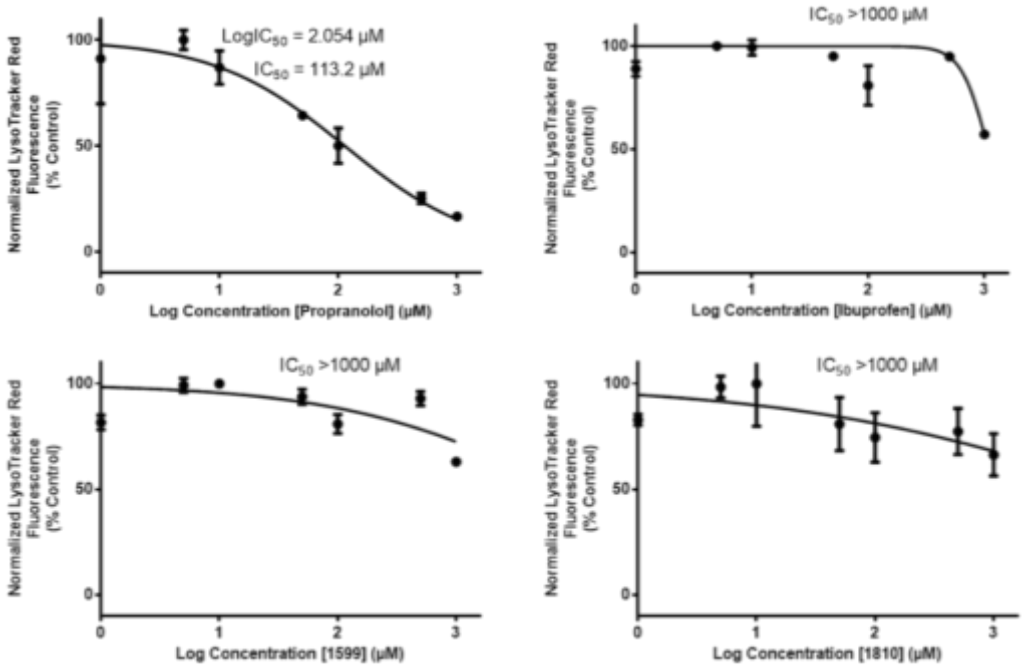

Figure 3-3. Displacement of LysoTracker Red fluorescence in Fa2N-4 cells by propranolol, ibuprofen, spectinamide 1599, and spectinamide 1810 interpreted in terms of IC_{50}.

System Specific or Physiological Parameters of Mouse, Rat, and Human

The physiological parameters in a PBPK model represent the anatomical structure and the physiological processes of the animal species researched [1]. Since these parameters are independent of the test compound, they are also known as drug-independent parameters. We borrowed the physiological parameters, such as organ volumes, organ blood flow rate, glomerular filtration rate, and subcompartmental organ volumes, from the literature [47-49], as listed in **Tables 3-2** and **3-3**.

To build a minimalistic PBPK model, we selected only the core tissues for which the experimental data were available, such as lung, liver, spleen, kidney, and blood, while all the remaining organs were lumped for the mass balance of the compound. Each tissue was divided into three subcompartments: vascular, interstitial, and cellular, and the volumes for each subcompartment were obtained from literature [49]. To model the intrapulmonary aerosol administration, the epithelial lining fluid (ELF) compartment was added to the lung compartment. The volume of ELF in human was obtained from the literature and was scaled to mouse and rat using allometric scaling based on body weight [2, 48].

Table 3-2. Physiological parameters of mouse, rat, and human utilized as building blocks of the minimal PBPK model.

Parameters	Units	Values		
		Mouse (0.02 kg)	**Rat (0.225 kg)**	**Human (71 kg)**
Q_{Lung}	L/h	0.618	4.83	340
Q_{Spleen}	L/h	0.00695	0.0412	4.67
Q_{Liver}	L/h	0.139	0.901	87.9
Q_{Kidney}	L/h	0.100	0.601	75.2
Q_{Other}	L/h	0.371	3.29	172
GFR	L/h	0.0168	0.088	7.58
$V_{Venous\ blood}$	L	0.00120	0.0115	3.98
$V_{Arterial\ blood}$	L	0.000515	0.00494	1.71
V_{Lung}	L	0.000194	0.00140	1.00
V_{ELF}	L	0.0000100	0.000100	0.0250
V_{Spleen}	L	0.000127	0.00277	0.221
V_{Liver}	L	0.00193	0.0157	2.14
V_{Kidney}	L	0.000525	0.00241	0.332
V_{Other}	L	0.0235	0.245	65.1
Q_{Lung}	L	0.618	4.83	340

Q = the tissue-specific blood flow rates, GFR = the glomerular filtration rate, V = the volume of the tissue, and ELF = the epithelial lining fluid.

Table 3-3. The fraction of tissue volume designated to the vascular, interstitial, and cellular subcompartments.

Tissue	Fraction Vascular	Fraction Interstitial	Fraction Cellular
Lung	0.26	0.19	0.55
Spleen	0.22	0.20	0.58
Liver	0.15	0.20	0.64
Kidney	0.10	0.15	0.75
Other	0.040	0.19	0.77

CHAPTER 4. ANIMAL EXPERIMENTATION AND BIOANALYSIS[3]

Introduction

The plasma and tissues pharmacokinetic data after single- and multiple-doses of spectinamide compounds 1599 and 1810 ranging from 10 to 200 mg/kg total daily dose in healthy mice after intravenous (IV), subcutaneous (SC), and intrapulmonary aerosol (IPA) administration were generated at the University of Tennessee Health Science Center. An extensive set of dose-ranging and dose-fractionation studies for spectinamide 1599 and 1810 in the *Mtb* infected mice were also performed at Colorado State University, and the plasma PK data were used to check the predictive performance of our PBPK model. The plasma and tissue PK data after a single 10 mg/kg dose of spectinamide 1599 administered *via* intravenous route to healthy rats were also generated at the University of Tennessee Health Science Center. A comprehensive list of data sets used for the PBPK model development are summarized **Appendix A.**

Chemical and Reagents

Spectinamide 1599 (2-(5-chloroypyridin-2-yl)-N-((2R,4R,4aS,5aR,6S,7S,8R,9S,9aR, 10aS) - 4a,7,9-trihydroxy-2-methyl-6,8-bis(methyl-amino)decahydro-2H-benzo[b]pyrano [2,3-e] [1,4]dioxin-4-yl)acetamide) and spectinamide 1810 (2-(5-hydroxypyridin-2-yl)-N-((2R,4R,4aS,5aR,6S,7S,8R,9S,9aR,10aS)-4a,7,9-trihydroxy-2-methyl-6,8-bis(methylamino) decahydro-2H-benzo[b]pyrano[2,3-e][1,4] diox-in-4-yl)acetamide) were synthesized in Dr. Richard E. Lee's laboratory at St. Jude Children's Research Hospital, Memphis, TN, as previously described [11]. Spectinomycin purchased from Sigma-Aldrich (St. Louis, MO) was used as an internal standard. Acetonitrile, methanol, HPLC grade water, formic acid and nonafluoropentanoic acid were purchased from Fisher Scientific (Pittsburgh, PA). Phosphate buffer saline (1x PBS) was purchased from Thermo Fisher Scientific (Waltham, MA).

Pharmacokinetic Studies on Healthy Animals

Single and multiple-dose (10 mg/kg) studies for the PK of spectinamide 1810 after intravenous administration in healthy mice, single-dose (50 mg/kg) study of spectinamide 1810 after subcutaneous administration in healthy mice, and single-dose (10 mg/kg) study of spectinamide 1599 after intravenous administration in healthy rats were performed at the University of Tennessee Health Science Center following approval by the Institutional Animal Care and Use Committee (IACUC).

---

[3] Modified from to-be-submitted article with permission. Keyur Parmar, Pradeep B. Lukka, Santosh Wagh, Zaid Temrikar, Richard E. Lee, Miriam Braunstein, Anthony J. Hickey, Gregory T. Robertson, Mercedes Gonzalez-Juarrero, Andrea Edginton and Bernd Meibohm. Development of a Minimalistic Physiologically-Based Pharmacokinetic (mPBPK) Model for the Preclinical Development of Spectinamide Antibiotics.

Mice

Female Balb/c mice, 8 weeks, weighing 18-22 g were purchased from Charles River Laboratories (CA, USA) and acclimatized for 72 hr with a 12 h light/dark cycle with access to food and water as libitum.

Dosing Procedure. Spectinamide compounds were formulated in PlasmaLyte A and water (9:1), and the dosing solutions were filtered through a 0.22 µm filter (MILLEX-GP, Millipore PES membrane, cat#SLGP033RB). The concentration in the dosing solution was prepared based on the average mouse body weight and a fixed volume of 50 µL was administered to each mouse.

Sampling Procedure. Groups of three mice were sacrificed at predefined time points post-dose, and blood samples were obtained by cardiac puncture under isoflurane anesthesia followed by euthanasia. Subsequently, organs of interest (lungs, liver, kidneys, spleen) were collected for single-dose studies. Samples were collected at 0.083, 0.25, 0.5, 1, 3, 8, 16, and 24 hr, and for multiple-dose studies at pre-dose (before the last dose administration), 0.083, 0.25, 0.5, 1, 3, 8, and 24 hr after the administration of the last dose. Plasma was immediately separated by centrifugation (~3,750 ×g for 10 min at 4 °C) and stored at -70 °C until LC-MS/MS analysis. For tissue samples, the tissues were weighed and homogenized in 4 volumes of phosphate buffered saline (1× PBS) and stored at -80 °C until LC-MS/MS analysis.

Rats

Double catheterized (jugular and femoral vein) male and female Sprague-Dawley rats (Envigo Laboratories, Indianapolis, IN) weighing 200-250 g were kept at a 12 hr light/dark cycle with access to food and water ad libitum.

Dosing Procedure. Single dose intravenous pharmacokinetic studies of spectinamide 1810 with serial blood sampling were performed to obtain the plasma concentration-time profiles in rats. Spectinamide 1810 (10 mg/mL) was formulated in PlasmaLyte (Baxter International, Deerfield, IL) and water (9:1) and injected *via* the femoral vein catheter as a rapid injection.

Sampling Procedure. For the serial blood sampling studies, 6 male rats (3 separate studies) for spectinamide 1810 were dosed at 10 mg/mL (same formulation and administration as described above) and blood samples (250 µL) were collected *via* the jugular vein catheter at 0.08, 0.25, 0.5, 0.75, 1, 1.5, 2, 4, 6, 8, 10, 24, and 48 hr post-dose. The plasma was separated from blood by centrifugation (~3,750 ×g for 10 min at 4 °C) and stored at -70 °C until LC-MS/MS analysis. Urine samples were collected at predetermined time intervals (0-6, 6-10, 10-24, 24-48 hr) up to 48 hr after dosing; volumes were recorded, and samples were processed by protein precipitation and analyzed by LC-MS/MS. The fraction of drug excreted unchanged (*fe*) in urine at each time interval and a cumulative *fe* were calculated.

Tissue PK Study. An additional single dose intravenous study of spectinamide 1599 with destructive sampling was performed to obtain the tissue pharmacokinetic profiles in rats. In this study, groups of 4 rats (2 male and 2 female) were euthanized either at 15 min or at 4 hr after dosing, and blood, lungs, liver, spleen, and kidneys were collected. For tissue samples, the tissues were weighed and homogenized in 4 volumes of phosphate buffered saline (1x PBS) and stored at -70 °C until LC-MS/MS analysis.

Quantitative Analysis of Spectinamide Antibiotics

Sample Preparation. Sample preparation was performed by protein precipitation using methanol. Plasma proteins were precipitated by the addition of 8-volumes (200 µL) of IS (spectinomycin;100 ng/mL) in methanol to a volume of 25 µL of plasma/tissue homogenate test sample. Samples were vortexed for 30 s and centrifuged at 10,000 ×g for 10 min at 4 °C, and the supernatants were collected for LC-MS/MS analysis.

Chromatographic Conditions. Chromatographic separations of the prepared samples were carried out using a Nexera XR liquid chromatograph (Shimadzu, Columbia, MD) consisting of two pumps, online degasser, system controller, and auto sampler. Mobile phase consisting of A) water with 5 mM ammonium formate buffer and B) methanol with 5 mM ammonium formate buffer was used at a flow rate of 0.4 mL/min in gradient mode as follows: 0-1 min, 30% B; 1-2 min, 70% B; 2-4 min, 70% B; 4-5 min, 30%B, 5-7 min, 30% B. A HILIC ® 3.5 µm C8, 100 × 4.6 mm column (Phenomenex, Torrance, CA) was used for the separation. Samples (5 µL) were injected on column and the eluate was led directly into the mass spectrometer.

Mass Spectrometric Conditions. An API 4500 triple quadruple mass spectrometer (Applied Biosystems, Foster City, CA) equipped with a turbospray ion source was operated in the positive ion mode. Selected reaction monitoring using precursor→product ion combinations of *m/z* 487.2→207.1, 418→207.1, and 365.1→333.2 was used for quantification of spectinamides 1599, 1810 and the IS spectinomycin, respectively.

Stock Solutions, Calibrants, and Quality Controls. Stock solution (1 mg/mL) of spectinamide compounds were prepared in water. Working solutions (29.3, 58.6, 117.2, 234.4, 468.75, 937.5, 1875, 3750, 7500, 15000, and 30000 ng/mL) were also prepared in water. Calibration standards (2.93, 5.86, 11.7, 23.4, 46.8, 93.7, 187.5, 375, 750, 1500, and 3000 ng/mL) were prepared by a 10-fold dilution of working solutions in blank tissue matrices (plasma, lung, liver, spleen, and kidney). A separate stock solution of spectinamide compounds was prepared, to be used as quality control at the final concentration of 54, 180, 600, and 2000 ng/mL. Each analytical run consisted of one set (triplicate) of quality control samples scattered in between calibrants and *in vivo* study samples. Linearity of the calibrants in duplicate was assessed by subjecting the spiked concentrations and the respective peak area to the least-square linear regression analysis with and without intercepts, and a weighted least-square regression ($1/x$ or $1/x^2$). A suitable calibration model was chosen after the examination of residuals and coefficient

of correlation in each case. The lowest limit of quantitation (LLOQ) in the standard curve measured with the acceptable accuracy and precision for spectinamide compounds was established as 2.93 ng/mL.

Results

Spectinamide 1810 Intravenous Single Dose Study in Mice

The concentrations of spectinamide 1810 were measured in mouse plasma, lung, liver, spleen, and kidney after 10 mg/kg single dose administration of spectinamide 1810. The concentration-time data are listed in **Appendix B** and the concentrations *vs.* time plots are shown in **Figure 4-1**. The concentration-time profiles in plasma and tissues (lung, liver, spleen, and kidney) showed biphasic disposition, i.e., a steep decline in the concentration at the initial time points (rapid distribution phase), followed by slower elimination phase at the later time points. The tissues showed almost flat concentration-time profiles after 3 hr, suggesting entrapment of spectinamide 1810, probably in the cellular subcompartment. These profiles are consistent with the previously reported data of spectinamide 1810 and 1599 [10, 12, 13, 15, 16, 51].

Spectinamide 1810 Intravenous Multiple Dose Study in Mice

The concentrations of spectinamide 1810 were measured in mouse plasma, lung, liver, spleen, and kidney after 10 mg/kg multiple dose (daily dosing for 5 consecutive days) administration of spectinamide 1810. The concentration-time data are listed in **Appendix C** and the concentrations *vs.* time plots are shown in **Figure 4-2**. The concentration-time profiles in plasma and tissues (lung, liver, spleen, and kidney) showed biphasic disposition, consistent to the data obtained after single dose. Despite of flat PK profiles in the tissues, we do not observe accumulation after multiple dose administrations. This could be due to saturable binding to the cellular subcompartment of the tissues.

Spectinamide 1810 Subcutaneous Single Dose Study in Mice

The concentrations of spectinamide 1810 were measured in mouse plasma after 50 mg/kg single dose administration of spectinamide 1810 *via* the subcutaneous route of administration. The concentration-time data in plasma are listed in **Table 4-1** and the concentration *vs.* time plot is shown in **Figure 4-3**. The concentration-time profile in plasma showed a biphasic disposition consistent with the data obtained after intravenous administration. We observed a rapid absorption phase, with the absorption half-life of ~5 min followed by rapid distribution phase and a slower elimination phase.

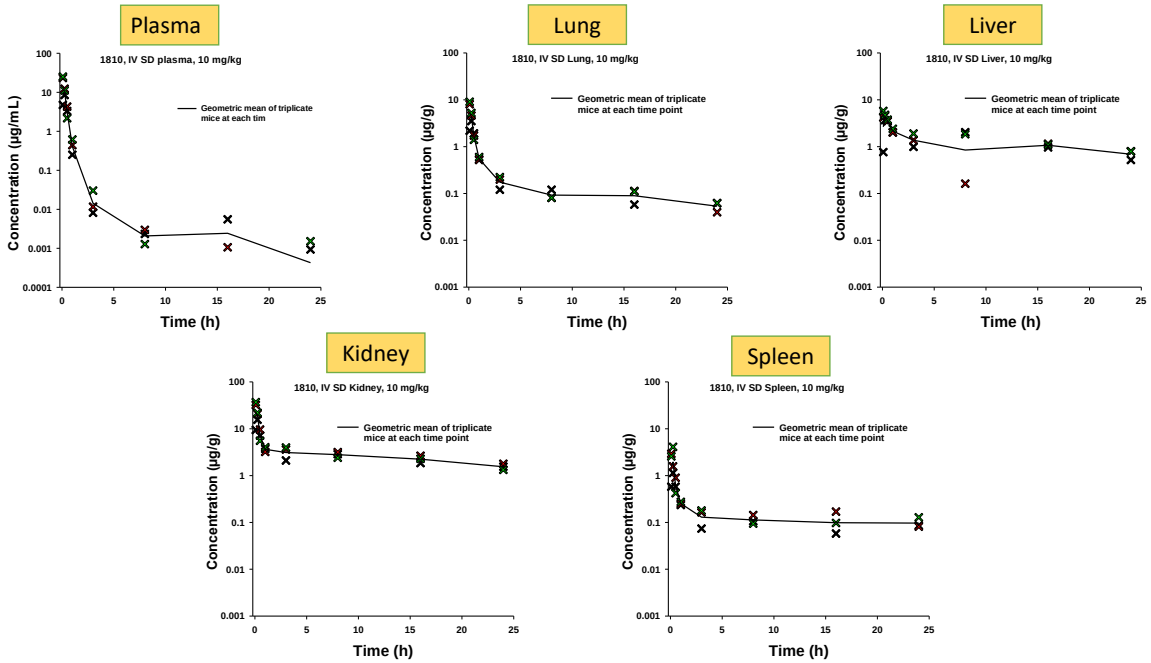

Figure 4-1. Concentration-time profiles of spectinamide 1810 in healthy mice plasma and tissues (lung, liver, spleen, and kidney) after single dose (10 mg/kg) administration *via* the intravenous route.

The solid line represents the geometric mean concentration, and the symbols represent the individual observations.

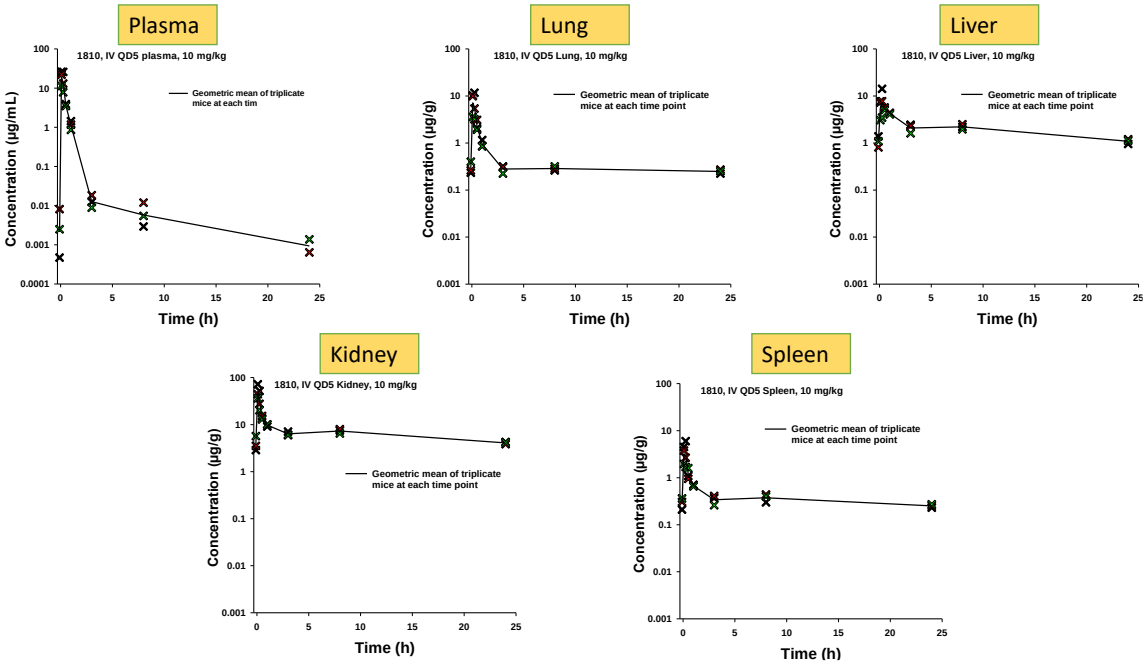

Figure 4-2. Concentration-time profiles of spectinamide 1810 in healthy mouse plasma and tissues (lung, liver, spleen, and kidney) after multiple dose (QD5, 10 mg/kg) administration *via* the intravenous route.
The solid line represents the geometric mean concentrations, and the symbols represent the individual observations.

Table 4-1. Plasma concentration-time data after single dose SC administration of spectinamide 1810 (50 mg/kg) to Balb/c mice (n = 3 mice per time point).

Time (h)	Concentration (mg/L)			Median	Mean	STDEV	Range	GEO MEAN	GEO STDEV
0.083	91.2	74.9	85.5	85.5	83.9	8.27	16.3	83.6	1.11
0.25	72.8	68.2	80.6	72.8	73.9	6.27	12.4	73.7	1.09
0.5	32.6	40.3	30.4	32.6	34.4	5.20	9.90	34.2	1.16
1	3.93	3.81	3.49	3.81	3.74	0.227	0.440	3.74	1.06
3	0.0465	0.0490	0.0311	0.0465	0.0422	0.00969	0.0179	0.0414	1.28
8	0.0215	0.0837	0.0196	0.0215	0.0416	0.0365	0.0641	0.0328	2.25
24	0.0122	0.00829	0.0178	0.0122	0.0128	0.00478	0.00951	0.0101	1.47

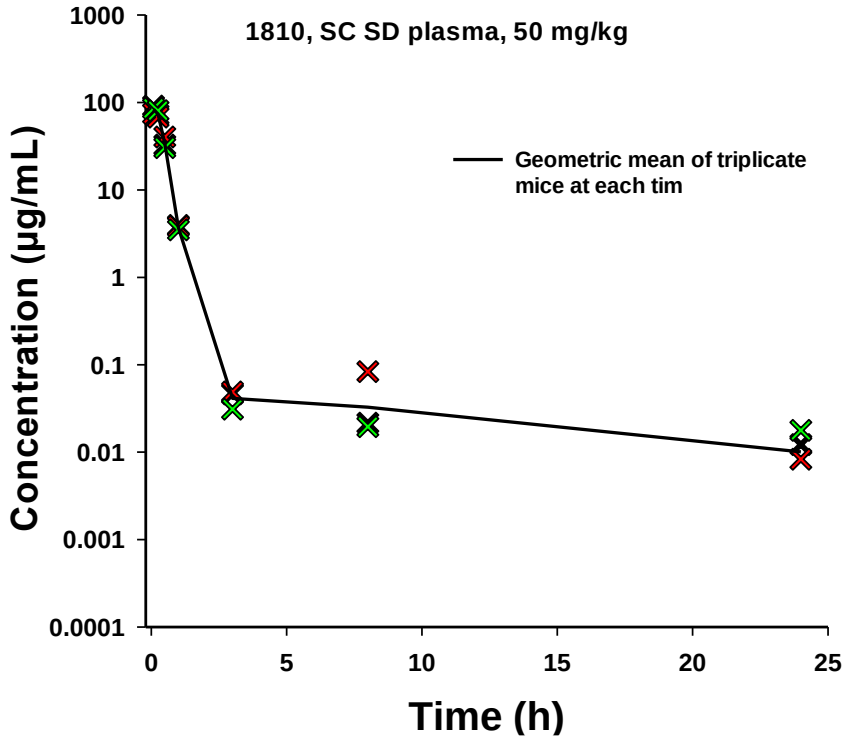

Figure 4-3. Concentration-time profile of spectinamide 1810 in healthy mouse plasma after single dose (50 mg/kg) administration via the subcutaneous route. The solid line represents the geometric mean concentrations, and the red and green symbols represent the individual observations.

Spectinamide 1810 Intravenous Single Dose Study in Rats

The concentrations of spectinamide 1810 were measured in rat plasma after 10 mg/kg single dose administration. The concentration-time data are listed in **Appendix D** and the concentration *vs.* time plots are shown in **Figures 4-4** to **4-6**. The concentration-time profiles were consistent across the three studies. We also observed the biphasic disposition, with a rapid decline in the concentration at the initial time points and a slower elimination phase after 6 hr post dosing.

Spectinamide 1599 Intravenous Single Dose Study in Rats

The concentrations of spectinamide 1599 were measured in rat plasma, lung, liver, spleen, and kidney after 10 mg/kg single dose administration of spectinamide 1599. The concentration-time data are listed in **Appendix E** and the bar plot of measured concentrations at two time-points is shown in **Figure 4-7**. The concentration-time profiles in plasma and tissues (lung, liver, spleen, and kidney) showed biphasic disposition, consistent to the data observed in mice. The difference in the concentrations between the two time points (15 min and 4 h) is highest in plasma. However, the tissue concentrations at the 4 h time point were greater than the plasma concentrations at the same time point. This is consistent with the data observed in mice, suggesting entrapment in the cellular subcompartment.

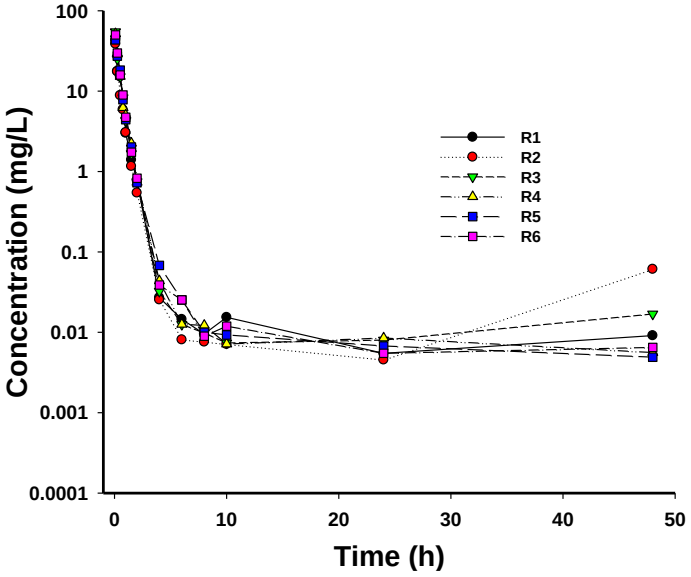

Figure 4-4. Study 1 plasma concentration-time profile of spectinamide 1810 after IV administration (10 mg/kg) to male Sprague-Dawley rats.

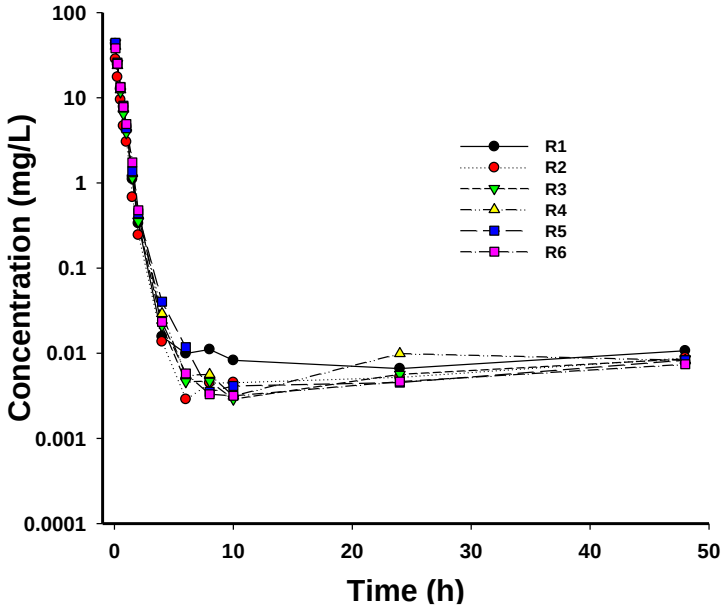

Figure 4-5. Study 2 plasma concentration-time profile of spectinamide 1810 after IV administration (10 mg/kg) to male Sprague-Dawley rats.

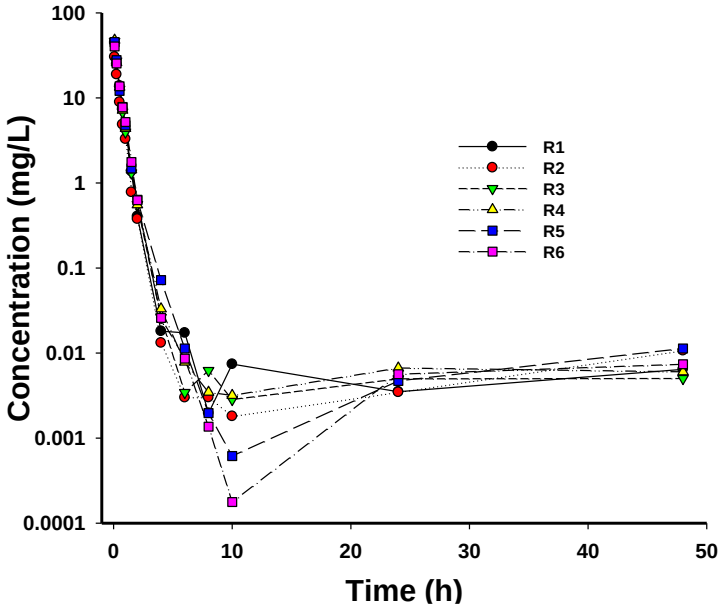

Figure 4-6. Study 3 plasma concentration-time profile of spectinamide 1810 after IV administration (10 mg/kg) to male Sprague-Dawley rats.

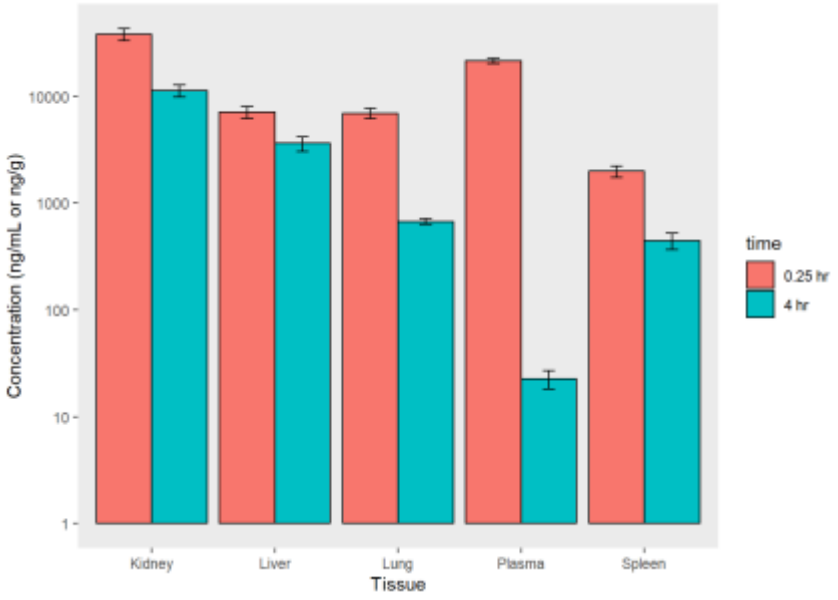

Figure 4-7. Spectinamide 1599 concentrations (ng/mL or ng/g) in rat plasma and tissues after 10 mg/kg single dose IV administration.
Red bars denote concentrations at 15 min, green bars denote concentrations at 4 h post dosing, and error bars denote standard deviations.

CHAPTER 5. DEVELOPMENT OF A MURINE MINIMAL PHYSIOLOGICALLY-BASED PHARMACOKINETIC MODEL FOR SPECTINAMIDE 1599[4]

Introduction

The minimalistic PBPK model was built by integrating the available information on the drug-specific and the system-specific parameters. The dynamic pharmacokinetic processes were described in terms of linear ordinary differential equations. The objective of the study was to build a murine PBPK model that can simultaneously characterize the pharmacokinetic behavior of spectinamide 1599 in plasma and tissues of interest. The model was intended to account for various routes of administrations, such as intravenous, subcutaneous, and intrapulmonary, and to be scaled to higher species. The plasma and tissue pharmacokinetic profiles of spectinamide 1599 after intravenous single dose administration were utilized in estimating the tissue-specific parameters by fitting the model to the data and validate it against the other sets of data. The intravenous model was then scaled to incorporate subcutaneous dosing and validated against various datasets from healthy and infected mice obtained after subcutaneous administration. Similarly, the model was scaled to incorporate the intrapulmonary administration and validated against observed datasets.

Methodology

Model Structure

For the PBPK model base structure, we utilized, adapted, and expanded the work published by Nasu et al [31]. The model structure included only the core tissues for which experimental data were available such as blood, lung, liver, spleen, and kidney, while all remaining organs and tissues were lumped together for the mass balance of the compound. Thus, the developed model can be classified as a partial or minimal PBPK model. The base model consists of five tissues (lung, liver, spleen, kidney, and others) and blood compartments (venous and arterial) representing the actual anatomical structure. The tissues are connected in parallel between the arterial and the venous blood compartment. The lung receives the blood from the venous blood compartment *via* the pulmonary artery, and blood flows out into the arterial blood compartment *via* the pulmonary vein. All other tissues are supplied from the arterial blood compartment, and the blood leaving from these tissues, except for the spleen, flows directly into the venous blood compartment. The blood leaving the spleen flows into the liver. In this model, the unbound spectinamide 1599 concentrations in plasma were assumed to be eliminated

[4] Modified from to-be-submitted article with permission. Keyur Parmar, Pradeep B. Lukka, Santosh Wagh, Zaid Temrikar, Richard E. Lee, Miriam Braunstein, Anthony J. Hickey, Gregory T. Robertson, Mercedes Gonzalez-Juarrero, Andrea Edginton and Bernd Meibohm. Development of a Minimalistic Physiologically-Based Pharmacokinetic (mPBPK) Model for the Preclinical Development of Spectinamide Antibiotics.

entirely by the kidney *via* glomerular filtration, as suggested by our previous work [10]. **Figure 5-1** represents the base model structure.

Each tissue is divided into three subcompartments: vascular, interstitial, and cellular. The distribution between the vascular and interstitial subcompartments was assumed to be instantaneous and thus we modeled both of these subcompartments together. In contrast, the distribution between the interstitial and cellular subcompartments was assumed to be slower and determined by first-order influx ($K_{I\rightarrow C}^{Organ}$) and backflux ($K_{C\rightarrow I}^{Organ}$) rate constants. We assumed that only the unbound fraction of spectinamide 1599 in plasma is distributed between the interstitial and cellular subcompartments. Also, the concentration in plasma was calculated by the blood-to-plasma ratio, which was determined experimentally.

For intravenous administration, the bolus dose was assumed to be mixed instantaneously into the venous blood. For subcutaneous administration, the dose was administered as an external compartment, absorbed into the venous compartment *via* a first-order absorption rate constant and a bioavailability component. For intrapulmonary aerosol administration, we modified the lung tissue by adding the epithelial lining fluid (ELF) subcompartment, as shown in **Figure 5-2**. The physiological volume of the ELF subcompartment was obtained from the literature [48]. The dose was administered as an external compartment absorbed into the ELF compartment *via* a first-order absorption rate constant and a bioavailability component. The compound was assumed to be bound to the ELF proteins and only the unbound fraction was distributed to the other subcompartments of the lungs and ultimately to the systemic circulation. The fraction unbound in ELF was calculated from the fraction unbound in plasma and the albumin ratio between plasma and ELF using the equation described by Poulin and Theil [25].

Model Parameterization for Spectinamide 1599

During the model development process, we utilized three different approaches to obtain values for model-related parameters: 1) System specific parameters (physiologic blood flow rates and organ volumes) were obtained from the literature; 2) Drug specific parameters (*fu* and k(b/p)) were experimentally determined; and 3) Transfer rate constants between model sub-compartments were estimated by fitting the model to experimentally observed data. Based on the observed biphasic disposition profiles of spectinamide compounds in plasma, lung, liver, spleen, and kidney after intravenous, subcutaneous, and intrapulmonary aerosol administration [13, 14, 18, 52] and the known hydrophilic character of spectinamide 1599 and 1810 (cLogP -2.52 and -3.03, respectively), we assumed a model structure where each compartment consists of subcompartments in rapid equilibrium with blood (vascular and interstitial) and a subcompartment in slow equilibrium with blood (cellular). The model was parameterized in terms of first-order influx and backflux rate constants between the rapidly and the slowly equilibrating sub-compartments in each tissue. Thereby, the observed concentration-time profiles are the result of the distribution and elimination of the drug in various tissues.

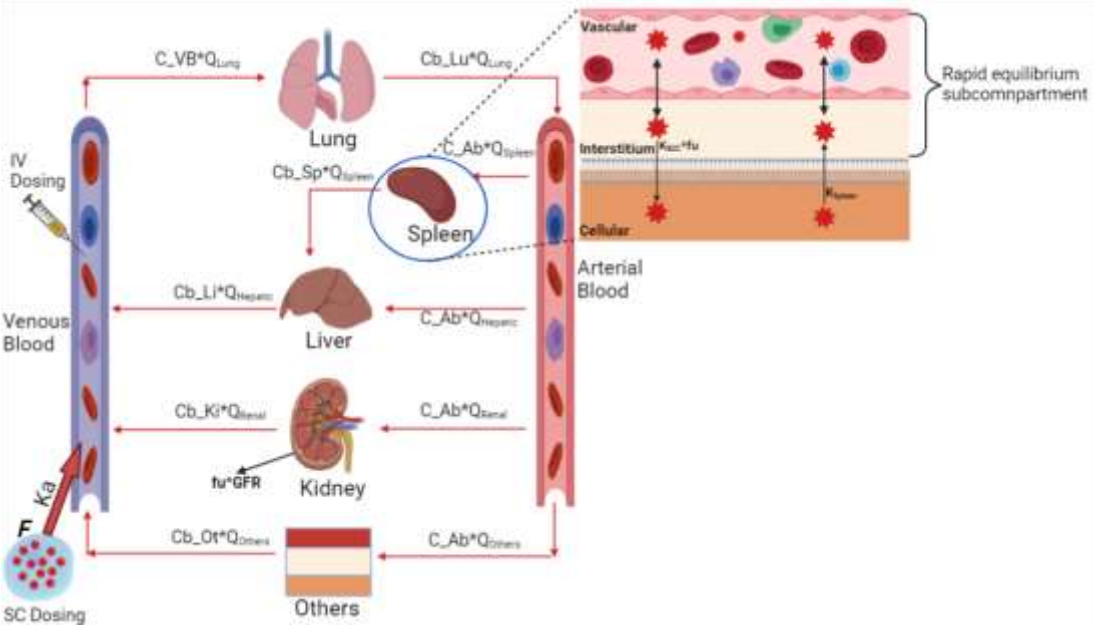

Figure 5-1. Schematic representation of the murine PBPK model accounting for intravenous and subcutaneous routes of administration.
The model is compartmentalized into blood (venous and arterial) and relevant tissues (lung, spleen, liver, kidney, and others), connected *via* blood flow rates (solid red arrows). Each tissue is divided into three sub-compartments, vascular, interstitial, and cellular. The vascular and interstitial sub-compartments were assumed to be in rapid equilibrium with blood, and the cellular subcompartment was assumed to be in slow equilibrium with blood.

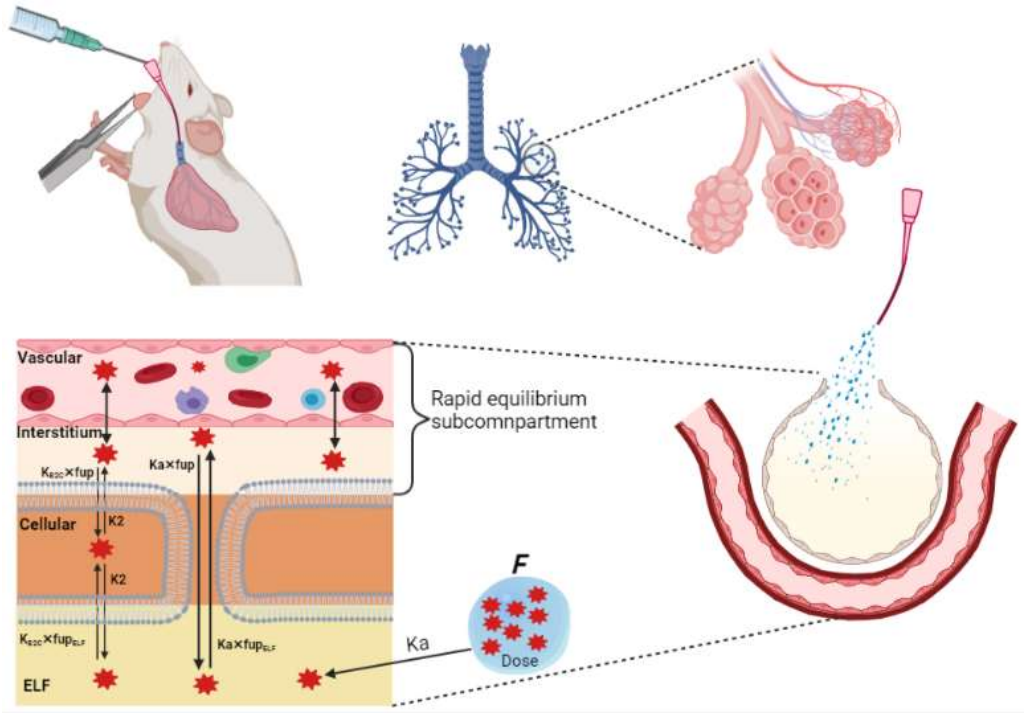

Figure 5-2. Schematic diagram of the modified lung compartment to model the drug dosing *via* intrapulmonary aerosol administration.
The aerosol was modeled to be administered intratracheally, absorbed into the epithelial lining fluid (ELF) compartment and distributed to the other sub-compartments of the lung and eventually reaching the systemic circulation.

Model Equations

All modeling and simulation were performed in the Monolix Suite (Lixoft, Antony, France). The dynamic pharmacokinetic processes were described in terms of balance equations for the PBPK model are listed below (**Equations 5-1** to **5-26**. All the model fittings were performed using the Stochastic Approximation Expectation Maximization (SAEM) algorithm of Monolix Version 2021R1 [53]. All plots were generated using ggplot2 in R [54]. The Monolix model scripts used to run the intravenous, subcutaneous, and intrapulmonary model are presented in the **Model Script Supplemental Data** file.

Venous Blood Compartment

$$V^{Venous\ Blood} \times \frac{d}{dt} C^{Venous\ Blood} = Q^{Liver} \times Cb^{Liver} + Q^{Kidney} \times Cb^{Kidney} + Q^{Other} \times Cb^{Other} - Q^{Lung} \times Cb^{Lung} \quad \textbf{Eq. 5-1}$$

Venous Plasma

$$C^{Venous\ Plasma} = \frac{C^{Venous\ Blood}}{k(b/p)} \quad \textbf{Eq. 5-2}$$

Lung Compartment

Lung Rapid Equilibrium Sub-Compartment

$$\left(V_{Vascular}^{Lung} + \left(\frac{V_{Interstitial}^{Lung}}{k(b/p)}\right)\right) \times \frac{d}{dt} Cb^{Lung} = Q_{Lung} \times (C^{Venous\ Blood} - Cb^{Lung}) - K_{I \to C}^{Lung} \times fu \times Cb^{Lung} \times \left(V_{Vascular}^{Lung} + \left(\frac{V_{Interstitial}^{Lung}}{k(b/p)}\right)\right) + K_{C \to I}^{Lung} \times C_{Cellular}^{Lung} \times V_{Cellular}^{Lung} \quad \textbf{Eq. 5-3}$$

Lung Cellular Sub-Compartment

$$V_{Cellular}^{Lung} \times \frac{d}{dt} C_{Cellular}^{Lung} = K_{I \to C}^{Lung} \times fu \times Cb^{Lung} \times \left(V_{Vascular}^{Lung} + \left(\frac{V_{Interstitial}^{Lung}}{k(b/p)}\right)\right) - K_{C \to I}^{Lung} \times C_{Cellular}^{Lung} \times V_{Cellular}^{Lung} \quad \textbf{Eq. 5-4}$$

Total Lung Concentration

$$C^{Lung} = \frac{\left(Cb^{Lung} \times \left(V_{Vascular}^{Lung} + \left(\frac{V_{Interstitial}^{Lung}}{k(b/p)}\right)\right) + C_{Cellular}^{Lung} \times V_{Cellular}^{Lung}\right)}{V^{Lung}} \quad \textbf{Eq. 5-5}$$

Arterial Blood Concentration

$$V^{Arterial\ Blood} \times \frac{d}{dt} C^{Arterial\ Blood} = Q^{Lung} \times (Cb^{Lung} - C^{Arterial\ Blood}) \quad \textbf{Eq. 5-6}$$

Spleen Compartment

Spleen Rapid Equilibrium Sub-Compartment

$$\begin{aligned} &\left(V_{Vascular}^{Spleen} + \left(\frac{V_{Interstitial}^{Spleen}}{k(b/p)}\right)\right) \times \frac{d}{dt} Cb^{Spleen} \\ &\quad = Q_{Spleen} \times (C^{Arterial\ Blood} - Cb^{Spleen}) \\ &\quad - K_{I\to C}^{Spleen} \times fu \times Cb^{Spleen} \times \left(V_{Vascular}^{Spleen} + \left(\frac{V_{Interstitial}^{Spleen}}{k(b/p)}\right)\right) \\ &\quad + K_{C\to I}^{Spleen} \times C_{Cellular}^{Spleen} \times V_{Cellular}^{Spleen} \end{aligned} \quad \textbf{Eq. 5-7}$$

Spleen Cellular Sub-Compartment

$$\begin{aligned} &V_{Cellular}^{Spleen} \times \frac{d}{dt} C_{Cellular}^{Spleen} \\ &\quad = K_{I\to C}^{Spleen} \times fu \times Cb^{Spleen} \times \left(V_{Vascular}^{Spleen} + \left(\frac{V_{Interstitial}^{Spleen}}{k(b/p)}\right)\right) \\ &\quad - K_{C\to I}^{Spleen} \times C_{Cellular}^{Spleen} \times V_{Cellular}^{Spleen} \end{aligned} \quad \textbf{Eq. 5-8}$$

Total Spleen Concentration

$$C^{Spleen} = \frac{\left(Cb^{Spleen} \times \left(V_{Vascular}^{Spleen} + \left(\frac{V_{Interstitial}^{Spleen}}{k(b/p)}\right)\right) + C_{Cellular}^{Spleen} \times V_{Cellular}^{Spleen}\right)}{V^{Spleen}} \quad \textbf{Eq. 5-9}$$

Liver Compartment

Liver Rapid Equilibrium Sub-Compartment

$$\begin{aligned} &\left(V_{Vascular}^{Liver} + \left(\frac{V_{Interstitial}^{Liver}}{k(b/p)}\right)\right) \times \frac{d}{dt} Cb^{Liver} \\ &\quad = Q_{Liver} \times (C^{Arterial\ Blood} - Cb^{Liver}) + Q_{Spleen} \times Cb^{Spleen} \\ &\quad - K_{I\to C}^{Liver} \times fu \times Cb^{Liver} \times \left(V_{Vascular}^{Liver} + \left(\frac{V_{Interstitial}^{Liver}}{k(b/p)}\right)\right) \\ &\quad + K_{C\to I}^{Liver} \times C_{Cellular}^{Liver} \times V_{Cellular}^{Liver} \end{aligned} \quad \textbf{Eq. 5-10}$$

Liver Cellular Sub-Compartment

$$V_{Cellular}^{Liver} \times \frac{d}{dt} C_{Cellular}^{Liver} = K_{I\to C}^{Liver} \times fu \times Cb^{Liver} \times \left(V_{Vascular}^{Liver} + \left(\frac{V_{Interstitial}^{Liver}}{k(b/p)} \right) \right) - K_{C\to I}^{Liver} \times C_{Cellular}^{Liver} \times V_{Cellular}^{Liver} \quad \textbf{Eq. 5-11}$$

Total Liver Concentration

$$C^{Liver} = \frac{\left(Cb^{Liver} \times \left(V_{Vascular}^{Liver} + \left(\frac{V_{Interstitial}^{Liver}}{k(b/p)} \right) \right) + C_{Cellular}^{Liver} \times V_{Cellular}^{Liver} \right)}{V^{Liver}} \quad \textbf{Eq. 5-12}$$

Kidney Compartment

Kidney Rapid Equilibrium Sub-Compartment

$$\left(V_{Vascular}^{Kidney} + \left(\frac{V_{Interstitial}^{Kidney}}{k(b/p)} \right) \right) \times \frac{d}{dt} Cb^{Kidney} = Q_{Kidney} \times (C^{Arterial\ Blood} - Cb^{Kidney}) - K_{I\to C}^{Kidney} \times fu \times Cb^{Kidney} \times \left(V_{Vascular}^{Kidney} + \left(\frac{V_{Interstitial}^{Kidney}}{k(b/p)} \right) \right) - GFR \times fu \times Cb^{Kidney} + K_{C\to I}^{Kidney} \times C_{Cellular}^{Kidney} \times V_{Cellular}^{Kidney} \quad \textbf{Eq. 5-13}$$

Kidney Cellular Sub-Compartment

$$V_{Cellular}^{Kidney} \times \frac{d}{dt} C_{Cellular}^{Kidney} = K_{I\to C}^{Kidney} \times fu \times Cb^{Kidney} \times \left(V_{Vascular}^{Kidney} + \left(\frac{V_{Interstitial}^{Kidney}}{k(b/p)} \right) \right) - K_{C\to I}^{Kidney} \times C_{Cellular}^{Kidney} \times V_{Cellular}^{Kidney} \quad \textbf{Eq. 5-14}$$

Total Kidney Concentration

$$C^{Kidney} = \frac{\left(Cb^{Kidney} \times \left(V_{Vascular}^{Kidney} + \left(\frac{V_{Interstitial}^{Kidney}}{k\left(\frac{b}{p}\right)} \right) \right) + C_{Cellular}^{Kidney} \times V_{Cellular}^{Kidney} \right)}{V^{Kidney}} \quad \textbf{Eq. 5-15}$$

Other Tissue Compartment

Other Tissue Rapid Equilibrium Sub-Compartment

$$\left(V_{Vascular}^{Other} + \left(\frac{V_{Interstitial}^{Other}}{k(b/p)}\right)\right) \times \frac{d}{dt} Cb^{Other} = Q_{Other} \times (C^{Arterial\ Blood} - Cb^{Other}) - K_{I\to C}^{Other} \times fu \times Cb^{Other} \times \left(V_{Vascular}^{Other} + \left(\frac{V_{Interstitial}^{Other}}{k(b/p)}\right)\right) + K_{C\to I}^{Other} \times C_{Cellular}^{Other} \times V_{Cellular}^{Other} \quad \textbf{Eq. 5-16}$$

Other Tissue Cellular Sub-Compartment

$$V_{Cellular}^{Other} \times \frac{d}{dt} C_{Cellular}^{Other} = K_{I\to C}^{Other} \times fu \times Cb^{Other} \times \left(V_{Vascular}^{Other} + \left(\frac{V_{Interstitial}^{Other}}{k(b/p)}\right)\right) - K_{C\to I}^{Other} \times C_{Cellular}^{Other} \times V_{Cellular}^{Other} \quad \textbf{Eq. 5-17}$$

Total Other Tissue Concentration

$$C^{Other} = \frac{\left(Cb^{Other} \times \left(V_{Vascular}^{Other} + \left(\frac{V_{Interstitial}^{Other}}{k(b/p)}\right)\right) + C_{Cellular}^{Other} \times V_{Cellular}^{Other}\right)}{V^{Other}} \quad \text{Eq. 5-18}$$

Subcutaneous Dosing

$$V_{Depot}^{Subcutaneous} = 50\ \mu L \quad \textbf{Eq. 5-19}$$

$$C_{Depot}^{Subcutaneous} = \frac{F \times Dose}{V_{Depot}^{Subcutaneous}} \quad \textbf{Eq. 5-20}$$

$$V_{Depot}^{Subcutaneous} \times \frac{d}{dt} C_{Depot}^{Subcutaneous} = -Ka \times C_{Depot}^{Subcutaneous} \quad \textbf{Eq. 5-21}$$

Intra-Pulmonary Aerosol Dosing (IPA)

Dosing Depot

$$V_{Depot}^{IPA} \times \frac{d}{dt} C_{Depot}^{IPA} = -Ka \times C_{Depot}^{IPA} \quad \textbf{Eq. 5-22}$$

ELF Sub-Compartment

$$V^{ELF} \times \frac{d}{dt} C^{ELF} = Ka \times C_{Depot}^{IPA} \times V_{Depot}^{IPA} - K_{ELF\to C} \times fu^{ELF} \times C^{ELF} \times V^{ELF} + K_{C\to I}^{Lung} \times C_{Cellular}^{Lung} \times V_{Cellular}^{Lung} - K_{ELF\to B} \times fu^{ELF} \times C^{ELF} \times V^{ELF} + K_{ELF\to B} \times fu \times Cb^{Lung} \times \left(V_{Vascular}^{Lung} + \left(\frac{V_{Interstitial}^{Lung}}{k(b/p)}\right)\right) \quad \textbf{Eq. 5-23}$$

Modified Lung Cellular Sub-Compartment

$$V_{Cellular}^{Lung} \times \frac{d}{dt} C_{Cellular}^{Lung} = K_{I\to C}^{Lung} \times fu \times Cb^{Lung} \times \left(V_{Vascular}^{Lung} + \left(\frac{V_{Interstitial}^{Lung}}{k(b/p)} \right) \right) - K_{C\to I}^{Lung} \times C_{Cellular}^{Lung} \times V_{Cellular}^{Lung} + K_{ELF\to C} \times fu^{ELF} \times C^{ELF} \times V^{ELF} \quad \textbf{Eq. 5-24}$$

Modified Lung Rapid Equilibrium Sub-Compartment

$$\left(V_{Vascular}^{Lung} + \left(\frac{V_{Interstitial}^{Lung}}{k(b/p)} \right) \right) \times \frac{d}{dt} Cb^{Lung} = Q_{Lung} \times (C^{Venous\ Blood} - Cb^{Lung}) - K_{I\to C}^{Lung} \times fu \times Cb^{Lung} \times \left(V_{Vascular}^{Lung} + \left(\frac{V_{Interstitial}^{Lung}}{k(b/p)} \right) \right) + K_{C\to I}^{Lung} \times C_{Cellular}^{Lung} \times V_{Cellular}^{Lung} + K_{ELF\to B} \times fu^{ELF} \times C^{ELF} \times V^{ELF} - K_{ELF\to B} \times fu \times Cb^{Lung} \times \left(V_{Vascular}^{Lung} + \left(\frac{V_{Interstitial}^{Lung}}{k(b/p)} \right) \right) \quad \textbf{Eq. 5-25}$$

Modified Lung Concentration

$$C^{Lung} = \frac{\left(Cb^{Lung} \times \left(V_{Vascular}^{Lung} + \left(\frac{V_{Interstitial}^{Lung}}{k(b/p)} \right) \right) + C_{Cellular}^{Lung} \times V_{Cellular}^{Lung} + C^{ELF} \times V^{ELF} \right)}{V^{Lung}} \quad \textbf{Eq. 5-26}$$

Results

Model Establishment for Intravenous Administration in Healthy Mice

The physiological (blood flow rates and organ volumes) and the drug-specific parameters (*fu* and k(b/p)) were fixed and used as building blocks of the model, as mentioned in **Chapter 3**. The remaining model parameters (tissue influx and backflux rate constants) were estimated by fitting the mouse PBPK model to the experimentally generated plasma, lung, liver, spleen, and kidney concentration-time data simultaneously. These plasma and tissue concentration-time profiles were obtained after intravenous single dose administration of spectinamide 1599 (10 mg/kg). The parameters were assumed to have log-normal distribution, and the residual unexplained variability (RUV) was characterized as a proportional error. The simulated median concentration-time

profiles along with the 95% prediction intervals overlaid by the observed concentrations, are shown in **Figure 5-3**.

To check the predictive performance of the model, we have simulated the plasma and tissue concentration-time after multiple dose intravenous administration (QD5) of 10 mg/kg spectinamide 1599. The model was verified using the visual inspection and 2-fold acceptance criteria between the observed and predicted AUCs. The simulated median concentration-time profiles along with the 95% prediction intervals, overlaid by the observed concentrations, are shown in **Figure 5-4**.

Model Expansion to Subcutaneous Administration in Healthy Mice

The intravenous model was also extended to accommodate subcutaneous (SC) administration by including a subcutaneous dosing compartment from which spectinamide is absorbed into the venous blood compartment *via* a first-order absorption rate constant (Ka) and where dose is corrected for bioavailability (F). The Ka, F, and RUV were estimated by fitting the model to the observed plasma and tissue concentration obtained after subcutaneous single dose administration of spectinamide 1599 (50 mg/kg) in healthy mice. Again, all tissue influx and backflux parameters were fixed to the values obtained from the intravenous model. The simulated median concentration-time profiles along with the 95% prediction intervals, overlaid by the observed concentrations, are shown in **Figure 5-5**.

To further validate the predictive performance of the model, we simulated the single (200 mg/kg) and multiple dose (QD5, TIW, and BIW at 200 mg/kg) plasma and tissue concentration profiles. The simulated median concentration-time profiles after SC QD5 200 mg/kg along with the 95% prediction intervals, overlaid by the observed concentrations, are shown in **Figure 5-6**. The model was verified using the visual inspection and twofold acceptance criteria between the observed and predicted AUCs.

Model Expansion to Intrapulmonary Administration in Healthy Mice

The developed intravenous model was extended to accommodate intrapulmonary aerosol (IPA) administration by including an external dosing compartment from which spectinamide is absorbed into the ELF compartment *via* a first-order absorption rate constant (Ka) and with a defined bioavailability (F). The Ka, F, and RUV were estimated by fitting the model to the observed plasma and tissue concentration-time profiles obtained after IPA single dose administration of spectinamide 1599 (50 mg/kg) in healthy mice. All tissue influx and backflux parameters were fixed to the values obtained from the intravenous model. The model fitting is shown in **Figure 5-7**. The model was used to simulate single (10 and 150 mg/kg) and multiple dose (QD5-once daily for 5 days, TIW-thrice weekly, and BIW-twice weekly at 10, 50, and 150 mg/kg dose levels) profiles. A

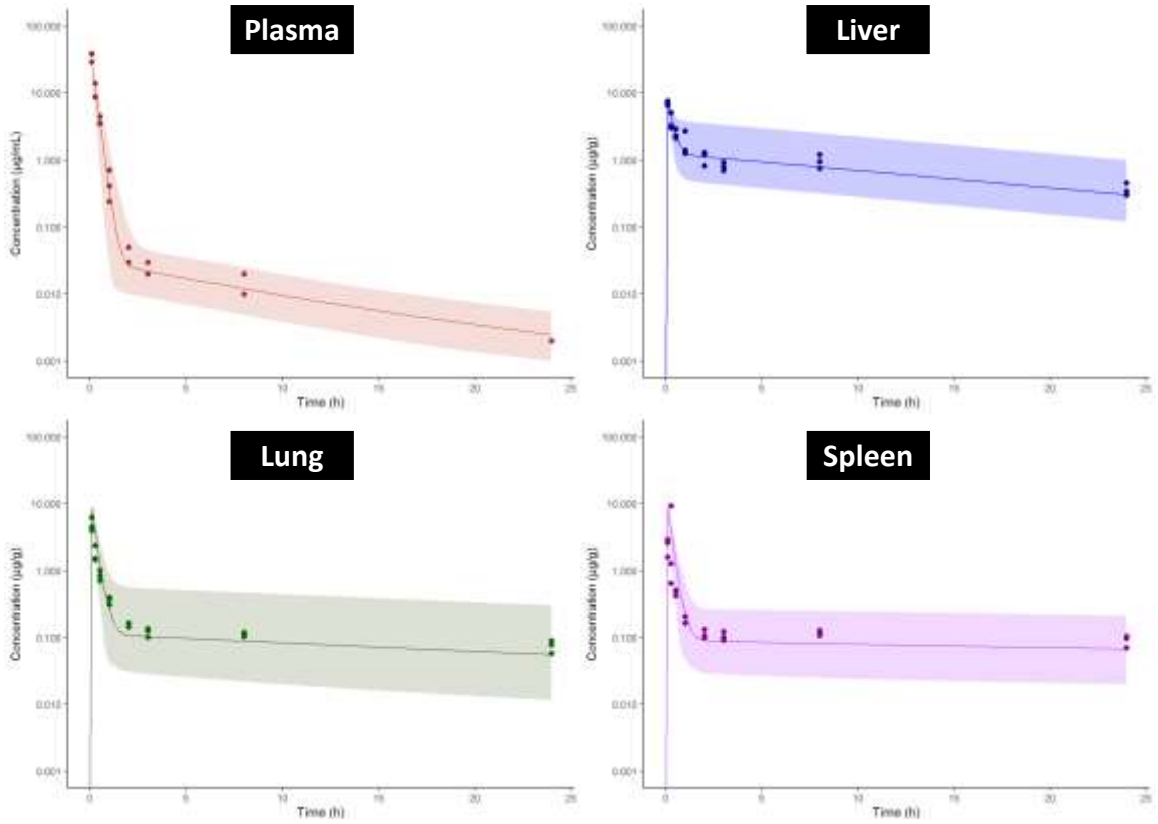

Figure 5-3. Concentration-time profiles of spectinamide 1599 in mouse plasma and tissues after administration of 10 mg/kg (IV).
Plasma (µg/mL); Liver (µg/g); Lung (µg/g); and Spleen (µg/g). The solid line represents the simulated median concentration profiles, and the shaded region is the 95% prediction interval overlaid by the experimentally observed concentrations represented by the dots.

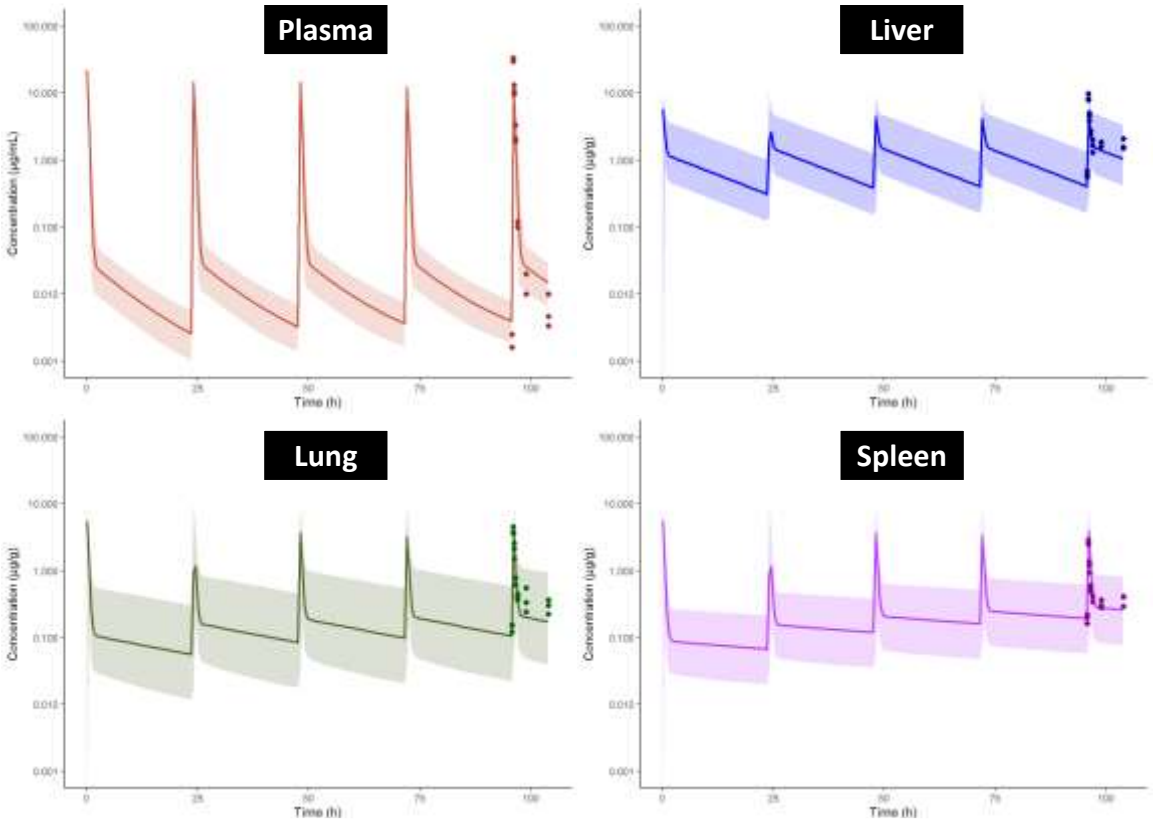

Figure 5-4. Concentration-time profiles of spectinamide 1599 in mouse plasma and tissues after multiple dose administration (QD5) of 10 mg/kg (IV).
Plasma (µg/mL); Liver (µg/g); Lung (µg/g); and Spleen (µg/g). The solid line represents the simulated median concentration profiles, and the shaded region is the 95% prediction interval overlaid by the experimentally observed concentrations represented by the dots.

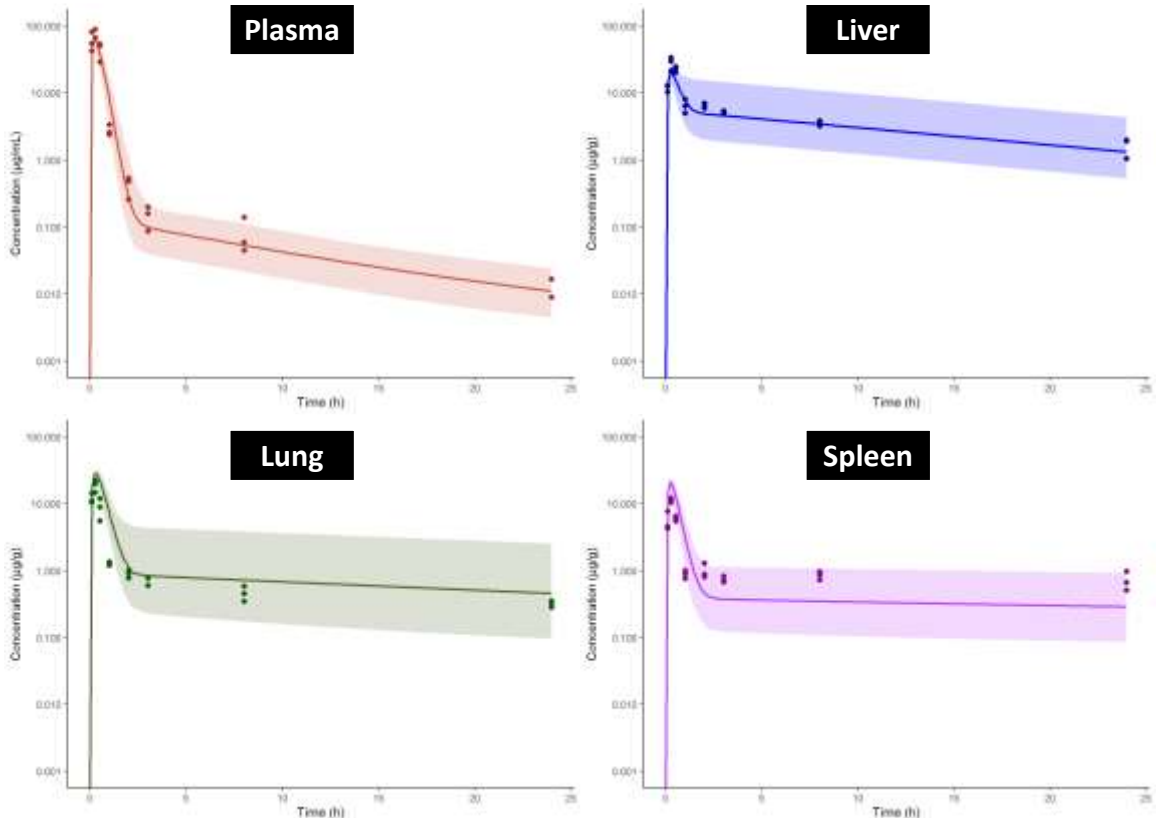

Figure 5-5. Concentration-time profiles of spectinamide 1599 in mouse plasma and tissues after subcutaneous administration of 50 mg/kg.
Plasma (µg/mL); Liver (µg/g); Lung (µg/g); and Spleen (µg/g). The solid line represents the simulated median concentration profiles, and the shaded region is the 95% prediction interval overlaid by the experimentally observed concentrations represented by the dots.

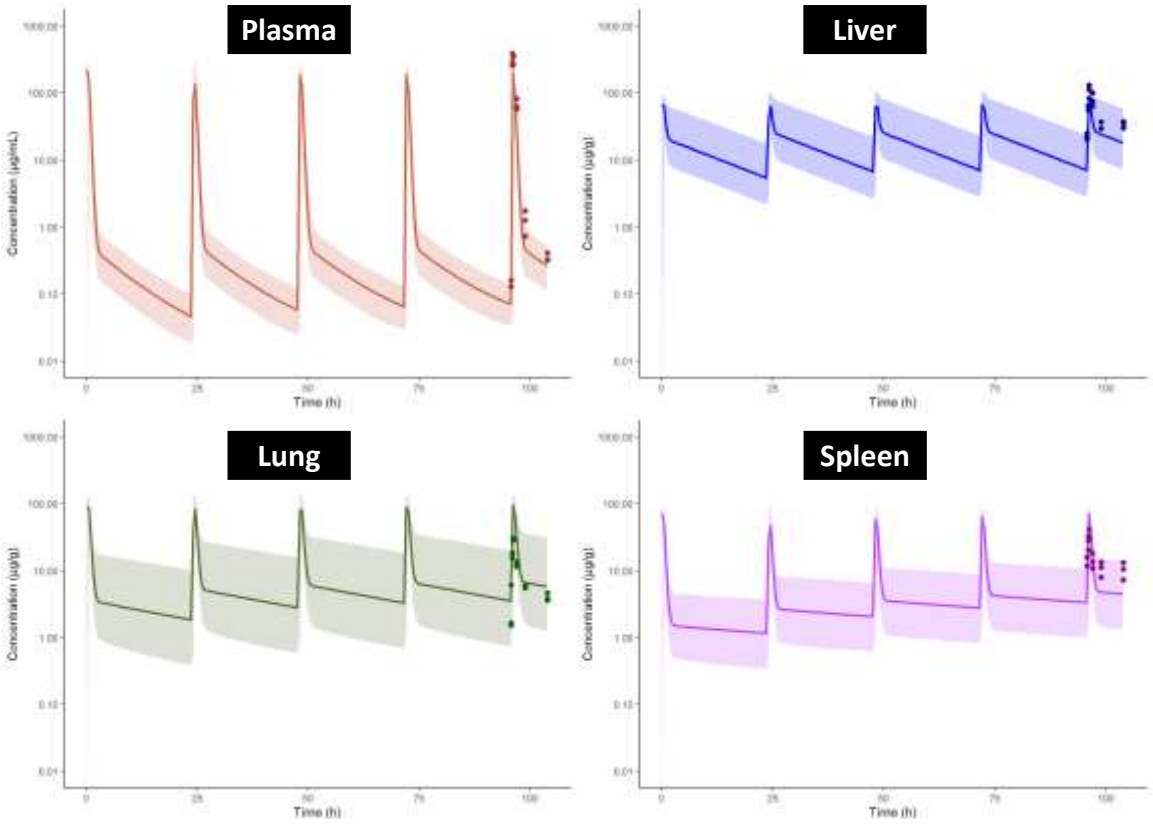

Figure 5-6. Concentration-time profiles of spectinamide 1599 in mouse plasma and tissues after multiple dose administration (QD5) of 200 mg/kg (SC).
Plasma (µg/mL); Liver (µg/g); Lung (µg/g); and Spleen (µg/g). The solid line represents the simulated median concentration profiles, and the shaded region is the 95% prediction interval overlaid by the experimentally observed concentrations represented by the dots.

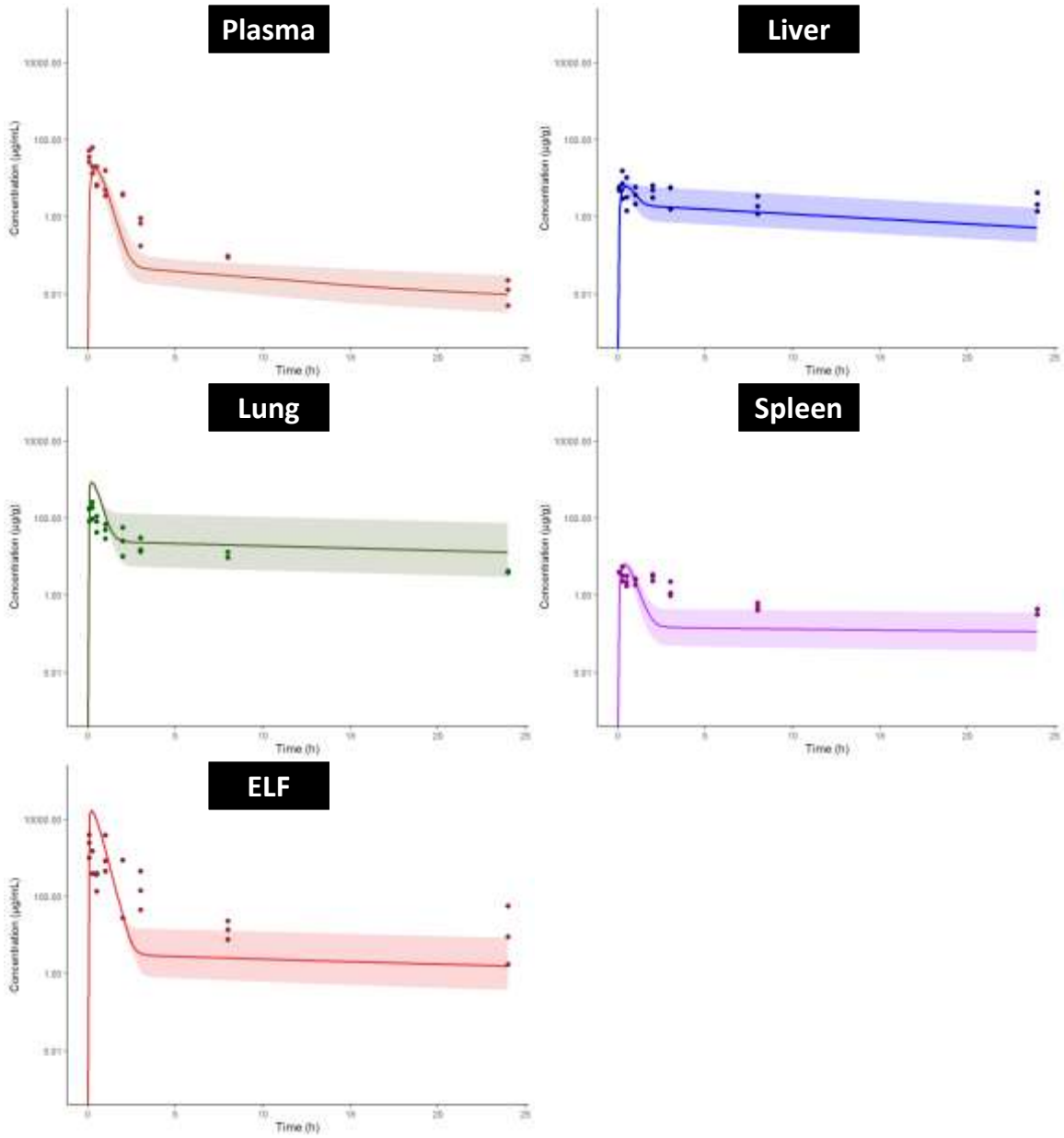

Figure 5-7. Concentration-time profiles of spectinamide 1599 in mouse plasma and tissues after intrapulmonary aerosol administration of 50 mg/kg.
Plasma (µg/mL); Liver (µg/g); Lung (µg/g); Spleen (µg/g); and ELF (µg/mL). The solid line represents the simulated median concentration-time profiles, and the shaded region is the 95% prediction interval overlaid by the experimentally observed concentrations represented by the dots.

select few plasma concentration profiles overlaid by observations are showed in **Figure 5-8**. The model was qualified by visual inspection of overlays of predicted and observed concentration-time profiles and the twofold criteria between the predicted and simulated AUCs.

Estimated Model Parameters and Predictive Performance for Healthy Mice

To describe the overall performance of the model with respect to the observations, **Figure 5-9** shows the goodness-of-fit plots of observed *vs.* predicted concentrations for all the available plasma and tissue data from uninfected animals. The estimated model parameters for IV, SC, and IPA administration of spectinamide 1599 are listed in **Table 5-1**. Overall, the model predictions were in reasonable agreement with the observations, with less than twofold difference in the predicted and observed AUCs in plasma (**Table 5-2**) and tissues (**Table 5-3**).

Model Expansion to Infected Mice

To this point, we utilized the model to characterize and predict the concentration-time profiles in healthy mice. Similarly, we used the subcutaneous model to simulate the plasma concentration-time profiles in a set of dose-ranging and dose fractionation studies that were performed in a standard mouse model of *Mtb* infection, which were recently reported [18, 50, 52]. The model predictions were in reasonable agreement with the observations, as shown in the corresponding goodness-of-fit diagnostic plot of observed *vs*. predicted plasma concentrations in infected mice (**Figure 5-10**). Thus, the model developed for the healthy mice was able to predict the plasma concentration-time profiles of infected mice, suggesting no significant difference in the pharmacokinetics of spectinamide 1599 between healthy and infected mice. This finding is in agreement with our previously published work [52].

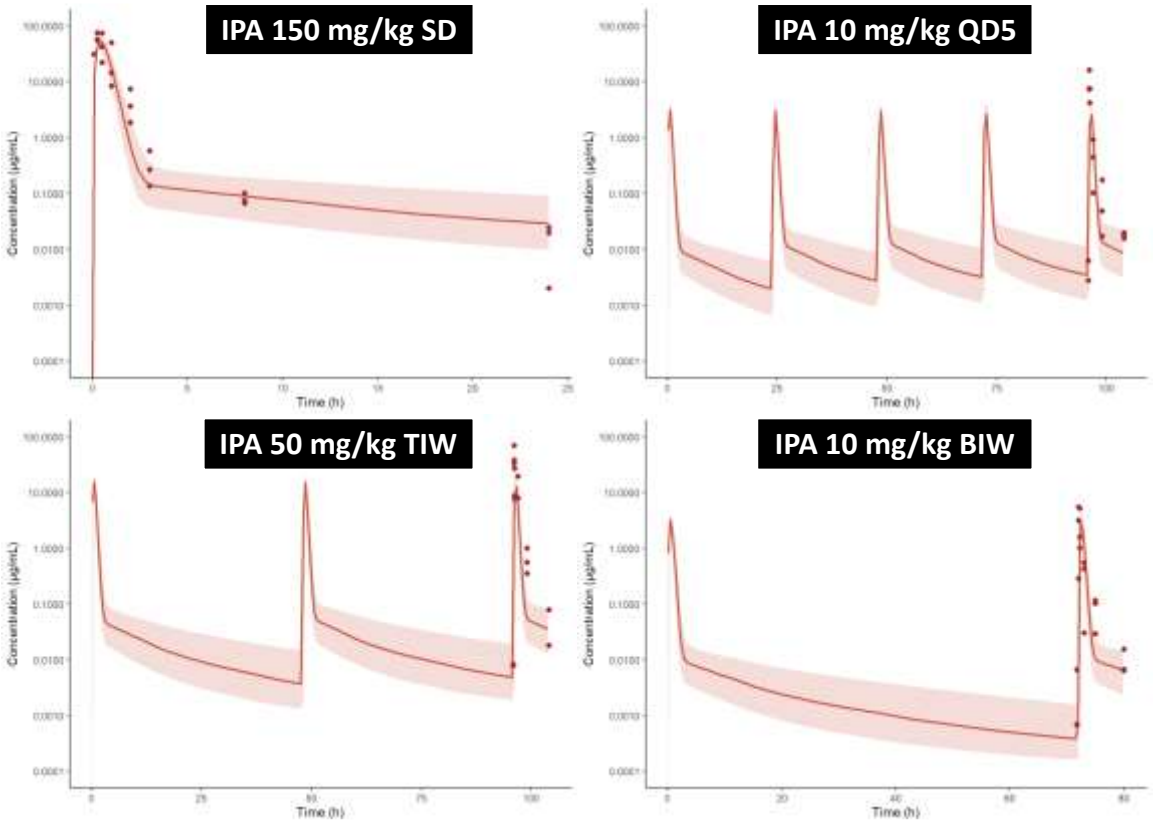

Figure 5-8. Concentration-time profiles of spectinamide 1599 in mouse plasma after single and multiple intrapulmonary aerosol (IPA) administration at dose levels ranging from 10-150 mg/kg.

150 mg/kg single dose; 10 mg/kg daily dosing for 5 consecutive days (QD5); 50 mg/kg three times a week (TIW) dosing on Monday, Wednesday, and Friday; and 10 mg/kg two times a week dosing on Monday and Thursday. The solid line represents the simulated median concentration-time profiles, and the shaded region is the 95% prediction interval overlaid by the experimentally observed concentrations represented by dots.

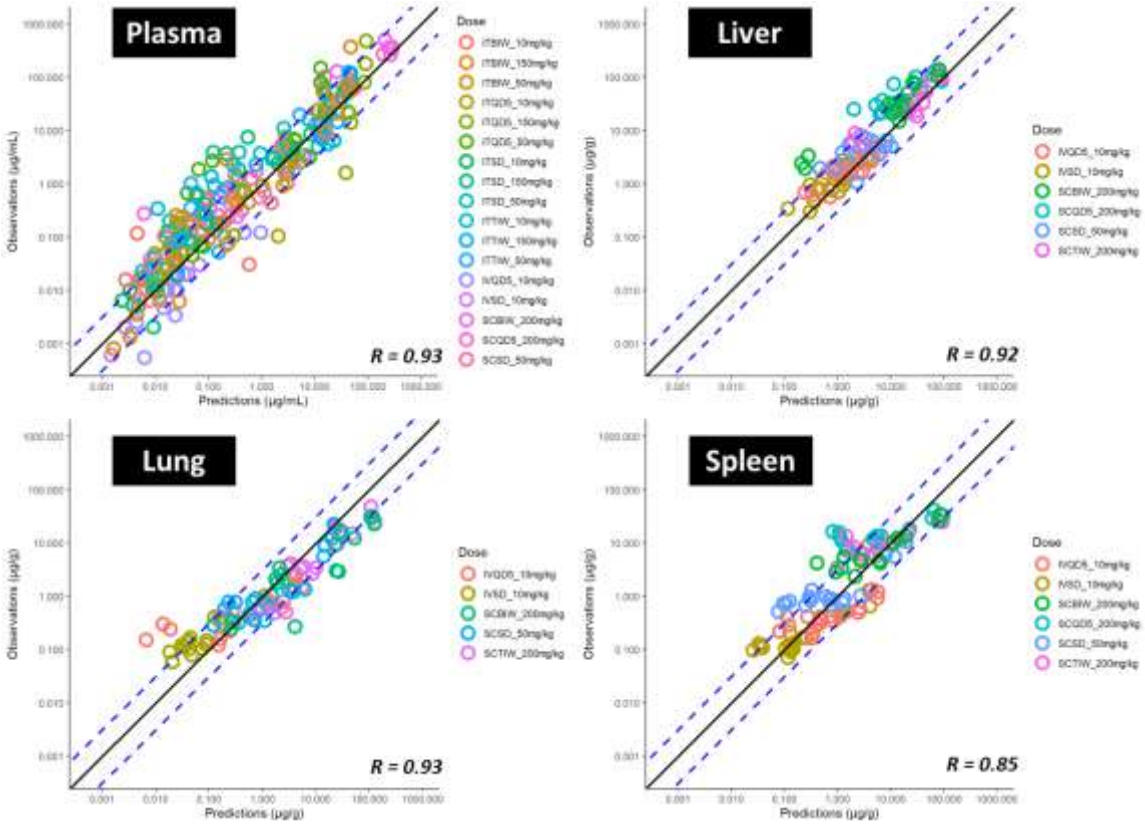

Figure 5-9. Predicted *versus* observed plasma and tissue concentrations of spectinamide 1599.

Plasma (µg/mL); Liver (µg/g); Lung (µg/g); and Spleen (µg/g) in healthy mice after intravenous (IV), subcutaneous (SC), and intrapulmonary aerosol (IPA) administration. SD = single dose; BIW = twice weekly on Monday and Thursday; QD5 = once daily for 5 consecutive days (Monday to Friday); TIW = thrice weekly on Monday, Wednesday, and Friday. The solid black line represents the line of unity, dashed blue lines are the twofold deviation, the symbols are the observed concentrations, and the R value is the Pearson correlation coefficient between the observations and predictions.

Table 5-1. Parameters, either fixed or estimated, used to build the PBPK model for spectinamide 1599.

Parameters	Description	Units	Intravenous Estimate (%RSE)	Intratracheal Estimate (%RSE)	Subcutaneous Estimate (%RSE)
$K_{I\to C}^{Lung}$	1st order uptake from the rapid equilibrium sub compartment (V+I) to the cellular sub compartment of the **lung**	1/h	0.068 (15.3)	Fixed	Fixed
$K_{C\to I}^{Lung}$	1st order backflux from the cellular sub compartment to the rapid equilibrium sub compartment of the **lung**	1/h	0.028 (41.5)	Fixed	Fixed
$K_{I\to C}^{Liver}$	1st order uptake from the rapid equilibrium sub compartment (V+I) to the cellular sub compartment of the **liver**	1/h	0.87 (10.1)	Fixed	Fixed
$K_{C\to I}^{Liver}$	1st order backflux from the cellular sub compartment to the rapid equilibrium sub compartment of the **liver**	1/h	0.061 (13.7)	Fixed	Fixed
$K_{I\to C}^{Spleen}$	1st order uptake from the rapid equilibrium sub compartment (V+I) to the cellular sub compartment of the **spleen**	1/h	0.048 (16.5)	Fixed	Fixed
$K_{C\to I}^{Spleen}$	1st order backflux from the cellular sub compartment to the rapid equilibrium sub compartment of the **spleen**	1/h	0.01 (106)	Fixed	Fixed
$K_{I\to C}^{Kidney}$	1st order uptake from the rapid equilibrium sub compartment (V+I) to the cellular sub compartment of the **Kidney**	1/h	12.1 (19.7)	Fixed	Fixed
$K_{C\to I}^{Kidney}$	1st order backflux from the cellular sub compartment to the rapid equilibrium sub compartment of the **Kidney**	1/h	0.15 (31.0)	Fixed	Fixed
$K_{I\to C}^{Others}$	1st order uptake from the rapid equilibrium sub compartment (V+I) to the cellular sub compartment of the **other tissues**	1/h	5.4 (4.92)	Fixed	Fixed
$K_{C\to I}^{others}$	1st order backflux from the cellular sub compartment to the rapid equilibrium sub compartment of the **other tissues**	1/h	7.0E-5 (142)	Fixed	Fixed
Ka	1st order absorption rate constant	-	-	5.03 (4.53)	4.36 (7.86)
F	Bioavailability component	-	-	0.33 (2.03)	0.86 (6.15)
ε_{Plasma}	Proportional error for plasma concentration-time profile		0.32 (15.1)	6.57 (8.62)	0.54 (17.6)
ε_{Lung}	Proportional error for lung concentration-time profile		0.35 (14.4)	0.95 (9.92)	0.50 (15.3)
ε_{Liver}	Proportional error for liver concentration-time profile		0.28 (14.4)	2.55 (10.3)	0.29 (19.1)
ε_{Spleen}	Proportional error for spleen concentration-time profile		0.53 (14.4)	8.48 (9.86)	0.97 (16.5)

RSE = relative standard error; K = first order rate constant; V+I = the combined vascular and interstitial sub-compartments; ε = the residual unexplained variance.

Table 5-2. Predicted *versus* observed plasma exposure of spectinamide 1599 in healthy mice.

Study	AUClast (h*µg/mL)		
	Observed	Median Predicted	Fold Difference
IV SD 10 mg/kg	7.52	8.85	1.18
IV QD5 10 mg/kg	6.37	8.83	1.39
SC SD 50 mg/kg	40.4	39.8	1.02
SC QD5 200 mg/kg	227	159	1.43
IPA SD 10 mg/kg	5.51	4.87	1.13
IPA QD5 10 mg/kg	3.57	4.85	1.36
IPA TIW 10 mg/kg	5.36	4.83	1.11
IPA SD 50 mg/kg	23.2	24.4	1.05
IPA QD5 50 mg/kg	39.8	24.2	1.64
IPA TIW 50 mg/kg	24.3	24.2	1.00
IPA BIW 50 mg/kg	14.2	24.1	1.70
IPA SD 150 mg/kg	59.5	73.1	1.23
IPA QD5 150 mg/kg	96.9	72.7	1.33
IPA TIW 150 mg/kg	61.7	72.5	1.18
IPA BIW 150 mg/kg	108	72.4	1.49

AUClast = area under the plasma concentration-time curve to the last measurable plasma concentration; IV = intravenous; SC = subcutaneous; IPA = intrapulmonary aerosol; SD = single dose; QD5 = once daily for 5 consecutive days (Monday to Friday); TIW = thrice weekly (Monday, Wednesday, and Friday); BIW = twice weekly (Monday and Thursday)

Table 5-3. Predicted *versus* observed exposure of spectinamide 1599 in lung, liver, and spleen.

Study	AUClast (h*µg/g)								
	Lung			Liver			Spleen		
	Observed	Predicted	Fold Difference	Observed	Predicted	Fold Difference	Observed	Predicted	Fold Difference
IV SD 10 mg/kg	3.79	6.24	1.65	19.9	16.6	1.2	3.42	5.02	1.47
IV QD5 10 mg/kg	4.05	5.62	1.39	19.6	12.4	1.58	3.91	5.62	1.44
SC SD 50 mg/kg	19.1	27	1.41	91.8	70.5	1.3	23.6	21.2	1.11
SC QD5 200 mg/kg	69.1	97.9	1.42	336	217	1.55	110	96.4	1.14

AUClast = area under the tissue concentration-time curve to the last measurable tissue concentration; IV = intravenous; SC = subcutaneous; SD =single dose; QD5 = once daily dosing for 5 consecutive days (Monday to Friday).

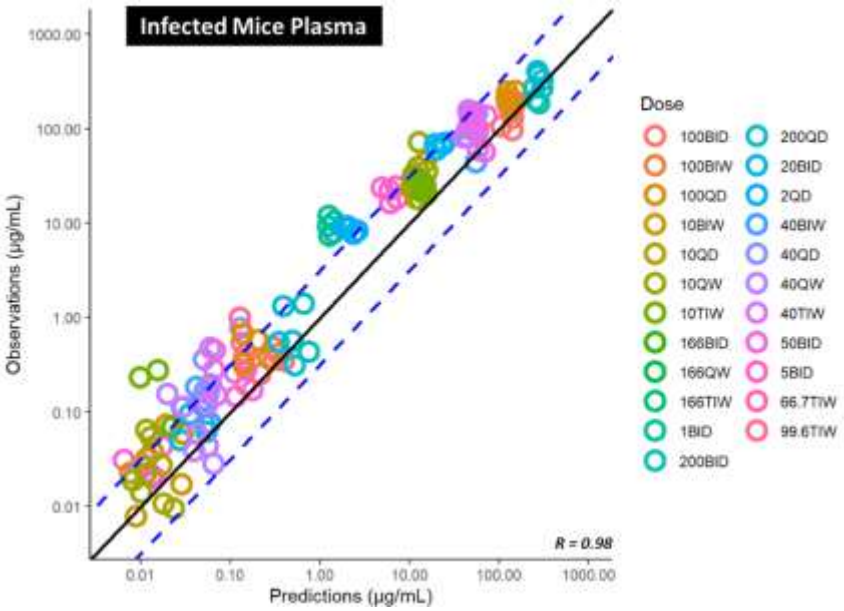

Figure 5-10. Predicted *versus* observed plasma concentrations (µg/mL) of spectinamide 1599 in infected mice after different dosing regimens using subcutaneous administration.

BID = twice daily; BIW = twice weekly; QD = once daily; QW = once weekly; TIW = thrice weekly. The solid black line represents the line of unity, dashed blue lines are the two-fold deviation, the symbols are the observed concentrations, and the R value is the Pearson correlation coefficient between the observations and predictions.

CHAPTER 6. DEVELOPMENT OF A MURINE MINIMAL PBPK MODEL FOR SPECTINAMIDE 1810[5]

Introduction

Next, we expanded the previously established minimal PBPK model to spectinamide 1810, a structurally highly similar spectinamide compared to 1599. The structural model for spectinamide 1599 was used unchanged and only updated with the drug-specific parameters of spectinamide 1810. The model parameters (tissue influx and backflux rate constants) were estimated by fitting the PBPK model to the PK data obtained after intravenous single dose administration of spectinamide 1810 (10 mg/kg). Here, we used the model to predict the PK profiles of spectinamide 1810 at various dose levels and dosing frequencies administered *via* the IV and the SC route in healthy mice. Thereafter, the model was used to predict the plasma concentrations of spectinamide 1810 in infected mice. The methodology for spectinamide 1810 was unchanged from the model developed for spectinamide 1599.

Results

Model Establishment for Intravenous Administration in Healthy Mice

The physiological (blood flow rates and organ volumes) and the drug-specific parameters (*fu* and k(b/p)) were fixed and used as building blocks of the model, mentioned in **Chapter 3**. The remaining model parameters (tissue influx and backflux rate constants) were estimated by fitting the mouse PBPK model to the experimentally generated plasma, lung, liver, spleen, and kidney concentration-time data simultaneously. These plasma and tissue concentration-time profiles were obtained after intravenous single dose administration of spectinamide 1810 (10 mg/kg). The parameters were assumed to have log-normal distribution and the residual unexplained variability (RUV) was characterized as a proportional error. The simulated median concentration-time profiles along with the 95% prediction intervals, overlaid by the observed concentrations, are shown in **Figure 6-1**.

To check the predictive performance of the model, we simulated the plasma and tissue concentration-time after multiple dose intravenous administration (QD5) of 10 mg/kg spectinamide 1810. The model was verified using the visual inspection and twofold acceptance criteria between the observed and predicted AUCs. The simulated median concentration-time profiles along with the 95% prediction intervals, overlaid by the observed concentrations, are shown in **Figure 6-2**.

---

[5] Modified from to-be-submitted article with permission. Keyur Parmar, Pradeep B. Lukka, Santosh Wagh, Zaid Temrikar, Richard E. Lee, Miriam Braunstein, Anthony J. Hickey, Gregory T. Robertson, Mercedes Gonzalez-Juarrero, Andrea Edginton and Bernd Meibohm. Development of a Minimalistic Physiologically-Based Pharmacokinetic (mPBPK) Model for the Preclinical Development of Spectinamide Antibiotics.

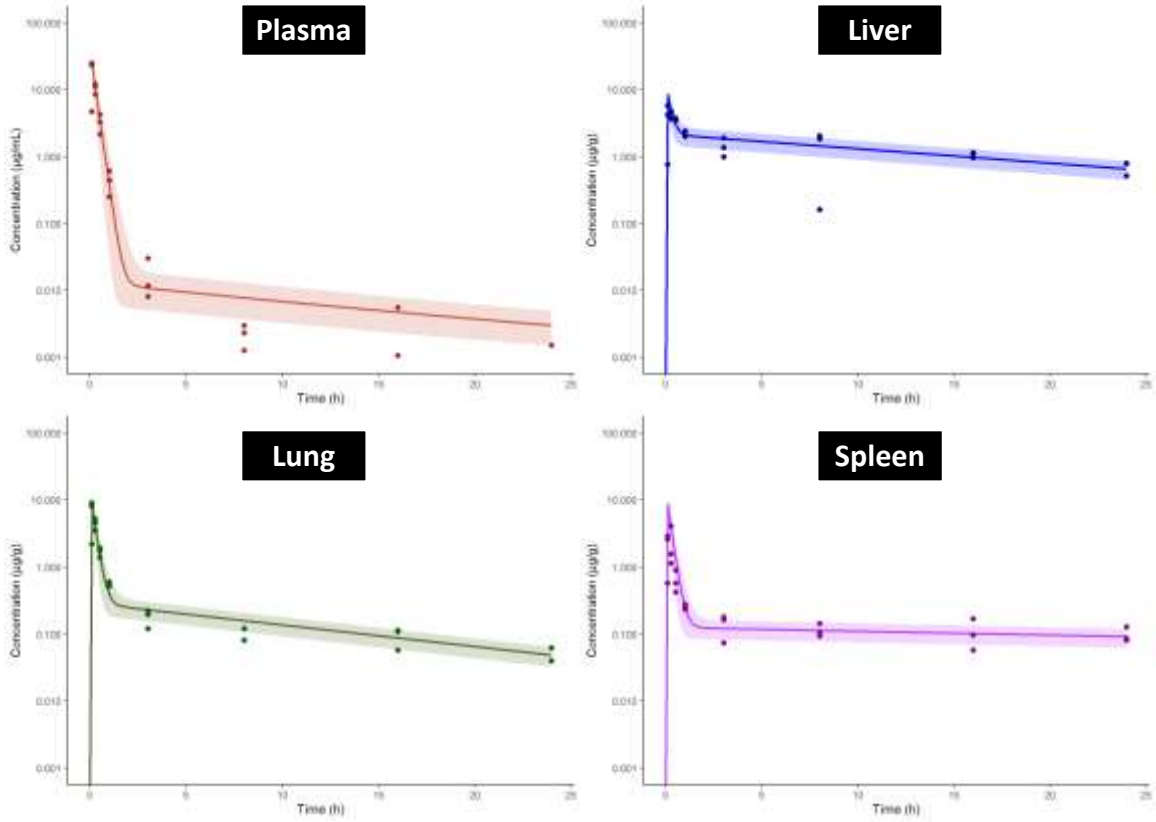

Figure 6-1. Concentration-time profiles of spectinamide 1810 in mouse plasma and tissues after intravenous administration of 10 mg/kg.
Plasma (µg/mL); Liver (µg/g); Lung (µg/g); and Spleen (µg/g). The solid line represents the simulated median concentration profiles, and the shaded region is the 95% prediction interval overlaid by the experimentally observed concentrations represented by dots.

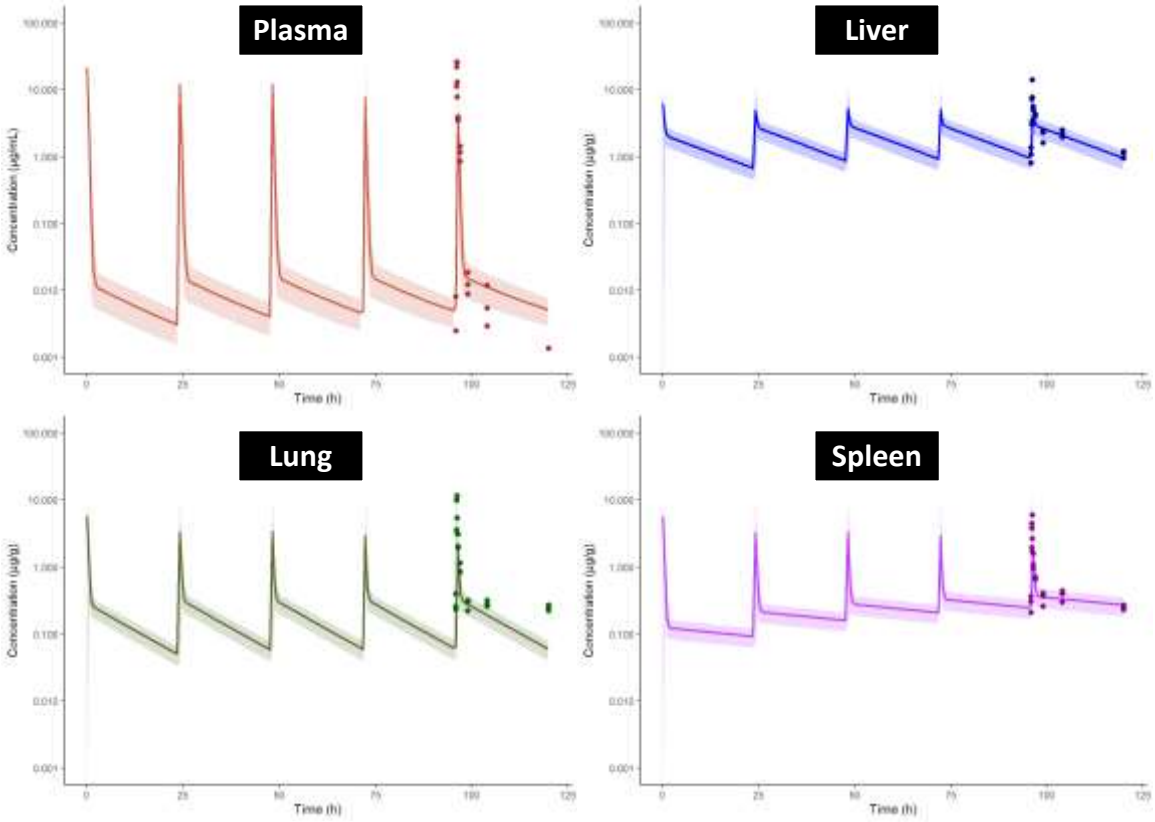

Figure 6-2. Concentration-time profiles of spectinamide 1810 in mouse plasma and tissues after multiple dose administration (QD5) of 10 mg/kg (IV).
Plasma (µg/mL); Liver (µg/g); Lung (µg/g); and Spleen (µg/g). The solid line represents the simulated median concentration-time profiles, and the shaded region is the 95% prediction interval overlaid by the experimentally observed concentrations represented by the dots.

Model Expansion to Subcutaneous Administration in Healthy Mice

The intravenous model was also extended to accommodate subcutaneous (SC) administration by including a subcutaneous dosing compartment from which spectinamide is absorbed into the venous blood compartment *via* a first-order absorption rate constant (Ka) and where dose is corrected for bioavailability (F). The Ka, F, and RUV were estimated by fitting the model to the observed plasma concentration obtained after subcutaneous single dose administration of spectinamide 1810 (46 mg/kg) in healthy mice. Again, all tissue influx and backflux parameters were fixed to the values obtained from the intravenous model. The model was simulated to predict the plasma concentration-time profiles of spectinamide1810 after single and multiple dose administration at the dose level of 50 and 200 mg/kg. The simulated median concentration-time profiles along with the 95% prediction intervals, overlaid by the observed concentrations, are shown in **Figure 6-3**.

Estimated Model Parameters and Predictive Performance for Healthy Mice

The estimated model parameters for IV and SC administration of spectinamide 1810 are listed in **Table 6-1**. Overall, the model predictions were in reasonable agreement with the observations, with less than twofold difference in the predicted and observed AUCs in plasma (**Table 6-2**) and tissues (**Table 6-3**).

Model Expansion to Infected Mice

Similar to spectinamide 1599, we have used the spectinamide 1810 subcutaneous model to simulate the plasma concentration-time profiles in a set of dose-ranging and dose fractionation studies that were performed in a standard mouse model of *Mtb* infection and were recently reported [18, 50, 52]. The model predictions were in reasonable agreement with the observations, as shown in the corresponding goodness-of-fit diagnostic plot of observed *vs*. predicted plasma concentrations in infected mice (**Figure 6-4**). Thus, the model developed for the healthy mice was able to predict the plasma concentration-time profiles in infected mice suggesting no significant difference in the pharmacokinetics of spectinamide 1810 between healthy and infected mice. This finding is in agreement with our previously published work [52].

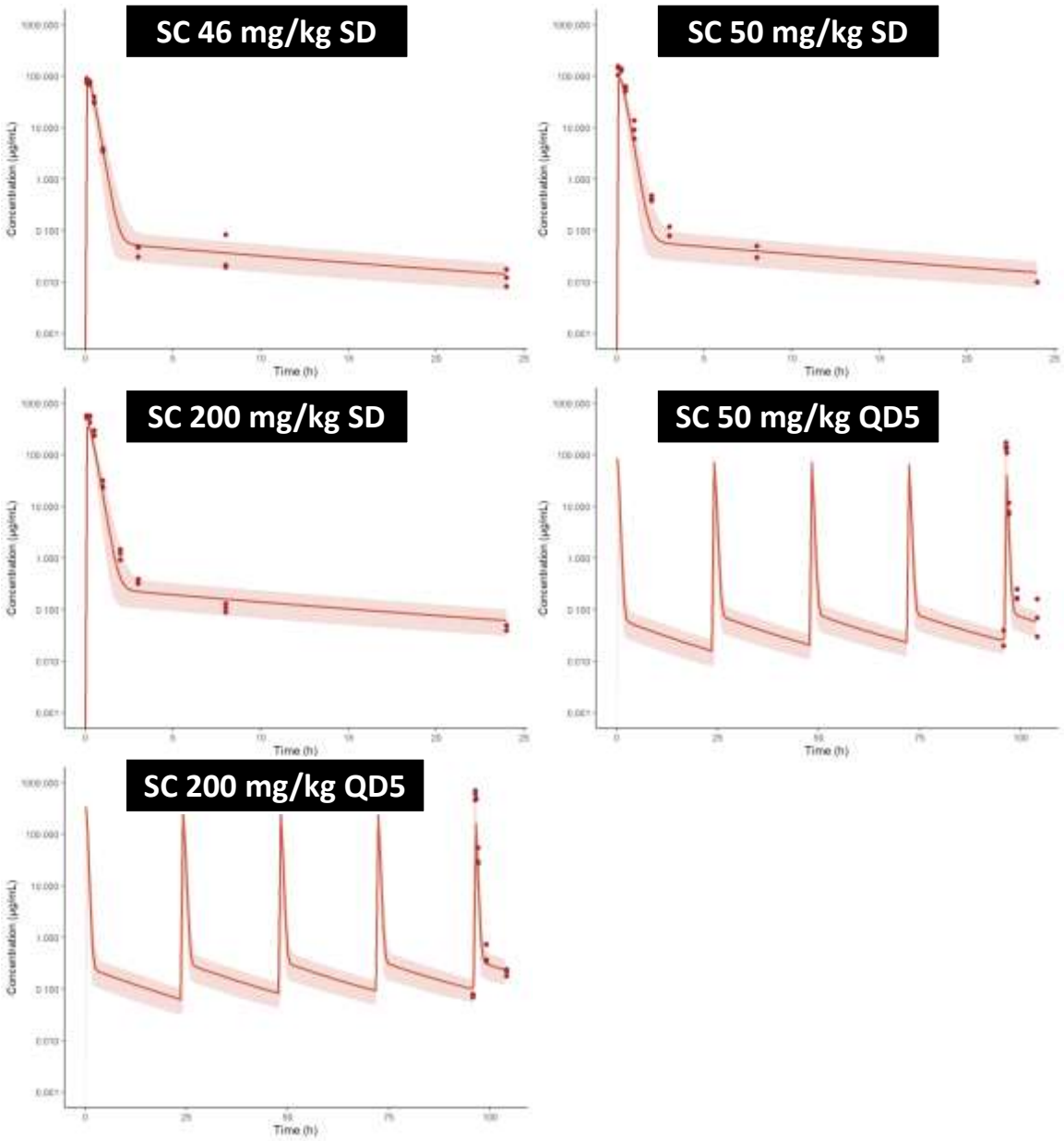

Figure 6-3. Concentration-time profiles of spectinamide 1810 in mouse plasma after single and multiple dose administration (QD5) of 46, 50, and 200 mg/kg (SC). The solid line represents the simulated median concentration profiles, and the shaded region is the 95% prediction interval overlaid by the experimentally observed concentrations represented by the dots. SC = subcutaneous, SD = single dose, QD5 = daily dosing for 5 consecutive days.

Table 6-1. Parameters, either fixed or estimated, used to build the PBPK model for spectinamide 1810.

Parameters	Description	Units	Intravenous Estimate (%RSE)	Subcutaneous Estimate (%RSE)
$K_{I\to C}^{Lung}$	1st order uptake from the rapid equilibrium sub compartment (V+I) to the cellular sub compartment of the **lung**	1/h	0.13 (16.0)	Fixed
$K_{C\to I}^{Lung}$	1st order backflux from the cellular sub compartment to the rapid equilibrium sub compartment of the **lung**	1/h	0.076 (17.6)	Fixed
$K_{I\to C}^{Liver}$	1st order uptake from the rapid equilibrium sub compartment (V+I) to the cellular sub compartment of the **liver**	1/h	1.19 (12.0)	Fixed
$K_{C\to I}^{Liver}$	1st order backflux from the cellular sub compartment to the rapid equilibrium sub compartment of the **liver**	1/h	0.051 (17.2)	Fixed
$K_{I\to C}^{Spleen}$	1st order uptake from the rapid equilibrium sub compartment (V+I) to the cellular sub compartment of the **spleen**	1/h	0.059 (23.1)	Fixed
$K_{C\to I}^{Spleen}$	1st order backflux from the cellular sub compartment to the rapid equilibrium sub compartment of the **spleen**	1/h	0.013 (120)	Fixed
$K_{I\to C}^{Kidney}$	1st order uptake from the rapid equilibrium sub compartment (V+I) to the cellular sub compartment of the **Kidney**	1/h	3.94 (43.9)	Fixed
$K_{C\to I}^{Kidney}$	1st order backflux from the cellular sub compartment to the rapid equilibrium sub compartment of the **Kidney**	1/h	0.097 (45.1)	Fixed
$K_{I\to C}^{Others}$	1st order uptake from the rapid equilibrium sub compartment (V+I) to the cellular sub compartment of the **other tissues**	1/h	4.77 (7.88)	Fixed
$K_{C\to I}^{others}$	1st order backflux from the cellular sub compartment to the rapid equilibrium sub compartment of the **other tissues**	1/h	7.0E-5 (0.00278)	Fixed
Ka	1st order absorption rate constant	-	-	8.26 (14.5)
F	Bioavailability component	-	-	1.00 (0.463)
ε_{Plasma}	Proportional error for plasma concentration-time profile		0.63 (15.1)	0.36 (15.6)
ε_{Lung}	Proportional error for lung concentration-time profile		0.30 (14.7)	0.30 (14.7)
ε_{Liver}	Proportional error for liver concentration-time profile		0.31 (14.7)	0.31 (14.7)
ε_{Spleen}	Proportional error for spleen concentration-time profile		0.43 (14.7)	0.43 (14.7)

RSE represents relative standard error; K represents first order rate constant; V+I represents the combined vascular and interstitial sub-compartments and ε is the residual unexplained variance.

Table 6-2. Predicted *versus* observed plasma exposure of spectinamide 1810 in healthy mice.

Study	AUClast (h*µg/mL)		
	Observed	**Median Predicted**	**Fold Difference**
IV SD 10 mg/kg	7.91	7.64	1.04
IV QD5 10 mg/kg	9.45	7.70	1.23
SC SD 46 mg/kg	38.6	36.8	1.05
SC SD 50 mg/kg	67.9	40.0	1.70
SC SD 200 mg/kg	267	160	1.67
SC QD5 50 mg/kg	65.5	40.3	1.63
SC QD5 200 mg/kg	265	161	1.65

AUClast = area under the plasma concentration-time curve to the last measurable plasma concentration; IV = intravenous; SC = subcutaneous; SD = single dose; QD5 = once daily for 5 consecutive days (Monday to Friday)

Table 6-3. Predicted *versus* observed exposure of spectinamide 1810 in lung, liver, and spleen.

Study	AUClast (h*µg/g)								
	Lung			**Liver**			**Spleen**		
	Observed	Predicted	Fold Difference	Observed	Predicted	Fold Difference	Observed	Predicted	Fold Difference
IV SD 10 mg/kg	5.75	8.53	1.48	31.6	25.2	1.25	4.29	4.43	1.03
IV QD5 10 mg/kg	11.2	9.79	1.14	51.2	37.4	1.37	9.45	7.91	1.19

AUClast = area under the tissue concentration-time curve to the last measurable tissue concentration; IV = intravenous; SD = single dose; QD5 = once daily dosing for 5 consecutive days (Monday to Friday).

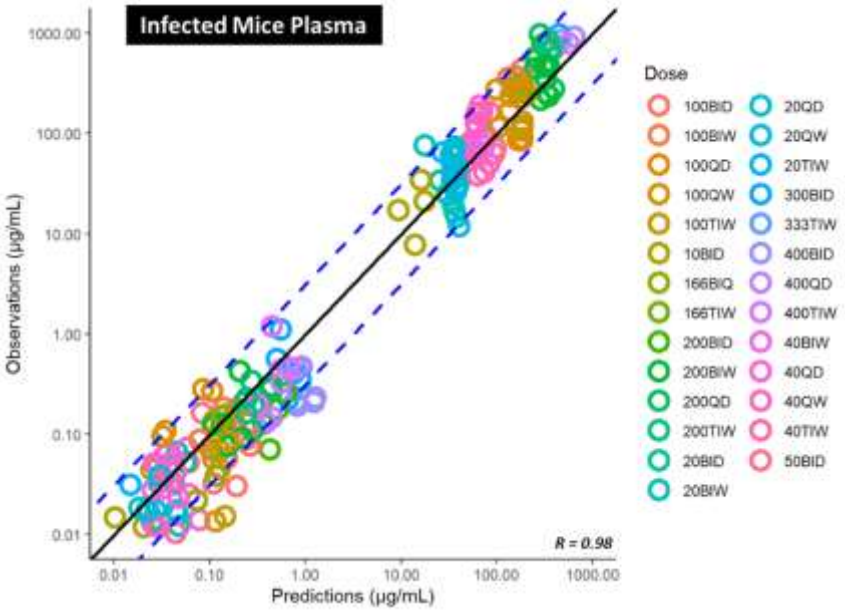

Figure 6-4. Predicted *versus* observed plasma concentrations (µg/mL) of spectinamide 1810 in infected mice after different dosing regimens using subcutaneous administration.

BID = twice daily; BIW = twice weekly; QD = once daily; QW = once weekly; TIW = thrice weekly. The solid black line represents the line of unity, dashed blue lines are the 2-fold deviation, the symbols are the observed concentrations, and the R value is the Pearson correlation coefficient between the observations and predictions.

CHAPTER 7. INTER-SPECIES EXTRAPOLATION OF THE PBPK MODEL[6]

Introduction

After the successful inter-route extrapolation of the model, we scaled the PBPK model between species by extending the model to rats. This was accomplished by incorporating the physiological parameters of a 225 g rat and updating the experimentally assessed drug specific parameters, k(b/p) and *fu*. The structural model was unchanged, and the model's estimated parameters (tissue influx and backflux rate constants) were fixed as well. Simulations were performed to predict the plasma and tissue PK profiles of spectinamide 1599 and 1810 after single dose administration *via* the intravenous route.

Results

Model Expansion to Rat for Spectinamide 1599

The scaled model was used to simulate the plasma and tissue concentration-time profiles after 10 mg/kg single dose intravenous administration of spectinamide 1599. Predicted profiles in rat plasma, lung, liver, and spleen were overlaid by the observations obtained after intravenous single dose administration of spectinamide 1599 (10 mg/kg) to healthy rats. While the plasma concentrations were in good agreement, the concentrations in the lung, liver, and spleen were slightly underpredicted compared to the observations. We believe this is most likely due to residual blood in the collected tissues, since the tissues were not perfused prior to harvesting.

We combined the mouse and rat model into a single integrated PBPK model for spectinamide 1599 that provides a single code structure that can estimate the parameters by fitting the model to the observed data in both species. We also estimated the inter-individual variability on the influx rate constant of lung, liver, spleen, and 'other tissue' by fitting the model to the mouse and rat data (plasma and tissues) after intravenous single dose administration of spectinamide 1599. The inter-individual variability (ω^2) was estimated as the variance ranging from 0.48 - 0.87, which corresponds to 69 to 93 %CV in the tissue concentrations in rats and mice. The predicted profiles (median and predictive intervals) overlaid by the observation in plasma and tissues are shown in **Figures 7-1** and **7-2**, respectively.

---

[6] Modified from to-be-submitted article with permission. Keyur Parmar, Pradeep B. Lukka, Santosh Wagh, Zaid Temrikar, Richard E. Lee, Miriam Braunstein, Anthony J. Hickey, Gregory T. Robertson, Mercedes Gonzalez-Juarrero, Andrea Edginton and Bernd Meibohm. Development of a Minimalistic Physiologically-Based Pharmacokinetic (mPBPK) Model for the Preclinical Development of Spectinamide Antibiotics.

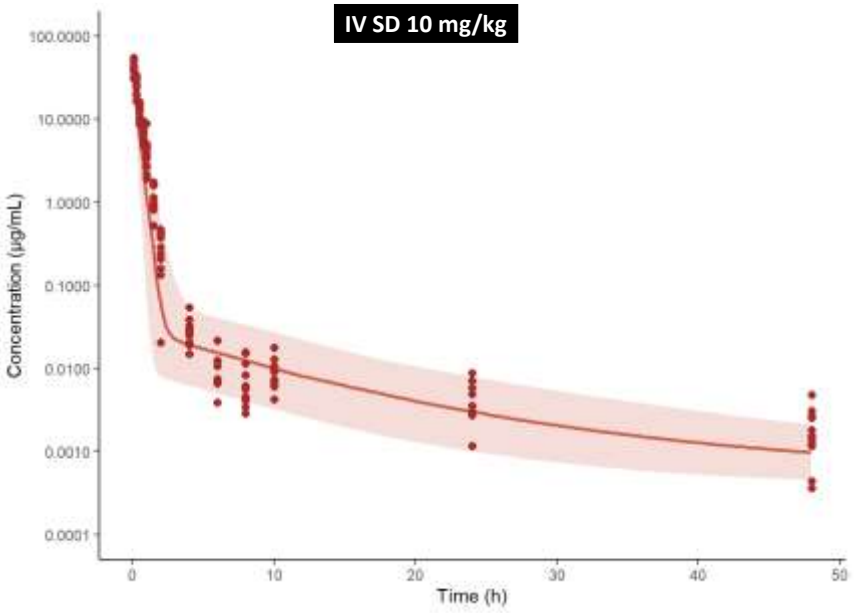

Figure 7-1. Concentration-time profiles of spectinamide 1599 in rat plasma after intravenous administration of 10 mg/kg.
The solid line represents the simulated median concentration profiles, and the shaded region is the 95% prediction interval overlaid by the experimentally observed concentrations represented by dots.

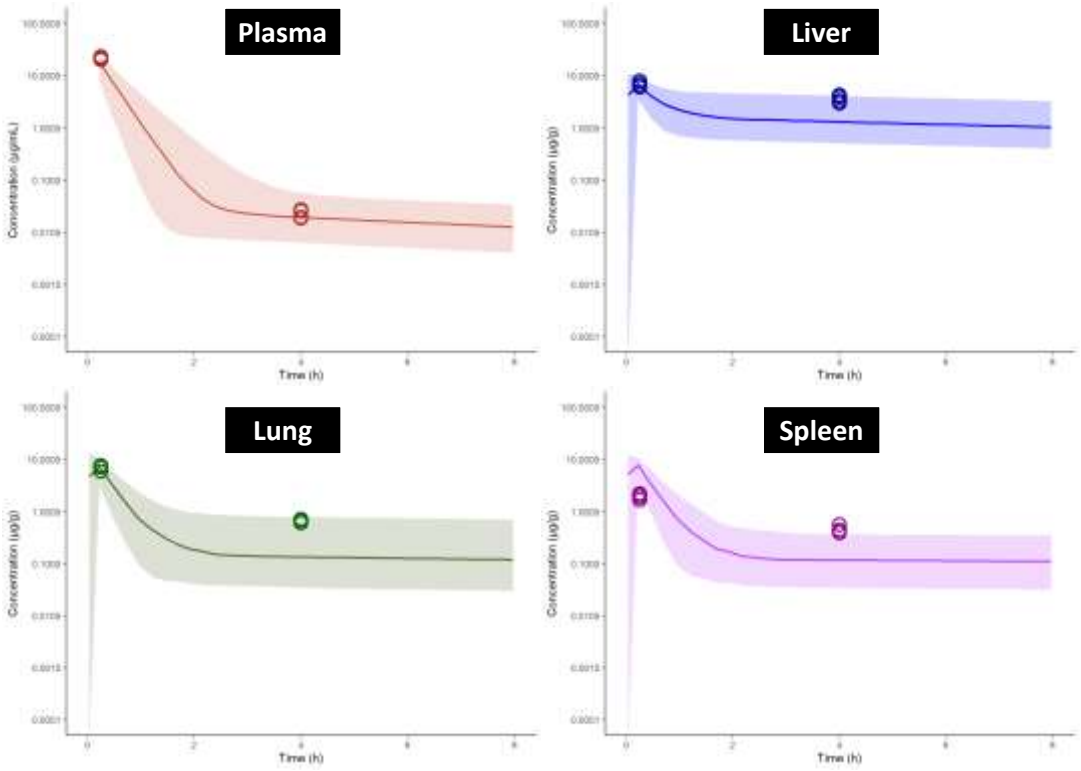

Figure 7-2. Concentration-time profiles of spectinamide 1599 in rat plasma and tissues after intravenous administration of 10 mg/kg.
Plasma (µg/mL); Liver (µg/g); Lung (µg/g); and Spleen (µg/g). The solid line represents the simulated median concentration profiles, and the shaded region is the 95% prediction interval overlaid by the experimentally observed concentrations represented by open circles.

Model Expansion to Rat for Spectinamide 1810

Similarly, we have scaled the spectinamide 1810 model to rats. The scaled model was used to simulate the plasma concentration-time profile after 10 mg/kg single dose intravenous administration of spectinamide 1810. Predicted plasma profile in rat was overlaid by the observations obtained after intravenous single dose administration of spectinamide 1810 (10 mg/kg) to healthy rats, as shown in **Figure 7-3**.

Overall, the model predictions were in reasonable agreement with the observations. The observed *vs.* predicted AUCs for both the compounds in rat plasma are shown in **Table 7-1**.

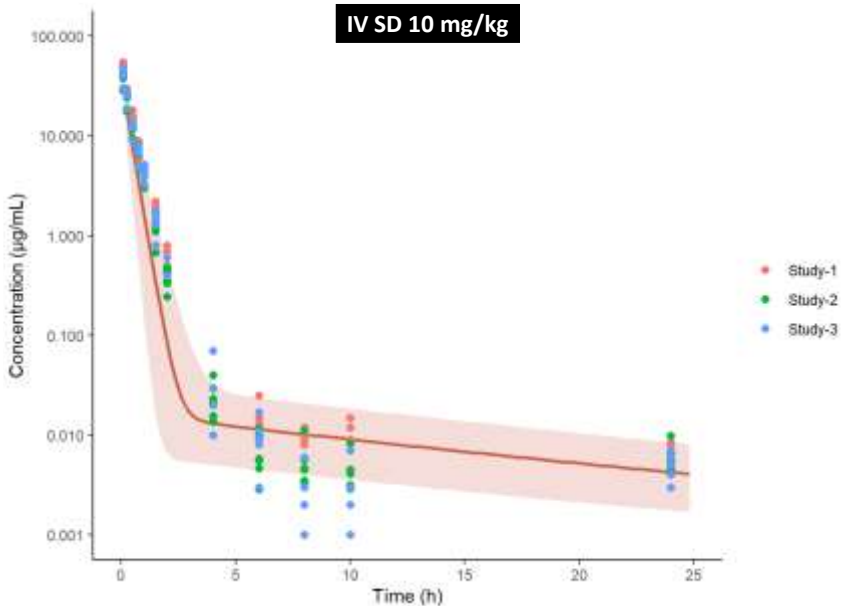

Figure 7-3. Concentration-time profiles of spectinamide 1810 in rat plasma after intravenous administration of 10 mg/kg.
The solid line represents the simulated median concentration-time profile, and the shaded region is the 95% prediction interval overlaid by the experimentally observed concentrations represented by dots. Different colors represent different studies that were performed.

Table 7-1. Predicted *versus* observed plasma exposure of spectinamide 1599 and 1810 in healthy rats.

Compounds	AUClast (h*µg/mL)		
	Observed	Median Predicted	Fold Difference
Spectinamide 1599	19.8	12.5	1.58
Spectinamide 1810	20.8	12.9	1.61

AUClast = under the plasma concentration-time curve to the last measurable plasma concentration.

CHAPTER 8. RELATIVE DRUG EXPOSURE IN GRANULOMATOUS LESION SUBSTRUCTURES[7]

Introduction

A hallmark feature of pulmonary *Mtb* infection in humans is the formation of distinct caseous granuloma that may harbor a substantial number of bacilli [55]. One of the recurrent questions and challenges in anti-TB drug development is therefore to assess the exposure of new drug candidates not only in the interstitial subcompartment of the lungs but also in the substructures of granulomatous lesions [56].

Methodology

While we did not have experimental data to build and implement granulomatous lesions into our murine PBPK model, we utilized the established multicompartmental human PBPK model of the lung and granuloma within the Simcyp simulator V21 R1 (Certara, Sheffield, UK) to translate our experimentally observed drug exposures in the lung intestinal subcompartment into relative drug exposures in different granuloma substructures. This allowed us to gain an understanding of the relative relationships between exposures in different lesion compartments and the lung interstitial sub-compartment under the assumption that similar exposures in the lung interstitial sub-compartments as experimentally observed in our rodent studies could also be achieved in humans.

As described by Gaohua et al., the mechanistic multicompartment permeability-limited lung model in the Simcyp simulator consists of 7 segments representing the upper and lower airways (2 segments) and the lobes of the lung (5 segments). Each segment is divided into four compartments (blood, mass, fluid, and air) [24]. This lung model has been extended to incorporate five additional compartments (capillary blood, interstitial fluid, macrophage, inner caseum and outer caseum) representing the granuloma in the lung of patients with TB [57]. A schematic diagram to explain the overall structure of the granuloma adopted from the Simcyp model structure is shown in **Figure 8-1**. The drug-specific parameters utilized to define the compound (spectinamide 1599) within the Simcyp simulator were molecular weight (486.95), cLogP (-2.52), pKa as diprotic base (8.69 and 6.95), and *fu* and k(b/p), as mentioned in **Chapter 3**. The model calculated effective passive permeability (13.9×10^{-4} cm/s), and Simcyp was used to define the distribution of spectinamide 1599 within the granuloma compartments.

[7] Modified from to-be-submitted article with permission. Keyur Parmar, Pradeep B. Lukka, Santosh Wagh, Zaid Temrikar, Richard E. Lee, Miriam Braunstein, Anthony J. Hickey, Gregory T. Robertson, Mercedes Gonzalez-Juarrero, Andrea Edginton and Bernd Meibohm. Development of a Minimalistic Physiologically-Based Pharmacokinetic (mPBPK) Model for the Preclinical Development of Spectinamide Antibiotics.

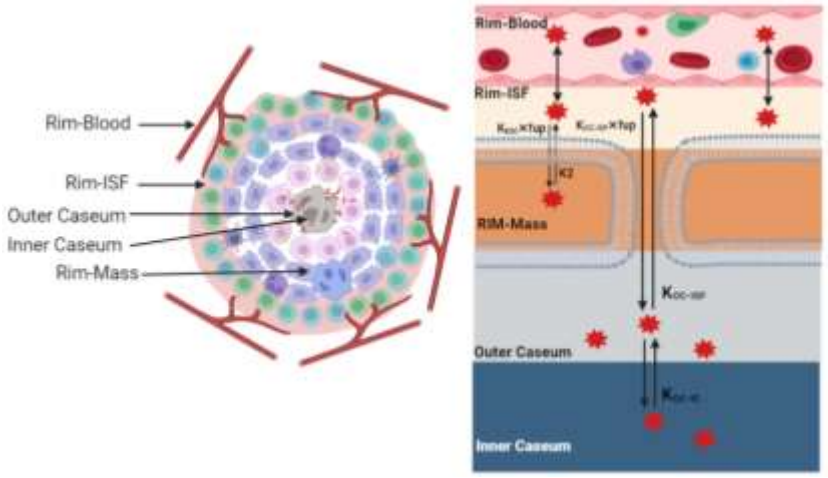

Figure 8-1. Schematic diagram representing the granulomatous lesion substructures.

Rim-Blood = outer rim of blood capillaries; Rim-ISF = rim interstitial fluid; Rim-Mass = rim of macrophages; Inner and Outer Caseum = the necrotic caseum (inner and outer); "K"= the permeability; *fu* = the fraction of drug unbound to plasma protein.

Results

We used the multicompartment permeability-limited lung model with an active granuloma model within the Simcyp simulator to perform an exploratory assessment of relative exposures between the various granuloma substructures. The granuloma structure within the Simcyp simulator consisted of an outer rim of blood capillaries and interstitial fluid enclosing a rim of macrophages and necrotic caseum (outer and inner). This was achieved by conducting simulations that achieved similar steady state concentrations (C_{ss}) of spectinamide 1599 in plasma and the pulmonary blood reservoir (PBR) compartment of the Simcyp lung model, similar to the observed C_{ss} in the plasma and the rapid equilibrium compartment of lung obtained following the efficacious subcutaneous dose of 200 mg/kg (QD5) in the standard mouse model of TB infection [4]. **Figure 8-2** shows the comparative C_{ss} of spectinamide 1599 in plasma and pulmonary blood reservoir (observed and simulated). While the mean C_{ss} in the capillary blood of the granuloma was the same as the C_{ss} in PBR, the C_{ss} in rim-interstitial fluid (rim-ISF) was 5.7-fold higher than PBR. Also, the simulation showed a ~57% lower C_{ss} in the caseum of the granuloma compared to the PBR, while the C_{ss} in the macrophage was more than 8,000-fold higher than PBR.

Spectinamide 1599 is reported to have a concentration-dependent intracellular uptake into the murine lung-derived dendritic cells and Balb/c-derived monocyte macrophage cell line [16]. The simulated terminal half-life of spectinamide 1599 in the rim-macrophage (58 h) was 7.45-fold greater than the terminal half-life in the rim-blood (7.75 h). This slower elimination from the intracellular to the interstitial space, since the distribution is permeability limited, could explain the accumulation of spectinamide 1599 in the intracellular space, as reported for moxifloxacin [58]. The substantial accumulation in the macrophages suggests that spectinamide 1599 might be efficacious in clearing the intracellular bacilli.

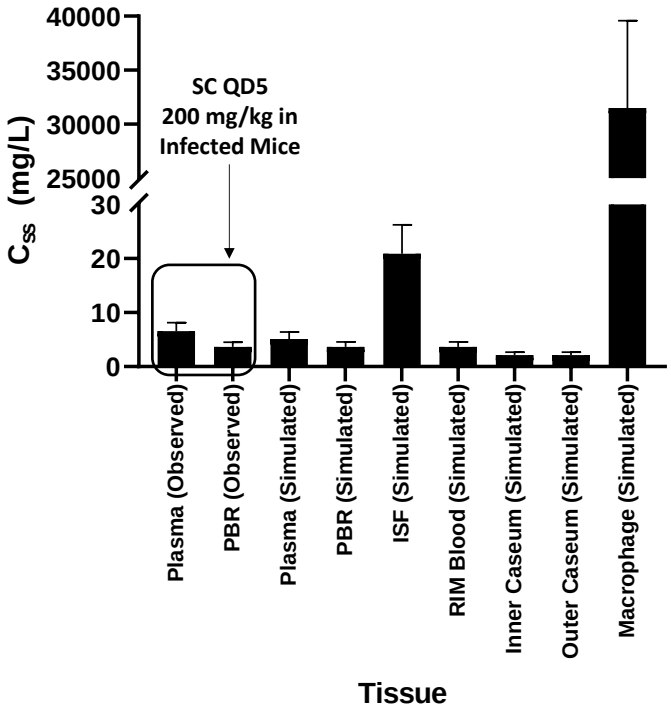

Figure 8-2. Observed and simulated steady state concentrations (mg/L) of spectinamide 1599 in plasma, pulmonary blood reservoir (PBR), rim-interstitial fluid, rim-capillary blood, macrophages, inner and outer caseum.
SC = subcutaneous; QD5 = once daily for 5 consecutive days.

CHAPTER 9. SUMMARY

Characterizing the disposition of a compound in the tissues of interest is important in understanding the pharmacology of novel antibiotic agents. TB is primarily a pulmonary disease, but extrapulmonary manifestations have been reported in 10-42% of patients [19]. Thus, understanding the drug disposition and exposure in the tissues in which *Mtb* is residing is of utmost importance for any new antitubercular drug.

In this study we used PBPK modeling to integrate preclinical *in vivo* pharmacokinetic data for an investigational class of anti-tuberculosis compounds from numerous experiments comprising different dosing regimens, routes of administration, disease status, and species to characterize their disposition behavior. We had hypothesized that a common PBPK model can be developed for spectinamide 1599 and 1810 that can reliably and accurately predict the concentration-time profiles in tissues relevant for *Mtb* infection across various dose-levels, dosing frequencies, routes of administration, health conditions (infected and uninfected), and different species.

We chose a minimalistic PBPK modelling approach because of its three major advantages over empirical pharmacokinetic approaches:

1. Richer information content: The model utilizes both drug-independent (organ volumes, blood flow rates, and other physiological parameters) and drug-specific (*fu*, k(b/p) permeability, clearance mechanism, etc.) parameters;
2. Modular structure: The model compartmentalization is derived from the anatomical structure of the body, which allows it to be adjusted for different conditions (e.g., disease status) and different routes of administration; and
3. Universality: The PBPK model structure is common across all mammalian species. This enables to scale the model from one species to another [1].

These features allowed the applicability of a PBPK model to describe the disposition of spectinamide compounds in plasma and tissues across various dosing levels, regimens, routes of administration, and species. Thus, the objective of this modeling exercise was to build a platform PBPK model which could be leveraged to predict the dose and regimens required to achieve desired drug exposures in target tissues relevant for TB infection in different preclinical species, and ultimately in humans.

As first step, we compiled the physiological parameters relevant for the investigated species and integrated them with experimentally measured or calculated drug-specific parameters into a structural model. Both spectinamides considered, 1599 and 1810, exhibit low plasma protein binding in mouse and rat, and measured unbound percentages ranged from 56 to 70%. The measured blood to plasma ratio of 0.5 to 0.8 for both of the compounds in mouse and rat blood reflects a preferential distribution in plasma as compared to the blood cells. In the PBPK model, the blood-to-plasma ratio was used to convert the model predicted blood concentrations to plasma concentrations, as determined in our experimental PK studies.

As a subsequent step, we decided on the model structure based on the available biphasic pharmacokinetic profiles in plasma and tissues for mice and rats [13, 14, 18, 52]. The dynamic pharmacokinetic processes within the model compartments and sub-compartments were described in terms of linear ordinary differential equations written in MlxTran format. The model parameters were estimated using a stochastic approximation expectation-maximization (SAEM) algorithm by fitting the model to the observed plasma and tissue data obtained after intravenous administration.

We assumed a rapid equilibrium between the vascular and the interstitial or extracellular space of a tissue by modeling them together. The distribution between the rapid equilibrium compartment and the cellular space was assumed to be permeability limited. The membrane permeation clearance is represented by the product of $K_{I\rightarrow C}^{Tissue}$, volume (interstitial and vascular) and the fraction unbound in plasma. The estimated membrane permeation clearance values for all the tissues (lung, liver, spleen, kidney, other) were substantially lower than the organ blood flow rates (Q_T), which supports our assumption of permeability-limited distribution.

One limitation of this approach is that these parameters are estimated by fitting the model to the data, making it more empirical than mechanistic. A more mechanistic approach would be to use the permeability surface area product as a membrane permeation clearance. However, we were unable to experimentally determine the passive permeability of spectinamides 1599 and 1810 with the parallel artificial membrane permeability assay (PAMPA) since spectinamides have very limited passive membrane permeability due to their high hydrophilicity and the concentrations in the acceptor compartment were below the limit of detection for the applied assay.

Therefore, we decided to estimate influx and backflux rate constants using the intravenous model fitting to the data obtained after single dose (10 mg/kg) administration and subsequent qualification of the model by comparing model-based predictions to data obtained after an intravenous multiple dose (10 mg/kg QD5) study. Thereafter, the model was expanded to include the subcutaneous route of administration by incorporating a subcutaneous dosing compartment. The estimated first-order absorption half-life from the subcutaneous administration site for spectinamides 1599 and 1810 was ~10 and 5 min, respectively, and the bioavailability was 86 and 100%, respectively. The subcutaneous model was used to simulate an extensive set of dose-ranging and dose fractionation studies for spectinamide 1599 and 1810 in the *Mtb* infected mice [50]. A total of 23 dose groups for spectinamide 1599 ranging from 10 to 2,000 mg/kg of total weekly dose were simulated and verified against the experimental observations. For spectinamide 1810, a total of 26 dose groups ranging from 20 to 4,000 mg/kg of total weekly dose were simulated and verified against the observations. The model predictions were in reasonable agreement with the observations for both spectinamides 1599 and 1810. This finding suggests that there is no significant difference in the pharmacokinetics of spectinamide 1599 and 1810 between healthy and infected animals, which is in agreement with our previously published work [52].

The intravenous model was also expanded to include the IPA route of administration by incorporating an external dosing compartment linked to the ELF compartment of the lung *via* a first-order absorption rate constant corrected for bioavailability. The estimated absorption half-life and bioavailability from the IPA administration site for spectinamide 1599 were ~8 min and 33%, respectively. The model was used to simulate single and multiple dose (QD5, TIW, and BIW) groups ranging from 10 to 150 mg/kg of total daily dose of spectinamide 1599 and verified against the observations. Overall, we successfully used the developed PBPK model in performing inter-route and inter-drug extrapolation.

The inter-species extrapolation from mouse to rat was achieved by incorporating the physiological parameters of a healthy rat and updating the experimentally assessed drug-specific parameters [*fu* and k(b/p)], while fixing the distribution parameters (tissue influx and backflux) estimated from the intravenous mouse model. The model predicted concentration-time profiles in rat plasma were in reasonable agreement. However, the predicted concentrations in rat tissues (lung, liver, and spleen) were slightly underpredicted compared to the observations. This disagreement shows the variability in the tissue concentrations in mice and rats, which we hypothesized is due to the residual blood in the collected tissues, particularly in rats [59]. It would be interesting to test this hypothesis by performing a whole-body perfusion before harvesting the tissues, followed by measuring the concentration levels. However, this disagreement also exposed a potential limitation of our approach—that is, the overreliance on one dataset at one dose level (10 mg/kg) used for the estimation of the model parameters, assuming dose-independent, linear pharmacokinetics of spectinamide 1599 and 1810. The latter, however, was reasonably well justified, as we had extensive PK data over a dose range of 10 to 400 mg/kg in mice that did not suggest any dose-dependencies in disposition of these compounds [18, 52].

Another potential limitation of the model is that we did not account for the cellular uptake or sequestration of the spectinamide compounds in the macrophage or dendritic cells, as previously reported [16]. This binding or trapping phenomenon could be a plausible reason for the slower elimination of the compound from the intracellular space and thus responsible for the higher concentrations at the terminal phase than the plasma concentrations. However, we did not observe lysosomal trapping of the spectinamide compounds in the Fa2N-4 cell line in which the uptake was mediated only by passive diffusion. Also, based on the results obtained from PAMPA assay, we were unable to determine the passive permeability of spectinamide compounds. Thus, an active or facilitated transport mechanism could be responsible for the cellular uptake of the spectinamide compounds, which needs to be explored in the future.

Lastly, we performed an exploratory evaluation of relative steady state concentrations (C_{ss}) of spectinamide 1599 in different granuloma compartments under the assumption that drug C_{ss} in plasma and the interstitial subcompartment of the lungs as observed in the standard mouse model of TB infection at a therapeutically efficacious dosing regimen could also be achieved in humans. The established granuloma model in the human Simcyp PBPK simulator was used to explore the disposition of spectinamide

1599 in granuloma compartments such as rim-interstitial fluid where extracellular bacteria reside, in macrophages where intracellular bacteria reside, and in caseum (inner and outer) where non-replicating bacteria reside [57]. The simulations suggested that spectinamide 1599 achieves a substantially higher exposure in the rim-ISF compared to the C_{ss} in PBR and accumulates in the alveolar macrophages, suggesting that spectinamide 1599 might be efficacious in clearing the intra- and extracellular *Mtb*, while the lower C_{ss} in the inner and outer caseum could suggest still substantial but lower efficacy towards the non-replicating *Mtb* phenotypes. Lesion distribution studies of spectinamides 1599 and 1810 in mouse models of chronic TB infection with pulmonary lesions are ongoing to further explore these hypotheses.

The model could be further extended to incorporate the pharmacodynamic (PD) component to understand the drug exposure needed to effectively eliminate the intra- and extracellular bacilli. The log reduction in the *Mtb* colony forming unit (CFU) data obtained from the dose ranging and fractionation study in the murine model of *Mtb* infection could be used along with the PBPK model predicted lung interstitial and intracellular concentrations. Also, the PD data obtained from the *in vitro* hollow fiber system could be used to explore the drug concentrations or exposures mediated antibacterial efficacy of the spectinamide compounds. Treatment of tuberculosis requires multiple drug therapy, first-line as well as second line, and thus it is imperative to understand the PK and PD of spectinamide compounds in combination with the standard anti-TB therapy. PBPK modeling approach is most appropriate in studying the drug-drug interactions and to study the synergy in the antibacterial activity between various combinations of drugs, which could be achieved by further evolving and refining this PBPK model.

In conclusion, the developed murine PBPK model was able to characterize and simultaneously predict plasma and tissue pharmacokinetic profiles of spectinamide 1599. The model was successfully expanded and accounted for a) various routes of administration, including intravenous, subcutaneous, and intrapulmonary aerosol delivery; b) healthy and infected animals; c) different species, mice, and rats; and d) another structurally similar compound, spectinamide 1810. The lesion distribution simulations performed on Simcyp showed higher steady state concentration (C_{ss}) in the rim-interstitial fluid and alveolar macrophages than in plasma, suggesting good tissue penetration for potential efficacy in clearing intra- and extracellular *Mtb*. The simulations also demonstrated a decent penetration of spectinamide 1599 in the necrotic caseum, suggesting substantial exposure in all lesion compartments. The overall modeling approach may be leveraged as an effective tool in planning and designing future development activities for spectinamide 1599 and 1810 in higher species in the context of a model-informed drug development (MIDD) paradigm [60].

LIST OF REFERENCES

1. Nestorov, I., *Whole body pharmacokinetic models.* J Clinical pharmacokinetics, 2003. **42**(10): p. 883-908.
2. Espié, P., et al., *Physiologically based pharmacokinetics (PBPK).* J Drug metabolism reviews, 2009. **41**(3): p. 391-407.
3. Shebley, M., et al., *Physiologically based pharmacokinetic model qualification and reporting procedures for regulatory submissions: a consortium perspective.* J Clinical Pharmacology Therapeutics, 2018. **104**(1): p. 88-110.
4. Cao, Y. and W.J. Jusko, *Applications of minimal physiologically-based pharmacokinetic models.* J Journal of pharmacokinetics pharmacodynamics, 2012. **39**(6): p. 711-723.
5. Bloomingdale, P., et al., *Minimal brain PBPK model to support the preclinical and clinical development of antibody therapeutics for CNS diseases.* Journal of Pharmacokinetics and Pharmacodynamics, 2021. **48**(6): p. 861-871.
6. Arya, V., et al., *Utilizing PBPK modeling to evaluate the potential of a significant drug–drug interaction between clopidogrel and dasabuvir: a scientific perspective.* Clinical Pharmacology & Therapeutics, 2017. **102**(4): p. 578-580.
7. Shebley, M., et al., *Physiologically based pharmacokinetic modeling suggests limited drug–drug interaction between clopidogrel and dasabuvir.* Clinical Pharmacology & Therapeutics, 2017. **102**(4): p. 679-687.
8. Jones, H., et al., *Physiologically based pharmacokinetic modeling in drug discovery and development: a pharmaceutical industry perspective.* Clinical Pharmacology & Therapeutics, 2015. **97**(3): p. 247-262.
9. Zhang, X., et al., *Application of PBPK modeling and simulation for regulatory decision making and its impact on US prescribing information: an update on the 2018-2019 submissions to the US FDA's office of clinical pharmacology.* The Journal of Clinical Pharmacology, 2020. **60**: p. S160-S178.
10. Lee, R.E., et al., *Spectinamides: a new class of semisynthetic antituberculosis agents that overcome native drug efflux.* Nature medicine, 2014. **20**(2): p. 152-158.
11. Liu, J., et al., *Structure–activity relationships of spectinamide antituberculosis agents: a dissection of ribosomal inhibition and native efflux avoidance contributions.* ACS infectious diseases, 2017. **3**(1): p. 72-88.
12. Golfar, Y. and A. Shayanfar, *Prediction of biopharmaceutical drug disposition classification system (BDDCS) by structural parameters.* Journal of Pharmacy & Pharmaceutical Sciences, 2019. **22**: p. 247-269.
13. Robertson, G.T., et al., *Spectinamides are effective partner agents for the treatment of tuberculosis in multiple mouse infection models.* J Journal of Antimicrobial Chemotherapy, 2016. **72**(3): p. 770-777.
14. Rathi, C., et al., *Comparative pharmacokinetics of spectinamide 1599 after subcutaneous and intrapulmonary aerosol administration in mice.* J Tuberculosis, 2019. **114**: p. 119-122.
15. *Tuberculosis*. Available from: https://www.who.int/tb/areas-of-work/drug-resistant-tb/en/.

16. Santos, K., et al., *Primary lung dendritic cell cultures to assess efficacy of spectinamide-1599 against intracellular Mycobacterium tuberculosis.* J Frontiers in microbiology, 2018. **9**: p. 1895.
17. *Working Group on New TB Drugs*. Available from: https://www.newtbdrugs.org/pipeline/clinical.
18. Gonzalez-Juarrero, M., et al., *Preclinical Evaluation of Inhalational Spectinamide-1599 Therapy against Tuberculosis.* ACS infectious diseases, 2021. **7**(10): p. 2850-2863.
19. Zumla, A., et al., *current concepts: Tuberculosis.* N Engl J Med, 2013. **368**: p. 745-55.
20. Ings, R., *Interspecies scaling and comparisons in drug development and toxicokinetics.* Xenobiotica, 1990. **20**(11): p. 1201-1231.
21. Mordenti, J., *Man versus beast: pharmacokinetic scaling in mammals.* Journal of pharmaceutical sciences, 1986. **75**(11): p. 1028-1040.
22. Ruelius, H.W., *Extrapolation from animals to man: predictions, pitfalls and perspectives.* Xenobiotica, 1987. **17**(3): p. 255-265.
23. SAWADA, Y., et al., *Prediction of the plasma concentration time courses of various drugs in humans based on data from rats.* Journal of pharmacobio-dynamics, 1985. **8**(9): p. 757-766.
24. Gaohua, L., et al., *Development of a multicompartment permeability-limited lung PBPK model and its application in predicting pulmonary pharmacokinetics of antituberculosis drugs.* CPT: pharmacometrics & systems pharmacology, 2015. **4**(10): p. 605-613.
25. Poulin, P. and F.P. Theil, *Prediction of pharmacokinetics prior to in vivo studies. 1. Mechanism-based prediction of volume of distribution.* J Journal of pharmaceutical sciences, 2002. **91**(1): p. 129-156.
26. Poulin, P. and F.P. Theil, *Prediction of pharmacokinetics prior to in vivo studies. II. Generic physiologically based pharmacokinetic models of drug disposition.* J Journal of pharmaceutical sciences, 2002. **91**(5): p. 1358-1370.
27. Wenlock, M.C., et al., *A method for measuring the lipophilicity of compounds in mixtures of 10.* journal of Biomolecular screening, 2011. **16**(3): p. 348-355.
28. Rodgers, T., D. Leahy, and M. Rowland, *Physiologically based pharmacokinetic modeling 1: predicting the tissue distribution of moderate-to-strong bases.* J Journal of pharmaceutical sciences, 2005. **94**(6): p. 1259-1276.
29. Wohnsland, F. and B. Faller, *High-throughput permeability pH profile and high-throughput alkane/water log P with artificial membranes.* Journal of medicinal chemistry, 2001. **44**(6): p. 923-930.
30. Di, L., et al., *High throughput artificial membrane permeability assay for blood–brain barrier.* European journal of medicinal chemistry, 2003. **38**(3): p. 223-232.
31. Nasu, R., et al., *Physiologically based pharmacokinetic model for pralmorelin hydrochloride in rats.* J Drug metabolism disposition, 2005. **33**(10): p. 1488-1494.
32. Wen, Z., et al., *Determination of red blood cell partitioning and whole blood to plasma ratio using human, rat, and mouse blood: Methods, model compounds and species differences.* AAPSJ abstracts W, 2010. **4305**.

33. Yu, S., et al., *A novel liquid chromatography/tandem mass spectrometry based depletion method for measuring red blood cell partitioning of pharmaceutical compounds in drug discovery.* Rapid Communications in Mass Spectrometry: An International Journal Devoted to the Rapid Dissemination of Up-to-the-Minute Research in Mass Spectrometry, 2005. **19**(2): p. 250-254.
34. Kariv, I., H. Cao, and K.R. Oldenburg, *Development of a high throughput equilibrium dialysis method.* Journal of pharmaceutical sciences, 2001. **90**(5): p. 580-587.
35. Bachmann, K. and R. Ghosh, *The use of in vitro methods to predict in vivo pharmacokinetics and drug interactions.* Current drug metabolism, 2001. **2**(3): p. 299-314.
36. Obach, R.S., *Prediction of human clearance of twenty-nine drugs from hepatic microsomal intrinsic clearance data: an examination of in vitro half-life approach and nonspecific binding to microsomes.* Drug Metabolism and Disposition, 1999. **27**(11): p. 1350-1359.
37. Kazmi, F., et al., *Lysosomal sequestration (trapping) of lipophilic amine (cationic amphiphilic) drugs in immortalized human hepatocytes (Fa2N-4 cells).* Drug Metabolism and Disposition, 2013. **41**(4): p. 897-905.
38. Aki, T., A. Nara, and K. Uemura, *Cytoplasmic vacuolization during exposure to drugs and other substances.* Cell biology and toxicology, 2012. **28**(3): p. 125-131.
39. Neuvonen, P.J., M. Niemi, and J.T. Backman, *Drug interactions with lipid-lowering drugs: mechanisms and clinical relevance.* Clinical Pharmacology & Therapeutics, 2006. **80**(6): p. 565-581.
40. Chadwick, B., D.G. Waller, and J.G. Edwards, *Potentially hazardous drug interactions with psychotropics.* Advances in Psychiatric treatment, 2005. **11**(6): p. 440-449.
41. Daniel, W. and J. Wojcikowski, *The role of lysosomes in the cellular distribution of thioridazine and potential drug interactions.* Toxicology and applied pharmacology, 1999. **158**(2): p. 115-124.
42. Funk, R.S. and J.P. Krise, *Cationic amphiphilic drugs cause a marked expansion of apparent lysosomal volume: implications for an intracellular distribution-based drug interaction.* Molecular pharmaceutics, 2012. **9**(5): p. 1384-1395.
43. Logan, R., et al., *Drug-drug interactions involving lysosomes: mechanisms and potential clinical implications.* Expert opinion on drug metabolism & toxicology, 2012. **8**(8): p. 943-958.
44. Kornhauser, D.M., R.E. Vestal, and D.G. Shand, *Uptake of propranolol by the lung and its displacement by other drugs: involvement of the alveolar macrophage.* Pharmacology, 1980. **20**(5): p. 275-283.
45. Hariparsad, N., et al., *Comparison of immortalized Fa2N-4 cells and human hepatocytes as in vitro models for cytochrome P450 induction.* Drug Metabolism and Disposition, 2008. **36**(6): p. 1046-1055.
46. Duvvuri, M., et al., *Weak base permeability characteristics influence the intracellular sequestration site in the multidrug-resistant human leukemic cell line HL-60.* Journal of Biological Chemistry, 2004. **279**(31): p. 32367-32372.
47. Davies, B. and T. Morris, *Physiological parameters in laboratory animals and humans.* Pharmaceutical research, 1993. **10**(7): p. 1093-1095.

48. Fröhlich, E., et al., *Measurements of deposition, lung surface area and lung fluid for simulation of inhaled compounds.* Frontiers in pharmacology, 2016. **7**: p. 181.
49. Shah, D.K. and A.M. Betts, *Towards a platform PBPK model to characterize the plasma and tissue disposition of monoclonal antibodies in preclinical species and human.* Journal of pharmacokinetics and pharmacodynamics, 2012. **39**(1): p. 67-86.
50. Wagh, S.J., *Model-Based Dose-Exposure-Response Assessment for Lead and Backup Spectinamide in a Mouse Model of Tuberculosis*. 2020, University of Tennessee Health Science Center: Memphis, Tennessee.
51. Rathi, C., *Translational Pharmacokinetic-Pharmacodynamic Modeling and Simulation in the Development of Spectinamides, a Novel Class of Anti-Tuberculosis Agents*. 2017, The University of Tennessee Health Science Center: Memphis, Tennessee.
52. Wagh, S., et al., *Model-based exposure-response assessment for spectinamide 1810 in a mouse model of tuberculosis.* Antimicrobial Agents and Chemotherapy, 2021. **65**(11): p. e01744-20.
53. Chan, P.L., et al., *The use of the SAEM algorithm in MONOLIX software for estimation of population pharmacokinetic-pharmacodynamic-viral dynamics parameters of maraviroc in asymptomatic HIV subjects.* Journal of pharmacokinetics and pharmacodynamics, 2011. **38**(1): p. 41-61.
54. Wickham, H., *Package 'ggplot2': elegant graphics for data analysis.* Springer-Verlag New York. doi, 2016. **10**: p. 978-0.
55. Sasindran, S.J. and J.B. Torrelles, *Mycobacterium Tuberculosis Infection and Inflammation: what is Beneficial for the Host and for the Bacterium?* Frontiers in microbiology, 2011. **2**: p. 2.
56. Dartois, V., *The path of anti-tuberculosis drugs: from blood to lesions to mycobacterial cells.* Nature Reviews Microbiology, 2014. **12**(3): p. 159-167.
57. *Development of a novel multi-compartment granuloma model to predict local drug distribution and its impact on pharmacodynamics and disease progression in tuberculosis*. 2016; Available from: https://www.page-meeting.org/pdf_assets/2649-Rose_2016_PAGE_TB.pdf.
58. Edginton, A.N., et al., *Defining the role of macrophages in local moxifloxacin tissue concentrations using biopsy data and whole-body physiologically based pharmacokinetic modelling.* Clinical pharmacokinetics, 2009. **48**(3): p. 181-187.
59. Khor, S., H. Bozigian, and M. Mayersohn, *Potential error in the measurement of tissue to blood distribution coefficients in physiological pharmacokinetic modeling. Residual tissue blood. II. Distribution of phencyclidine in the rat.* Drug metabolism and disposition, 1991. **19**(2): p. 486-490.
60. Rostami-Hodjegan, A. and S. Toon, *physiologically based pharmacokinetics as a component of model-informed drug development: where we were, where we are, and where we are heading.* The Journal of Clinical Pharmacology, 2020. **60**: p. S12-S16.

APPENDIX A. DATASETS FOR SPECTINAMIDE 1599 AND 1810 USED FOR THE PBPK MODELING, INCLUDING ADMINISTRATION ROUTES, DOSE LEVELS AND DOSING REGIMENS, SPECIES, AND DISEASE STATUS

Drug	Species	Disease Status	Route of Administration	Dosing Frequency	Dose Level (mg/kg)	No. of Animals	No. of Data Points/ Animal (Tissues)	No. of Animals/ Sampling Time Point	Reference
Spectinamide 1599	Balb/c mice	Healthy	Intravenous	Single dose	10	24	1 (plasma, lung, liver, spleen)	3	[18]
Spectinamide 1599	Balb/c mice	Healthy	Intravenous	Daily dosing for 5 days (QD5)	10	21	1 (plasma, lung, liver, spleen)	3	[18]
Spectinamide 1599	Balb/c mice	Healthy	Subcutaneous	Single Dose	50	24	1 (plasma, lung, liver, spleen)	3	[14, 18]
Spectinamide 1599	Balb/c mice	Healthy	Subcutaneous	Single Dose	200	27	1 (plasma, lung, liver, spleen)	3	[14, 18]
Spectinamide 1599	Balb/c mice	Healthy	Subcutaneous	Daily dosing for 5 days (QD5)	200	18	1 (plasma, lung, liver, spleen)	3	[14, 18]
Spectinamide 1599	Balb/c mice	Healthy	Subcutaneous	Twice a week (BIW)	200	18	1 (plasma, lung, liver, spleen)	3	[14, 18]
Spectinamide 1599	Balb/c mice	Healthy	Subcutaneous	Three times a week (TIW)	200	18	1 (plasma, lung, liver, spleen)	3	[14, 18]
Spectinamide 1599	Balb/c mice	Infected	Subcutaneous - Study 1A	Twice daily (QD5 for 4 weeks)	1, 5, 20, 50, 100, 200	30	2 (plasma)	5	[50]

Table Continued.

Drug	Species	Disease Status	Route of Administration	Dosing Frequency	Dose Level (mg/kg)	No. of Animals	No. of Data Points/ Animal (Tissues)	No. of Animals/ Sampling Time Point	Reference
Spectinamide 1599	Balb/c mice	Infected	Subcutaneous - Study 1A	Once daily (QD5 for 4 weeks)	2, 10, 40, 100, 200	25	2 (plasma)	5	[50]
Spectinamide 1599	Balb/c mice	Infected	Subcutaneous - Study 1A	TIW for 4 weeks	10, 40, 99.6	15	2 (plasma)	5	[50]
Spectinamide 1599	Balb/c mice	Infected	Subcutaneous - Study 1A	BIW for 4 weeks	10, 40	10	2 (plasma)	5	[50]
Spectinamide 1599	Balb/c mice	Infected	Subcutaneous - Study 1A	Once every week for 4 weeks	10, 40	10	2 (plasma)	5	[50]
Spectinamide 1599	Balb/c mice	Infected	Subcutaneous - Study 1B	Twice daily (QD5 for 4 weeks)	100, 166	12	2 (plasma)	6	[50]
Spectinamide 1599	Balb/c mice	Infected	Subcutaneous - Study 1B	TIW for 4 weeks	66, 166	12	2 (plasma)	6	[50]
Spectinamide 1599	Balb/c mice	Infected	Subcutaneous - Study 1B	BIW for 4 weeks	100	6	2 (plasma)	6	[50]
Spectinamide 1599	Balb/c mice	Infected	Subcutaneous - Study 1B	Once every week for 4 weeks	166	6	2 (plasma)	6	[50]
Spectinamide 1599	Balb/c mice	Infected	Subcutaneous - Study 1C	Twice daily (QD5 for 4 weeks)	50	6	2 (plasma)	6	[50]
Spectinamide 1599	Balb/c mice	Infected	Subcutaneous - Study 1C	Once daily (QD5 for 4 weeks)	100	6	2 (plasma)	6	[50]
Spectinamide 1599	Balb/c mice	Infected	Subcutaneous - Study 1C	TIW for 4 weeks	166	6	2 (plasma)	6	[50]
Spectinamide 1599	Balb/c mice	Infected	Subcutaneous - Study 1C	BIW for 4 weeks	100	6	2 (plasma)	6	[50]
Spectinamide 1599	Balb/c mice	Healthy	Intrapulmonary Aerosol	Single Dose	10, 50, 150	72	1 (plasma, lung, liver, spleen, ELF)	3	[14, 18]

Table Continued.

Drug	Species	Disease Status	Route of Administration	Dosing Frequency	Dose Level (mg/kg)	No. of Animals	No. of Data Points/ Animal (Tissues)	No. of Animals/ Sampling Time Point	Reference
Spectinamide 1599	Balb/c mice	Healthy	Intrapulmonary Aerosol	QD5	10, 50, 150	54	1 (plasma, lung, liver, spleen, ELF)	3	[14, 18]
Spectinamide 1599	Balb/c mice	Healthy	Intrapulmonary Aerosol	BIW	10, 50, 150	54	1 (plasma, lung, liver, spleen, ELF)	3	[14, 18]
Spectinamide 1599	Balb/c mice	Healthy	Intrapulmonary Aerosol	TIW	10, 50, 150	54	1 (plasma, lung, liver, spleen, ELF)	3	[14, 18]
Spectinamide 1599	Sprague-Dawley Rats	Healthy	Intravenous	Single Dose	10	5 males	13 (plasma)	5	[10]
Spectinamide 1599	Sprague-Dawley Rats	Healthy	Intravenous	Single Dose	10	6 females	13 (plasma)	6	[10]
Spectinamide 1599	Sprague-Dawley Rats	Healthy	Intravenous	Single Dose	10	4 males	1 (plasma, lung, liver, spleen)	4	Generated in this study as described above
Spectinamide 1599	Sprague-Dawley Rats	Healthy	Intravenous	Single Dose	10	4 females	1 (plasma, lung, liver, spleen)	4	
Spectinamide 1810	Balb/c Mice	Healthy	Intravenous	Single Dose	10	24	1 (plasma, lung, liver, spleen)	3	[50-52]
Spectinamide 1810	Balb/c Mice	Healthy	Intravenous	QD5	10	24	1 (plasma, lung, liver, spleen)	3	[50-52]
Spectinamide 1810	Balb/c Mice	Healthy	Subcutaneous	Single Dose	46	21	1 (plasma)	3	[50-52]
Spectinamide 1810	Balb/c Mice	Healthy	Subcutaneous	Single Dose	50, 200	48	1 (plasma)	3	[50-52]
Spectinamide 1810	Balb/c Mice	Healthy	Subcutaneous	QD5	50, 200	36	1 (plasma)	3	[50-52]
Spectinamide 1810	Balb/c Mice	Infected	Subcutaneous - Study 2A	Twice daily (QD5 for 4 weeks)	10, 20, 50, 100, 200, 300, 500	35	2 (plasma)	5	[50-52]

Table Continued.

Drug	Species	Disease Status	Route of Administration	Dosing Frequency	Dose Level (mg/kg)	No. of Animals	No. of Data Points/ Animal (Tissues)	No. of Animals/ Sampling Time Point	Reference
Spectinamide 1810	Balb/c Mice	Infected	Subcutaneous - Study 2A	Once daily (QD5 for 4 weeks)	20, 40, 100, 200, 400	25	2 (plasma)	5	[50-52]
Spectinamide 1810	Balb/c Mice	Infected	Subcutaneous - Study 2A	TIW for 4 weeks	20, 40, 100, 200, 400	25	2 (plasma)	5	[50-52]
Spectinamide 1810	Balb/c Mice	Infected	Subcutaneous - Study 2A	BIW for 4 weeks	20, 40, 100, 200	20	2 (plasma)	5	[50-52]
Spectinamide 1810	Balb/c Mice	Infected	Subcutaneous - Study 2A	Once every week for 4 weeks	20, 40, 100	15	2 (plasma)	5	[50-52]
Spectinamide 1810	Balb/c Mice	Infected	Subcutaneous - Study 2B	Twice daily (QD5 for 4 weeks)	50, 200	12	2 (plasma)	6	[50-52]
Spectinamide 1810	Balb/c Mice	Infected	Subcutaneous - Study 2B	Once daily (QD5 for 4 weeks)	100	6	2 (plasma)	6	[50-52]
Spectinamide 1810	Balb/c Mice	Infected	Subcutaneous - Study 2B	TIW for 4 weeks	166, 333	12	2 (plasma)	6	[50-52]
Spectinamide 1810	Sprague-Dawley Rats	Healthy	Intravenous	Single Dose	10	18 males	13 (plasma)	18	Generated in this study as described above

APPENDIX B. MEASURED CONCENTRATION-TIME DATA IN PLASMA AND TISSUE AFTER SINGLE DOSE INTRAVENOUS ADMINISTRATION OF SPECTINAMIDE 1810

Table B-1. Plasma concentration-time data after single dose IV administration of spectinamide 1810 (10 mg/kg) to Balb/c mice (n = 3 mice per time point).

Time (h)	Concentration (mg/L)			Median	Mean	STDEV	Range	GEO MEAN	GEO STDEV
0.083	4.76	23.3	25.2	23.3	17.8	11.3	20.4	14.1	2.56
0.25	8.54	12.4	11.2	11.2	10.7	1.95	3.81	10.6	1.21
0.5	3.32	4.30	2.17	3.32	3.26	1.06	2.13	3.14	1.41
1	0.251	0.443	0.616	0.443	0.437	0.183	0.365	0.409	1.57
3	0.00820	0.0117	0.0303	0.0117	0.0167	0.0119	0.0221	0.0143	1.96
8	0.00234	0.00298	0.00128	0.00234	0.00220	0.000856	0.00170	0.00207	1.54
16	0.00554	0.00106	-	0.00330	0.00330	0.00316	0.00447	0.00242	3.21
24	0.000933	0.0000551	0.00152	0.000933	0.000834	0.000735	0.00146	0.000427	5.99

Table B-2. Lung concentration-time data after single dose IV administration of spectinamide 1810 (10 mg/kg) to Balb/c mice (n = 3 mice per time point).

Time (h)	Concentration (µg/g)			Median	Mean	STDEV	Range	GEO MEAN	GEO STDEV
0.083	2.19	8.05	9.10	8.05	6.45	3.72	6.91	5.43	2.20
0.25	3.52	4.62	5.25	4.62	4.46	0.876	1.73	4.40	1.23
0.5	1.92	1.73	1.41	1.73	1.69	0.260	0.515	1.67	1.17
1	0.520	0.535	0.600	0.535	0.552	0.0425	0.0800	0.551	1.08
3	0.121	0.198	0.224	0.198	0.181	0.0538	0.104	0.175	1.39
8	0.121	0.0810	0.0810	0.0810	0.0942	0.0228	0.0395	0.0925	1.26
16	0.0580	0.114	0.110	0.110	0.0937	0.0310	0.0555	0.0897	1.46
24	0.0620	0.0398	0.0625	0.0620	0.0548	0.0130	0.0227	0.0536	1.29

Table B-3. Liver concentration-time data after single dose IV administration of spectinamide 1810 (10 mg/kg) to Balb/c mice (n = 3 mice per time point).

Time (h)	Concentration (µg/g)			Median	Mean	STDEV	Range	GEO MEAN	GEO STDEV
0.083	0.765	4.20	5.80	4.20	3.59	2.57	5.04	2.65	2.97
0.25	3.69	4.55	4.78	4.55	4.34	0.575	1.09	4.31	1.15
0.5	3.54	3.50	3.77	3.54	3.60	0.145	0.270	3.60	1.04
1	2.01	2.03	2.41	2.03	2.15	0.224	0.395	2.14	1.11
3	0.990	1.38	1.91	1.38	1.42	0.459	0.915	1.37	1.39
8	2.04	0.162	1.85	1.85	1.35	1.03	1.87	0.847	4.19
16	0.965	1.16	1.11	1.11	1.08	0.0985	0.190	1.07	1.10
24	0.520	0.800	0.790	0.790	0.703	0.159	0.280	0.690	1.28

Table B-4 Spleen concentration-time data after single dose IV administration of spectinamide 1810 (10 mg/kg) to Balb/c mice (n = 3 mice per time point).

Time (h)	Concentration (µg/g)			Median	Mean	STDEV	Range	GEO MEAN	GEO STDEV
0.083	0.580	2.92	2.58	2.58	2.03	1.26	2.34	1.63	2.46
0.25	1.14	1.58	4.12	1.58	2.28	1.61	2.98	1.95	1.95
0.5	0.580	0.900	0.423	0.580	0.634	0.243	0.478	0.604	1.46
1	0.236	0.251	0.275	0.251	0.254	0.0197	0.0390	0.253	1.08
3	0.0740	0.164	0.180	0.164	0.139	0.0571	0.106	0.130	1.63
8	0.107	0.144	0.0945	0.107	0.115	0.0258	0.0495	0.113	1.24
16	0.0580	0.171	0.0975	0.0975	0.109	0.0571	0.113	0.0988	1.71
24	0.0865	0.0815	0.129	0.0865	0.0988	0.0258	0.0470	0.0968	1.28

Table B-5. Kidney concentration-time data after single dose IV administration of spectinamide 1810 (10 mg/kg) to Balb/c mice (n = 3 mice per time point).

Time (h)	Concentration (µg/g)			Median	Mean	STDEV	Range	GEO MEAN	GEO STDEV
0.083	9.45	32.3	37.0	32.3	26.3	14.7	27.6	22.4	2.12
0.25	15.6	20.8	22.0	20.8	19.4	3.37	6.35	19.2	1.20
0.5	7.15	9.60	5.55	7.15	7.43	2.04	4.05	7.25	1.32
1	3.74	3.21	4.03	3.74	3.66	0.416	0.820	3.64	1.12
3	2.10	3.61	3.98	3.61	3.23	0.994	1.875	3.11	1.41
8	2.88	3.17	2.41	2.88	2.82	0.383	0.760	2.80	1.15
16	1.86	2.66	2.29	2.29	2.27	0.401	0.800	2.24	1.20
24	1.56	1.79	1.33	1.56	1.56	0.230	0.460	1.55	1.16

APPENDIX C. MEASURED CONCENTRATION-TIME DATA IN PLASMA AND TISSUE AFTER MULTIPLE-DOSE INTRAVENOUS ADMINISTRATION OF SPECTINAMIDE 1810

Table C-1. Plasma concentration-time data after multiple-dose IV administration of spectinamide 1810 (QD5, 10 mg/kg) to Balb/c mice (n = 3 mice per time point).

Time (h)	Concentration (mg/L)			Median	Mean	STDEV	Range	GEO MEAN	GEO STDEV
Pre-Dose	0.000472	0.00816	0.00250	0.00250	0.00371	0.00399	0.00769	0.00213	4.19
0.083	26.1	22.0	11.4	22.00	19.8	7.61	14.8	18.7	1.55
0.25	26.0	13.1	7.84	13.05	15.6	9.32	18.1	13.8	1.82
0.5	3.91	3.60	3.49	3.60	3.67	0.220	0.425	3.66	1.06
1	1.44	1.17	0.859	1.170	1.16	0.291	0.582	1.13	1.30
3	0.0124	0.0185	0.00890	0.012	0.0133	0.00486	0.00961	0.0127	1.44
8	0.00293	0.0120	0.00546	0.005	0.00678	0.00465	0.00902	0.00576	2.02
24	-	0.000641	0.00137	0.001	0.00101	0.000518	0.000733	0.000938	1.71

Table C-2. Lung concentration-time data after multiple-dose IV administration of spectinamide 1810 (QD5, 10 mg/kg) to Balb/c mice (n = 3 mice per time point).

Time (h)	Concentration (µg/g)			Median	Mean	STDEV	Range	GEO MEAN	GEO STDEV
Pre-Dose	0.234	0.262	0.402	0.262	0.299	0.0897	0.168	0.291	1.33
0.083	10.3	9.90	3.59	9.90	7.91	3.75	6.66	7.14	2.05
0.25	11.7	5.40	3.20	5.40	6.77	4.41	8.51	5.87	1.92
0.5	2.06	3.11	1.92	2.06	2.36	0.648	1.19	2.31	1.30
1	1.16	0.860	0.850	0.860	0.957	0.176	0.310	0.947	1.19
3	0.319	0.308	0.225	0.308	0.284	0.0512	0.0935	0.281	1.21
8	0.262	0.285	0.319	0.285	0.288	0.0284	0.0565	0.287	1.10
24	0.225	0.272	0.252	0.252	0.250	0.0238	0.0475	0.249	1.10

Table C-3. Liver concentration-time data after multiple-dose IV administration of spectinamide 1810 (QD5, 10 mg/kg) to Balb/c mice (n = 3 mice per time point).

Time (h)	Concentration (µg/g)			Median	Mean	STDEV	Range	GEO MEAN	GEO STDEV
Pre-Dose	1.39	0.810	1.09	1.09	1.10	0.288	0.575	1.07	1.31
0.083	7.65	7.25	3.07	7.25	5.99	2.54	4.59	5.54	1.84
0.25	14.2	7.75	3.48	7.75	8.48	5.40	10.73	7.26	2.03
0.5	5.20	5.70	5.00	5.20	5.30	0.361	0.700	5.29	1.07
1	4.37	4.33	4.07	4.33	4.25	0.164	0.300	4.25	1.04
3	2.45	2.31	1.61	2.31	2.12	0.450	0.840	2.09	1.26
8	2.21	2.51	1.96	2.21	2.22	0.275	0.550	2.21	1.13
24	0.955	1.21	1.13	1.13	1.10	0.128	0.250	1.09	1.13

Table C-4. Spleen concentration-time data after multiple-dose IV administration of spectinamide 1810 (QD5, 10 mg/kg) to Balb/c mice (n = 3 mice per time point).

Time (h)	Concentration (µg/g)			Median	Mean	STDEV	Range	GEO MEAN	GEO STDEV
Pre-Dose	0.211	0.306	0.363	0.306	0.293	0.0771	0.153	0.286	1.32
0.083	4.51	3.78	1.96	3.78	3.42	1.31	2.55	3.22	1.59
0.25	6.00	2.67	1.69	2.67	3.45	2.26	4.31	3.00	1.90
0.5	1.09	0.950	1.60	1.09	1.21	0.339	0.645	1.18	1.31
1	0.710	0.660	0.660	0.660	0.677	0.0289	0.0500	0.676	1.04
3	0.371	0.410	0.261	0.371	0.347	0.0773	0.149	0.341	1.27
8	0.300	0.440	0.401	0.401	0.380	0.0723	0.140	0.375	1.22
24	0.231	0.254	0.272	0.254	0.252	0.0206	0.0410	0.252	1.09

Table C-5. Kidney concentration-time data after multiple-dose IV administration of spectinamide 1810 (QD5, 10 mg/kg) to Balb/c mice (n = 3 mice per time point).

Time (h)	Concentration (µg/g)			Median	Mean	STDEV	Range	GEO MEAN	GEO STDEV
Pre-Dose	2.88	3.53	5.70	3.53	4.04	1.48	2.83	3.87	1.42
0.083	72.0	44.3	36.2	44.3	50.8	18.8	35.9	48.7	1.15
0.25	52.0	27.7	20.2	27.7	33.3	16.6	31.9	30.7	1.62
0.5	13.6	15.3	12.9	13.6	13.9	1.21	2.35	13.9	1.09
1	9.10	10.1	10.1	10.1	9.75	0.563	1.00	9.74	1.06
3	7.10	5.95	6.10	6.10	6.38	0.625	1.15	6.36	1.10
8	7.50	8.00	6.50	7.50	7.33	0.764	1.50	7.31	1.11
24	4.28	3.84	4.16	4.16	4.09	0.227	0.440	4.09	1.06

APPENDIX D. MEASURED PLASMA CONCENTRATION-TIME DATA AFTER SINGLE DOSE INTRAVENOUS ADMINISTRATION OF SPECTINAMIDE 1810 IN HEALTHY RATS

Table D-1. Study 1 plasma concentration-time data after single dose IV administration of spectinamide 1810 (10 mg/kg) to male Sprague-Dawley rats (n=6).

Time (h)	Concentration (mg/L)						Mean	SD	%CV
	R1	R2	R3	R4	R5	R6			
0.08	43.0	38.8	54.8	51.7	43.5	50.0	47.0	6.12	13.0
0.25	17.7	17.5	25.1	29.6	27.3	29.8	24.5	5.61	22.9
0.5	15.1	8.90	15.1	15.3	18.2	15.9	14.8	3.10	21.0
0.75	8.20	5.90	8.30	6.20	7.80	9.00	7.57	1.24	16.4
1	3.00	3.10	4.30	5.00	4.40	4.70	4.08	0.838	20.5
1.5	1.40	1.20	1.70	2.20	2.00	1.70	1.70	0.369	21.7
2	0.800	0.500	0.700	0.700	0.700	0.800	0.700	0.110	15.6
4	0.0300	0.0300	0.0300	0.0400	0.0700	0.0400	0.0400	0.0155	38.7
6	0.0150	0.00800	0.0130	0.0130	0.0250	0.0250	0.0165	0.00698	42.3
8	0.0100	0.00800	0.0100	0.0120	0.0100	0.00900	0.00983	0.00133	13.5
10	0.0150	0.00700	0.00700	0.00700	0.00900	0.0120	0.00950	0.00333	35.1
24	0.00550	0.00460	0.00800	0.00850	0.00680	0.00550	0.00648	0.00155	23.8
48	0.00910	0.0611	0.0169	0.00560	0.00490	0.00650	0.0174	0.0219	126

Table D-2. Study 2 plasma concentration-time data after single dose IV administration of spectinamide 1810 (10 mg/kg) to male Sprague-Dawley rats (n=6).

Time (h)	Concentration (mg/L)						Mean	SD	%CV
	R1	R2	R3	R4	R5	R6			
0.08	43.2	28.5	44.0	40.3	44.2	38.1	39.7	5.99	15.1
0.25	24.6	17.5	25.2	23.9	25.9	25.1	23.7	3.11	13.1
0.5	12.9	9.50	11.7	12.4	13.4	13.3	12.2	1.46	12.0
0.75	7.84	4.68	6.47	7.39	8.07	7.77	7.04	1.28	18.3
1	4.55	3.04	3.88	4.42	4.40	4.91	4.20	0.658	15.7
1.5	1.11	0.681	1.14	1.28	1.37	1.74	1.22	0.348	28.5
2	0.336	0.245	0.353	0.416	0.440	0.477	0.378	0.0839	22.2
4	0.0157	0.0137	0.0210	0.0292	0.0403	0.0233	0.0239	0.00977	40.9
6	0.00993	0.00288	0.00463	0.00552	0.0118	0.00579	0.00676	0.00339	50.2
8	0.0111	0.00450	0.00469	0.00563	0.00352	0.00330	0.00546	0.00289	53.0
10	0.00827	0.00455	0.00289	0.00314	0.00413	0.00316	0.00436	0.00202	46.4
24	0.00661	0.00526	0.00565	0.00990	0.00452	0.00465	0.00610	0.00201	33.0
48	0.0107	0.00888	0.00858	0.00826	0.00829	0.00742	0.00869	0.00110	12.7

Table D-3. Study3 plasma concentration-time data after single dose IV administration of spectinamide 1810 (10 mg/kg) to male Sprague-Dawley rats (n=6).

Time (h)	Concentration (mg/L)						Mean	SD	%CV
	R1	R2	R3	R4	R5	R6			
0.08	45.2	30.4	46.0	47.8	45.4	40.2	42.5	6.45	15.2
0.25	25.0	18.9	27.1	26.0	27.8	25.4	25.0	3.18	12.7
0.5	13.9	9.00	12.6	13.4	12.1	13.7	12.5	1.82	14.6
0.75	7.50	4.90	6.80	7.20	7.80	7.70	6.98	1.08	15.5
1	4.50	3.30	4.00	4.40	4.80	5.20	4.37	0.659	15.1
1.5	1.40	0.800	1.30	1.40	1.50	1.80	1.37	0.327	23.9
2	0.400	0.400	0.600	0.600	0.600	0.600	0.533	0.103	19.4
4	0.0200	0.0100	0.0300	0.0300	0.0700	0.0300	0.0317	0.0204	64.5
6	0.0170	0.00300	0.00300	0.00800	0.0110	0.00900	0.00850	0.00528	62.1
8	0.00200	0.00300	0.00600	0.00300	0.00200	0.00100	0.00283	0.00172	60.8
10	0.00700	0.00200	0.00300	0.00300	0.00100	0.00	0.00267	0.00242	90.8
24	0.00400	0.00300	0.00500	0.00700	0.00500	0.00600	0.00500	0.00141	28.3
48	0.00600	0.0110	0.00500	0.00600	0.0110	0.00700	0.00767	0.00266	34.7

APPENDIX E. MEASURED CONCENTRATION-TIME DATA IN PLASMA AND TISSUE AFTER SINGLE-DOSE INTRAVENOUS ADMINISTRATION OF SPECTINAMIDE 1599 IN HEALTHY RATS

Table E-1. Plasma concentration-time data after single dose IV administration of spectinamide 1599 (10 mg/kg) to Sprague-Dawley rats (n = 4 rats per time point, 2 males and 2 females).

Time (h)	Concentration (mg/L)					
	Male-1	Male-2	Mean (SD)	Female-1	Female-2	Mean (SD)
0.25	23.0	21.6	22.3 (0.955)	21.2	19.9	20.5 (0.884)
4	0.0192	0.0185	0.0188 (0.000495)	0.0269	0.0255	0.0262 (0.00103)

Table E-2. Lung concentration-time data after single dose IV administration of spectinamide 1599 (10 mg/kg) to Sprague-Dawley rats (n = 4 rats per time point, 2 males and 2 females).

Time (h)	Concentration (µg/g)					
	Male-1	Male-2	Mean (SD)	Female-1	Female-2	Mean (SD)
0.25	7.05	7.05	7.05 (0.0)	7.65	5.90	6.78 (1.24)
4	0.610	0.705	0.658 (0.658)	0.695	0.670	0.683 (0.0177)

Table E-3. Liver concentration-time data after single dose IV administration of spectinamide 1599 (10 mg/kg) to Sprague-Dawley rats (n = 4 rats per time point, 2 males and 2 females).

Time (h)	Concentration (µg/g)					
	Male-1	Male-2	Mean (SD)	Female-1	Female-2	Mean (SD)
0.25	7.80	7.75	7.78 (0.0354)	5.98	6.73	6.35 (0.530)
4	3.86	3.32	3.59 (0.387)	4.24	2.99	3.62 (0.887)

Table E-4. Spleen concentration-time data after single dose IV administration of spectinamide 1599 (10 mg/kg) to Sprague-Dawley rats (n = 4 rats per time point, 2 males and 2 females).

Time (h)	Concentration (µg/g)					
	Male-1	Male-2	Mean (SD)	Female-1	Female-2	Mean (SD)
0.25	2.13	1.67	1.90 (0.325)	1.90	2.20	2.05 (0.212)
4	0.386	0.442	0.414 (0.0396)	0.555	0.393	0.474 (0.115)

Table E-5. Kidney concentration-time data after single dose IV administration of spectinamide 1599 (10 mg/kg) to Sprague-Dawley rats (n = 4 rats per time point, 2 males and 2 females).

Time (h)	Concentration (µg/g)					
	Male-1	Male-2	Mean (SD)	Female-1	Female-2	Mean (SD)
0.25	32.0	40.6	36.3 (6.12)	36.0	42.9	39.4 (4.84)
4	10.1	11.4	10.7 (0.919)	13.2	10.4	11.8 (2.02)

VITA

Keyur Parmar was born in the Valsad district of Gujarat, India, in 1989 and was raised in Daman and Diu. He obtained his Diploma in Pharmacy from Dr. Dayaram Patel Pharmacy College located in Bardoli, Gujarat, in 2009; Bachelor's degree in Pharmacy from L.M. College of Pharmacy located in Ahmedabad, Gujarat, in 2012; and Master's degree in Pharmaceutical Analysis from the National Institute of Pharmaceutical Education and Research (NIPER) located in Mohali, in 2014. After completing his Master's degree, he joined the Drug Metabolism and Pharmacokinetic (DMPK) department at Syngene International Limited in Bengaluru and worked there for three years. Following that, he joined the Pharmaceutical Sciences Ph.D. program with a major focused in Pharmacometrics at the University of Tennessee Health Science Center (UTHSC) with Dr. Bernd Meibohm as his advisor. During his tenure as a Ph.D. student, he has presented his work as a poster presentation at the American Association of Pharmaceutical Scientists (AAPS) PharmSci 360 conference 2019, San Antonio, and received a college of Graduate Health Science (CGHS) travel grant award from UTHSC. While at UTHSC, he was involved with various leadership positions such as Vice-Chair elect of the AAPS student chapter in 2018 and 2019. He was also actively involved in the Seed Grant Review Committee at UTHSC from 2020 to 2022. During this period, he was also a summer intern in Cell Therapy Clinical Pharmacology at Takeda Pharmaceuticals, Cambridge, MA in the summer of 2021. He presented the internship work at the American Society of Clinical Pharmacology and Therapeutics conference 2022 and received a Presidential Trainee Award. He expects to receive the Doctor of Philosophy degree in Pharmaceutical Sciences in March 2023. After completion of his Ph.D., he will be joining the Quantitative Pharmacology and Pharmacometrics group at Merck & Co., Rahway, NJ, as a Senior Scientist.